Investigation of Space Charge Profile on the Flashover Characteristics of Fiberglass Reinforced Plastic (FRP) Tools Under HVDC Conditions

by

Jeffrey Laninga

A thesis submitted to the Faculty of Graduate Studies of
The University of Manitoba
in partial fulfilment of the requirements of the degree of

Master of Science

Department of Electrical and Computer Engineering
University of Manitoba
Winnipeg, Canada

Abstract

In high voltage direct current (HVDC) electric power systems, live-line maintenance methods, using fibreglass reinforced plastic (FRP) tools, are being applied to enhance their reliability and avoid costly outages. The effects of direct current (DC) space charges are not well understood or accounted for in live-line working standards.

Surface charge is generated by a ring of needles, pre-stressing and wiping. Surface potentials are measured using a vibrating Kelvin probe and converted to charge densities using a probe response matrix. Surface charging characteristics of FRP are compared to silicone rubber (SIR) and wood hot stick insulator samples.

The effects on flashover voltage due to the presence of surface charge are investigated by applying both polarities of voltage when charges pre-existed on the surface. It is discovered that the presence of surface charge does impact the flashover voltage of FRP insulator samples. Mitigation methods are investigated and discussed.

Acknowledgements

Firstly, I would like to thank Dr. Behzad Kordi for his guidance, help and support through this process. He provided excellent advice during my research to ensure the thesis would come to the finish line successfully. Working full time, having a family and completing a M. Sc. degree comes with its challenges but his calm nature and sense of humour was exactly what was needed by myself.

Thanks to my co-advisor Dr. David Swatek, from Manitoba Hydro, for advocating and supporting this project. His passion for my topic and encouraging words provided great motivation for completion of the project.

I would like to thank my examining committee, Dr. Ahmed Shalaby and Dr. Ioni Fernando for accepting to review this thesis and providing constructive comments. Thank you as well to Bill McDermid from Manitoba Hydro for sharing his valuable expertise.

I want to give many thanks to Ph. D. student Mohammed Amer, whom spent many hours with myself in the high voltage laboratory helping me carry out the research and testing. We had challenges, but many more good times during our 400 plus hours of testing together. We shared many technical conversations to understand our results. He was of great help to me and I will always consider him a friend.

Thank you to Manitoba Hydro and NSERC for their funding of the project, for without this support the completion of the project would have not been possible. Thank you specifically to my manager, Trevor Smith, for supporting the project and giving me time to work on the project until completion.

I also want to thank Daryl Hamelin for all the work he completed and knowledge he shared in setting up our laboratory equipment. He designed and fabricated our setups of the utmost quality and with great professionalism. He also put our safety in the high voltage laboratory as paramount. A big thanks as well to Cory Smit for the machining of all of our insulator samples.

Last but definitely not least, I would like to thank my wife and four children for their support and understanding. Without my wifes encouragement, I would have never started the M. SC. program, but she believed in me and it has turned out to be a great decision.

Dedication

To my loving and supportive wife and children.

Table of Contents

List of Figures

List of Tables

Chapter 1

Introduction

1.1 Background

There is a growing interest worldwide for high voltage direct current (HVDC) systems for bulk transmission of electric power over long distances. HVDC transmission systems operate at voltages up to 800 kV and higher levels are emerging [1]. Live-line maintenance methods are used to safely secure continuous and reliable transportation of electric energy in such systems while avoiding revenue loss. Live-line maintenance methods employ fibreglass reinforced plastic (FRP) insulating materials to safely insulate the energized conductors from each other and from the ground, as well as ensuring the safety of the personnel. During live-line maintenance work, space charges accumulate on the surface of FRP hot sticks (commonly used in live-line work) due to corona discharge from energized nearby objects and/or by direct contact with energized objects. This work can be carried out using FRP tools from structures where the tool is the worker's sole line of defense. There are also barehanding techniques (worker is at the same potential as the energized conductor) where aerial devices are used or a ladder is used from the structure (Figure 1.1) . In these latter cases, leakage monitoring is used in conjunction with the insulation to provide extra security,

as measurable leakage current is a precursor to a contamination-type flashover. Workers are visually required to monitor the leakage current during the duration of energized contact.

Industry and recent research is taking interest in the space charge accumulation and flashover performance for insulators of various materials under direct current (DC) conditions. The impact of surface charge is being investigated and given extra consideration under DC conditions as studies have shown, for example, that the flashover characteristics can be affected by charges residing on the surface of cylindrical polymer insulators [2]. This phenomenon will need to be better understood for live line tools made from FRP used for HVDC maintenance since existing standards do not consider the effect of space charge for DC minimum approach distances. The effects of DC corona space charge is not well understood as of yet on FRP tools.

After two flashover accidents, in 1997 and 2002 at 500 kV AC (alternating current) at Manitoba Hydro, extensive research was carried out to study and understand the root cause [3]. Testing and research have shown that the root cause of the AC accidents was light salt pollution on the surface of the FRP tools combined with surface moisture/ice. Follow-up testing at 500 kV HVDC at Institut de recherche d'Hydro-Québec (IREQ) revealed a "fast flashover" phenomenon [3], [4] that appears to be due to space charge from DC corona. The fast flashover phenomenon was characterized as occurring at low humidity, with absence of leakage current, at less than the system's operating voltage, light to no contamination, and occurs exclusively at negative voltages. There are well distinguished differences that characterize the fast flashover from the well understood pollution flashover which always occurred with prior leakage current of greater than 2 mA. The test procedure was such that the electrodes were pre-stressed for about 30 minutes with HVDC, and then a series of voltage ramps were started along with increasing humidity. The DC withstand voltage of clean FRP surface was shown to be reduced compared to their AC withstand voltage, due to the accumulation of surface charges [5].

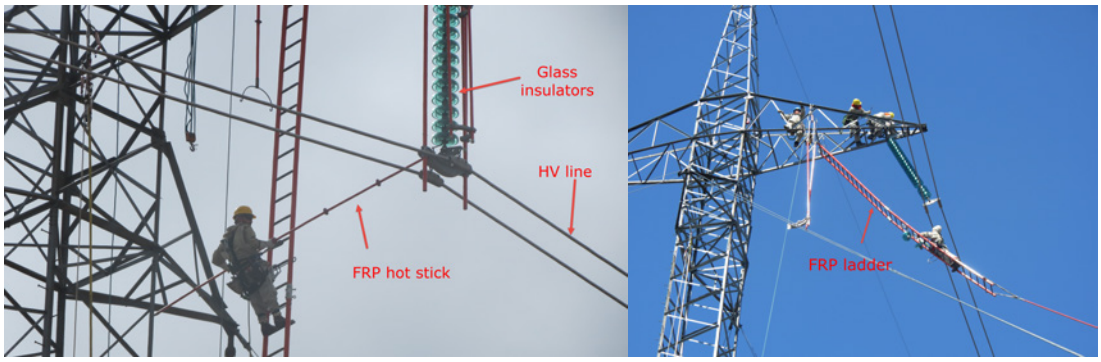

(a) **(b)**

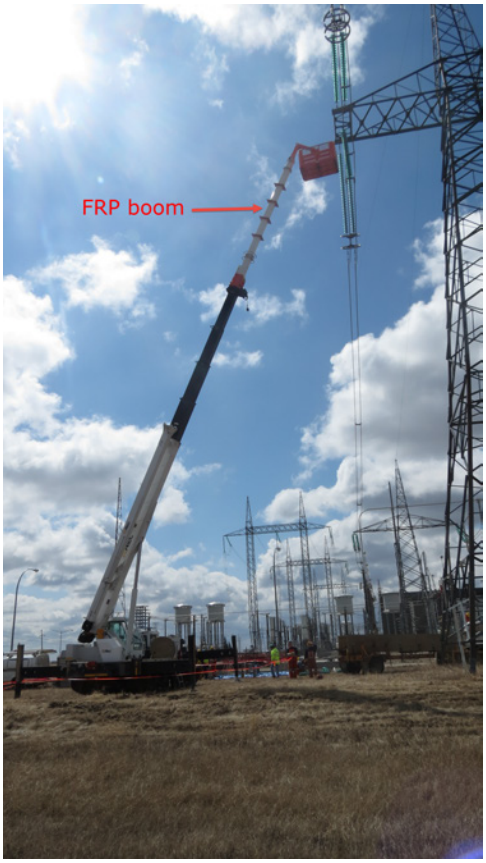

(c)

Fig. 1.1: Pictures illustrating live-line work on HVDC using a) FRP hot stick from the structure(ladder), b) barehand method from a ladder and c) barehand method from an aerial device. Photographs courtesy of Manitoba Hydro.

At the same time flashover incidents are occurring in industry all at the negative peak of the AC waveform [6]. At the same time Manitoba Hydro experiences anomalous flashovers on their 500 kV HVDC transmission lines during summer months always on the negative poles during the afternoon to early evening. Many of the flashovers occur in the northern part of the line where the towers are more likely to be standing in or surrounded by water [7]. Further understanding is required as to why these flashovers are all occurring at negative polarity and the cause of the anomalous flashover, as it is suspected to be caused by space charge as well.

The benefits of this thesis to industry are an increased safety of live-line workers and the economic benefit of avoiding outage costs by maintaining or allowing the ability to carry out live-line maintenance on HVDC transmission lines. The results of this research can aid utilities that currently carry out live-line maintenance or plan to on HVDC lines, in the understanding of the possible effects of DC corona on FRP tools and on live working procedures.

1.2 Problem Definition and Existing Solution

There is a large worldwide experience on live-line work on AC lines but the knowledge and experience of live-line work on DC is much more limited. Also of great significance is that present minimum approach distances, for DC live-line work, such as those found in IEEE 516-2009 [8] are based on AC test results with no surface charge considerations under DC conditions. The minimum approach distances are based on switching surge tests in the absence of DC space charge. Other live working standards such as IEC 61472-2013 [9] make no recommendation for the calculation of minimum approach distances for live-line work on HVDC transmission lines. Standards such as ASTM F711-02 [10] specifies AC tests for the design of FRP tools and no consideration is given for the effects of space charge under DC conditions as well.

Based on tests done previously by Manitoba Hydro and others [2], there is some belief that the dielectric withstand of DC, and therefore at the suggested minimum approach distance, the strength may be reduced compared to AC because of the presence of space charge. Previous testing at Manitoba Hydro [11] also showed that AC corona tends to cause static charge on a FRP tool to decay rapidly. Under AC conditions, due to the alternating polarity, space charge will reside very close to the energized apparatus while under DC conditions space charge will spread out due to the repelling nature of the charge. There are many similarities between live work on HVDC systems and live work on high voltage alternating current (HVAC) systems. Live work methods on DC lines were derived from AC live work, and, in general, the two employ the same work methods and tools. There are also several very important differences and issues that require special consideration and further research, including possible effects of DC space charge produced on HVDC lines.

It is critical that the effects of DC corona on FRP tools are understood so that future incidents can be avoided which could result in the inability to perform live-line work and the associated economic benefits. This thesis is based on the testing that was completed by Manitoba Hydro at the IREQ laboratories which resulted in the discovery of a "fast flashover" phenomenon [3], [4] and the previous work of Kumara *et al.* on the effects of DC charge on cylindrical polymer insulators [2], [12].

Concerns with surface charging of polymeric insulators is increasing as the durations that charges reside on surfaces are significantly longer due to the progression of material types. Prior to the 1950s FRP tools were made from wood but have been replaced with the FRP material and in recent years there have been an increasing amount of hot stick flashovers in industry. It has been shown that epoxy resin can have an even slower charge decay times than silicone rubber (SIR) and the charges will reside even longer [13]. This thesis will consider a FRP (composed of fibreglass reinforced epoxy resin) hot stick, SIR, and a wood insulator sample.

Experiments have been performed to better understand the phenomenon and these showed that electric charges can be deposited on polymeric surfaces in different ways, such as being activated by corona discharges in the surrounding air [12]. The issue with most of the past studies on corona charged polymeric surfaces is that they were conducted on very thin flat samples. Few studies involved thick samples or cylindrical shapes, which are more relevant to the case of high voltage insulation and live working tools such as hot sticks, strain poles, and aerial device booms. No study to date have successfully characterized the surface charging and flashover characteristics of FRP tools. Studies of cylindrical insulators to date have mainly focused on streamer propagation.

Previous work done [14] by EPRI (Electric Power Research Institute) concluded that quantifying the possible effects of DC charge on tool performance is a difficult task. An approach to measure the voltage profile along FRP tools with a non-contact measuring device, which could help address this task, was suggested. More recent testing by EPRI attempted to measure surface charge along a FRP tool from a corona brush but due the failure of an electric field probe it was not possible. The effects of wiping with silicone clothes, buffed with wax and rubbed by leather gloves was to be investigated but the work was not successfully completed due to a lack of measurement equipment [15].

Manitoba Hydro was not successful at reproducing fast flashovers at their own high voltage laboratory as completed at IREQ. This was deemed to be due to the ground electrode being closer to the ground and shorter lengths of bundled conductor on the energized side of the FRP tool which resulted in lower space charge potentials [7]. It was recommended that the size of the laboratory be increased along with the length of conductor or testing should be carried out on smaller sized hot sticks. These recommendations would result in higher space charge potentials.

Manitoba Hydro is the only utility in the world that is applying mitigation measures for HVDC live-line work, using polymer sheds and inhibitor electrodes, and interest is growing.

Polymer sheds have the effect of increasing the flashover voltage required for surface charge based flashovers under HVDC conditions, while inhibitor electrodes suppress the formation of positive streamers. This topic will be discussed later in the thesis in the Results and Discussion chapter. Other utilities are not currently performing live line work until further research is carried out and the risks associated with HVDC space charge on FRP tools are fully understood. There is great interest currently in industry to better understand the effects of space charge on FRP tools and its effects on minimum approach distances for HVDC live-line work.

1.3 Objective of the Thesis

The objective of this thesis is to investigate the effects of DC corona on the surface charge and flashover characteristics of an FRP hot stick. Laboratory testing will be carried out in combination with computer simulation to determine the effects of electrical surface charges on FRP tools under DC conditions. The characteristics of the deposited surface charge (surface potential profile) and flashover performance will be investigated using various methods of charging. It is expected that the surface charge on the tool surface will decrease the flashover voltage and increase the probability of a flashover at the system operating voltage. The effects of different material properties on the charge profile and flashover characteristics will be investigated. The thesis will provide an understanding of the impact of surface charges and their characteristics on the DC flashover voltage of FRP tools, which is essential to consider in live-line working standards, live-line methods, and flashover prevention. Possible mitigation methods are discussed for improving worker safety during live-line work on HVDC transmission lines.

1.4 Contributions

The contributions of this thesis are as follows:

- Determination of the DC surface charging characteristics of cylindrical FRP, SIR and wood insulator samples using three charging methods of direct and non-direct contact. These characteristics included charging time, voltage and decay.
- The influence of distance from the non-contact corona source to the insulator surface is determined for all insulator materials.
- Comparisons between all insulator materials is made in regards to their surface charging characteristics. The difference between polarity of charging voltage and the materials properties effect on charge collection and decay is determined.
- Determination that the wiping method, as completed in live-line work just prior to hot stick contact, could be hazardous prior to live line work for DC.
- Provided a full understanding of the effects of triple point junctions and electrode configurations for pre-stressing insulator samples from one side with the other side grounded.
- The DC flashover characteristics of a FRP cylindrical sample are determined for surface charge applied by direct and non-direct corona charging. Flashovers are repeatably produced in the absence of leakage current, in low humidity, and in the absence of contamination.
- The impact of sheds on a clean FRP insulator sample is evaluated along with their optimum location.
- Validation of flashover characteristics for a cylindrical SIR insulator sample as performed in [2].

- Confirmation that the effect of DC space charge needs to be given consideration in existing live-line working standards.

1.4.1 Publications

The outcome of this research have been submitted and accepted as conference papers. One paper [16] focuses on the surface charging characteristics of FRP hot sticks while the other [17] focuses on the flashover performance of FRP hot sticks considering space charge under DC conditions.

1.5 Thesis Outline

This thesis is divided into six chapters as described below:

Chapter 1: Introduction of the thesis, giving the background, problem definition and existing solution, objectives, and contributions.

Chapter 2: Discussion on the literature review of research completed on surface charging of insulators under DC conditions, streamer propagation in air and along surfaces and flashover characteristics of insulators under DC voltage. This chapter also discusses surface measurement techniques and details on the vibrating Kelvin probe.

Chapter 3: Discussion on the experimental setup and methodology used for the surface charging characteristics and DC flashover tests for all insulator samples. A discussion on the computer simulation technique used to develop the probe response matrix required for converting the measured surface potential distribution to a charge density distribution is provided.

Chapter 4: Discussion on results of the DC charging characteristics study using the direct and non-direct surface charging methods and the DC flashover investigation. Mitigation methods are discussed.

Chapter 5: Conclusion of this thesis, with a discussion on future work.

Chapter 2

Literature Review

This chapter of the thesis summarizes research completed on the effects of DC space charge on insulators samples. Firstly the literature on surface charging characteristics of insulators under DC voltage is summarized. Streamer propagation research is then discussed which includes positive and negative streamers and ice surfaces. The literature on flashover of insulators under DC voltage is then reviewed which includes the fast flashover phenomenon. The effects of DC space charge on cylindrical FRP samples is not yet fully understood or characterized.

2.1 Surface Charging on Insulators under DC Voltage

Kumara *et al.* investigated the characteristics of charge distribution on a cylindrical insulator composed of a silicone rubber layer (SIR) over a fiberglass reinforced epoxy resin core [12]. The sample was charged using a corona ring of needles and by pre-stressing from an electrode. It was shown, in the case of a corona ring of needles, that charging by negative voltage results in a slightly higher surface potential than charging by positive voltage. It was also observed that under certain conditions a bell shaped surface potential was measured while under charging scenarios back discharges were observed as seen in Figure 2.1. Back discharges appear to occur when the voltage source is turned off and grounded as the

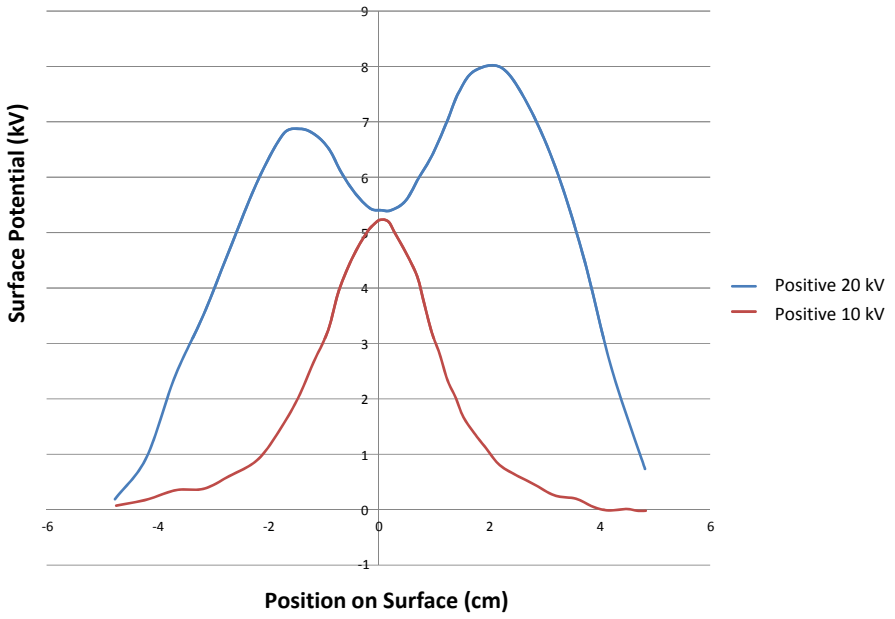

Fig. 2.1: Surface potential on the surface of a SIR cylindrical insulator showing the bell curve and a back discharge for different charging conditions [12].

charge on the surface discharges back to the needles if the electric field strength is approximately 30 kV/cm, which is the ionization threshold. Back discharges are discussed further in Section 4.1.2.5. Under positive charging using the ring of needles, a charging voltage above 10 kV did not result in a noticeable change of potential at the center of sample where as for negative charging, there was an increase in potential, for all charging voltages, along the sample at all locations. In areas close to the electrodes hetero-charges (charges of the opposite polarity to the charging voltage) are found.

It was also discovered in [12] that the net charge on the surface of the samples was higher for negative charging than positive charging. The amount of charge was shown to increase linearly with charging voltage for positive and negative charging. Higher charging voltages displayed that charge was spread further away from the center as well. As reported in [12]

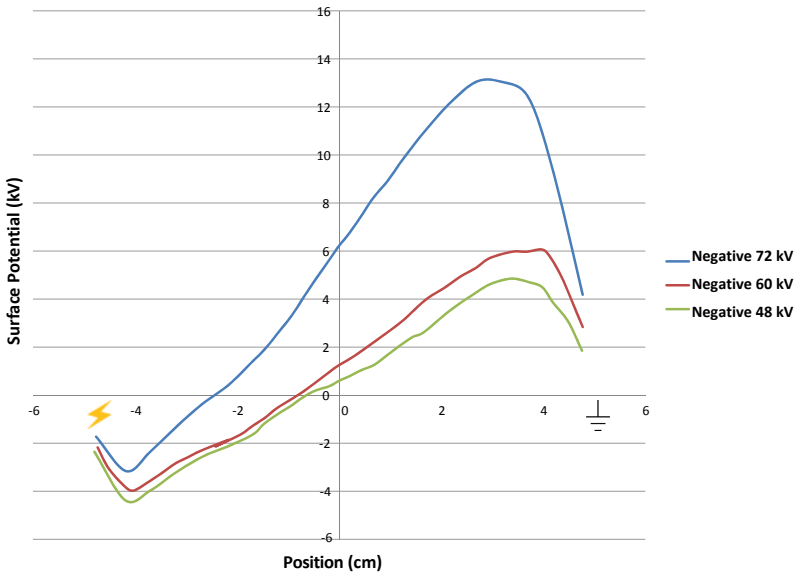

Fig. 2.2: Surface potential on the surface of a SIR cylindrical insulator after pre-stressing with negative voltage [12]. (-5 cm is energized electrode, +5 cm is grounded electrode)

the charging time using the ring of needles did not have a sizable effect on the resultant charging time when 1, 2 or 3 minutes was utilized. When moving the location of the ring of needles to the left or right of the center, symmetry is found for the same locations (*i.e.* $\pm$ 2.5 cm) on either side.

When the pre-stressing method was used to deposit charge on the surface of the insulator in [12], with one electrode grounded and the other energized with negative voltage, a positive charge was produced on the majority of the surface of the insulator as seen in Figure 2.2. Large hetero-charges (charges of the opposite polarity of the charging voltage) exist near the grounded electrode while homo-charges (charges of the same polarity of the charging voltage) exist near the energized electrode. Higher pre-stressing voltages did not significantly increase the amount of surface charge at the energized electrode while there was a noticeable increase at the grounded side especially at 72 kV.

Research in [18] for flat PTFE (polytetrafluoroethylene) insulators showed that negative charges accumulate more easily on insulator surfaces than positive charge. It was concluded that in high humidity, surface charge decays faster than in low humidity. Also it was found that about 65% of the total charge on the insulator surface was accumulated in the first 2 minutes as compared to 200 minutes.

Yamano *et al.* [19] studied the surface charging characteristics of a flat dielectric sample in a vacuum chamber where a triple junction was used to broadcast the charge. It was determined that when charging with negative DC voltage, a larger magnitude of charge is distributed on the surface than when charging with positive DC voltage. In the case of a negative DC voltage, the charge is more widely distributed over the surface as compared to a positive DC voltage where the charge distribution is steeper and more localized. This speaks again of the higher mobility of electrons versus positive ions. Similar observations were made in [20] for flat silicone samples. It was noted that the spread of negative charge is over a wider area than positive charge which stays in a much more concentrated area near the high voltage electrode.

2.1.1 Decay of Surface Charge

Kumara *et al.* [21] studied surface charge decay on polymeric flat materials. It was determined that positive impulse corona resulted in a higher surface charge and a larger area of charge than in the case of negative corona. Locations with higher potentials had a faster decay of potential. No significant differences were found if positive or negative charge existed on the surface and the associated decay rate, of surface charge, for either polarity. However, the difference in decay rates of surface charge for different materials is found to be significant.

In [22], the charging characteristics of flat EDPM (ethylene propylene diene monomer) and SIR was investigated. It was determined that under positive impulse voltage, a larger

amount of accumulated charge was deposited. It was shown that positive or negative charges do not decay at different rates. The decay rate of different materials was also found to be significantly dissimilar.

In [23] it was discovered that positive charge decays faster than negative charge, for room temperature vulcanized (RTV) silicone rubber (SIR) although the difference is not considerable. When the SIR was treated by direct fluorination, the decay rate of positive and negative surface charge was found to increase and the accumulation of charge was found to decrease.

It was shown in [13] for surface decay studies that surface charge on epoxy resin does decay considerably slower than SIR. FRP insulators are composed of an epoxy resin as well and reinforced with fibreglass.

2.2 Streamer Propagation

Streamer propagation was first studied mainly in air and later research initiated on the effect of insulator surfaces on the propagation of streamers. Streamers can be thought of as a transient electrical discharge. Research on streamer propagation mainly focuses on positive streamers as they tend to propagate under lower electric field strengths and are thus much more common. The majority of the work on streamer propagation dates back to the 1990's. DC surface charge and flashover characteristics research tended to focus on flat samples while streamer propagation investigations focused on cylindrical insulators. The following review is presented in chronological order from the oldest to newest research on this topic.

Allen and Ghaffar in [24] studied the conditions required for a positive streamer in air. The minimum electric field that is required for propagation was discovered of 440 kV/m. It was shown that the velocity of streamers increases linearly with the electric field strength.

Allen and Ghaffar in [25] studied the impact of cylindrical insulator surfaces on the

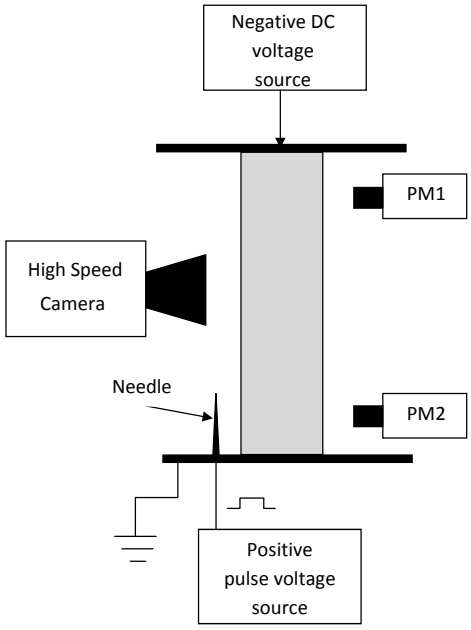

Fig. 2.3: Typical setup for streamer propagation investigations in literature [24–36]. The setup includes a negative DC voltage source, photomultipliers, two electrodes, a cylindrical insulator sample, a needle which is pulsed by a positive pulse to generate positive streamers, and a high speed camera.

propagation of positive streamers. Much of the work on streamer propagation carries commonalities in that photomultipliers are used to measure the velocities of streamers from one end of the sample to the other. Photomultipliers are able to detect the light emitted due to streamer propagation and are used to measure the speed of the streamers by using multiple photomultipliers along the sample. High speed cameras are used to capture images of streamers. One electrode is energized with a negative constant DC voltage while the other ground electrode will have a sharp point or needle which is pulsed with a positive pulse of voltage to start a positive streamer. A typical is setup is shown in Figure 2.3.

The work in [25] demonstrated that the minimum electric fields for propagation along insulator surfaces are elevated as compared to air only by studying cylindrical insulators of

glazed ceramic, PTFE and silicone rubber. At the same time, the streamer velocity (the speed at which the streamer propagates) is higher along insulator surfaces than through air. Distinct air and surface components of streamers were discovered where the air component was described as slow and the surface component was described as fast. This concept was further discussed by Allen and Mikropoulos [26] where it was shown that the stable propagation of a streamer is dependent on a propagation field(electric field required for streamer propagation) and a streamer velocity which are related to the dielectric properties of the insulator. Both the propagation field and the velocity are larger for a surface than for propagation in air alone. When an electric field is higher than that required for stable streamer propagation and a pulse is given, a streamer will propagate with a surface component that is faster than the speed of a streamer in air with no insulator. With an insulator surface present, the air component of the streamer has a velocity slower than in air alone.

Serdyuk *et al.* [37] studied the propagation of positive streamers in a weak and uniform background electric field. Two electrodes were separated by air. A needle was located at one of the electrodes to trigger streamers. The distance between the electrodes was 33 mm. It was determined that at a field strength of 500 kV/m, one could create stable propagation of a streamer which had a constant velocity. The streamers could however cross the 33 mm distance in field strengths as low as 300 kV/m.

Positive streamers are investigated along a silicone rubber surface by Akyuz *et al.* [27]. Again, it was determined that the voltage and electric field required for a streamer to cross with stable constant velocity are both increased in the presence of an insulator as compared to air. It is discussed that when a streamer travels through air the positive charge tends to be located mainly in the front head of the channel however when a surface is present the positive charge spreads along the streamer channel as it interacts with the surface of the insulator.

Allen *et al.* [28] used their same setup as previous work [24–26] for streamer propaga-

tion studies except they investigated the impact of a shed on a cylindrical rubber silicone insulator. The distance to be traveled by streamers between the electrodes in the study was 12 cm. The shed was shown to cause a loss of energy about $\frac{1}{3}$ of what is required for streamers to cross the gap. The shed was shown to increase the electric field required for streamer propagation to higher levels than those required to produce flashovers in air or along smooth SIR surfaces. Three factors are suggested that may impact why insulating surfaces cause a faster velocity for the propagation of streamers. These are suggested as the relative permittivity of the material, photoemission of electrons from the surface insulator, and attachment and detachment of electrons on the surface. Electric field stresses of 700 kV/m are noted as very likely to cause flashover across the gap and a shed will raise the electric field stress required for this to occur.

Further work with sheds is carried out in [29] and [30] where the authors studied cylindrical insulator surfaces again with a similar setup as that used in [24–28]. Previous observations were confirmed such as streamers propagate at higher electric field along surfaces than air alone. If the needle, where positive streamers are generated from, corona source is displaced away from the surface horizontally, the effect of the sheds and surface, lessens as the streamer travels in air and not on the surface. The insulator with a single shed weakens the strength of the gap compared to an air gap but strengthens the air gap compared to only a smooth insulator surface. The shed is shown to be more effective when placed closer to the high voltage electrode which in this experimentation is where the positive streamer propagates from. It is suggested that the permittivity of the insulator has an effect on the performance of the shed. The higher the permittivity of the material, the more effective the shed is in blocking the progression of the positive streamer. Photographic evidence displays that there is still considerable positive streamer propagation through the air around the shed to the ground electrode. The first shed is shown to be the most crucial and the second shed does not significantly increase the electric field strength required for

breakdown. In [29] the higher permittivity of porcelain vs PTFE is suggested as the reason PTFE has a higher flashover voltage.

Mikropoulos [31] investigated positive streamer propagation on cylindrical insulators covered in room temperature vulcanized (RTV) silicone rubber coatings and compared to bare nylon insulators. It was established that RTV silicone insulators increase the required electric field for streamer propagation and increase the velocity of stable propagation as compared to nylon alone. Changes in the coating chemistry led to differences in the properties of streamers, again reinforcing that material types can influence the flashover voltage. RTV silicone coatings have been proven to improve insulator flashover performance under various conditions including ice [38].

Mikropoulos went on to further study the influence of humidity on positive streamer propagation and flashover voltage [32]. Higher stable propagation electric fields are required for streamer propagation under high humidity. The velocity of stable streamer propagation also increases with humidity. The electric field required for flashover increases with humidity as well. Interestingly, the time to breakdown of air decreases with higher electric fields and humidity. In [33], it is suggested that as humidity is increased the conductivity of the streamer channel is lowered thus higher electric fields are required for stable streamer propagation.

Recently, work was carried out on the characteristics of streamer propagation along different insulator surfaces to determine the influence of the material by Meng et al. [35]. Six different dielectric materials were studied and the same setup was used with photomultipliers, high speed cameras, and a pulsed needle which dates back to the work of Allen in the early 1990's [24–26]. It is observed that the electric field required for streamer propagation in air is less than along an insulator surface. It is reconfirmed that materials with higher permittivities require higher electric fields for streamers to propagate. The work of Allen [39] was validated as Meng *et al.* found only one peak of light when the streamer

propagated in air alone but two peaks of light were observed when the streamer propagated along the insulator surface. Also from the photographs that were taken, a fast and a slow component can be seen when an insulator surface is present. The fast component is shown to be dependent on the dielectric material type while the slow component is not significantly different for the different materials. It is demonstrated that the velocity of the fast surface streamers is inversely proportional to the dielectric permittivity.

Meng *et al.* carried out further investigation on the influence of permittivity and surface properties in [34]. The amount of charge deposited on the insulator surface increases with permittivity. Negative charges accumulated on the insulator surface before streamer propagation reduces the electric field. Higher electric fields are required for positive streamer propagation along dielectric material with higher permittivity due to the negative charge on the surface. Under identical electric fields, the streamer propagation velocity and permittivity are inversely related. When the permittivity of a material is increased, more charge accumulates on the surface, which means that more charge in a positive streamer will attach to the surface with a larger permittivity. This will weaken the streamer and thus the streamers require a higher electric field for propagation. Nylon was found to be most favourable for streamer propagation followed by PTFE and silicone rubber.

The effects of sheds and their configuration were researched further by Meng *et al.* [36]. The first shed, closer to where the positive streamer starts has primary influence. Other sheds didn't have a significant influence. The shed causes the fast component on the surface to be cut off. The slow component through the air still can bypass the shed and reach the cathode. The electric field required for streamer propagation is required to be larger with a shed. The velocity of slow components along insulators with shed are higher than along insulators without sheds. The electric field required for streamer stable streamer propagation was directly proportional to the diameter of the shed, and the velocity of the slow component were shown to be inversely proportional to the shed diameter. Sheds are

discussed to cause an energy loss of the streamer. There is a decrease in the electric field strength at the shed, an increase in the length of propagation path for the streamers over the shed, and streamer charges will attach and interact with the shed which cause energy losses to the streamer.

2.2.1 Positive and Negative Streamers

Streamer propagation studies mainly focus on positive streamers as discussed in the previous section. Interestingly, flashover incidents in industry all are occurring at the negative peak of the AC waveform and seem to indicate a positive streamer was initiated from the ground side to the negative source side.

Luque *et al.* [40] showed that at high electric fields, positive and negative streamers have similar behaviour, however at lower electric fields positive streamers are produced at lower strengths than negative. They move with a higher velocity, and are longer in length and the radius of the streamers is smaller. Electron drift in the case of negative streamers actually leads to the growth of radius of the head of the streamer and leads to weakening of the electric field, a slower streamer, and likely extinction. Positive streamers depend more on the impact ionization and the radius of the streamer stays smaller and results in a stronger electric field and faster moving streamer.

Briels *et al.* [41] used a voltage pulse through a needle to grounded plane in air across a 40 mm gap to study the differences between positive and negative streamers. At voltages from 5 to 40 kV, only positive streamers propagated. A negative glow discharge is only visible above 20 kV and there are no negative streamers and no branching. The positive streamers branch easily at low applied voltages. Negative streamers only form at voltages greater than 40 kV but do not cross the air gap until a voltage of 56 kV. The negative streamers travel at a speed less than positive streamers.

Research shows that stable propagation of positive streamers can occur in an electric

field of approximately 5 kV/cm and at 10 kV/cm for negative streamers [42]. Due to the high electric field in the head of a positive streamer, the size of the positive streamer head tends to be smaller than a negative streamer. Negative streamers have a much larger radius of their heads which can be up to 12 times large than a positive streamer. Positive streamers have higher electric fields and are much narrower. Negative streamers can not propagate at as low an electric field due to the large radius of the streamer head and more difficulty with streamer branching. Negative streamers have weaker electric fields in the head compared to positive streamers thus require stronger electric fields in the channel to propagate.

2.2.2 Ice Surface

Ghassemi *et al.* carried out various studies [6,43–46] researching the incidents that occurred on Manitoba's 500 kV AC line and a Saskatchewan 230 kV AC line. The role of light pollution combined with a layer of ice are considered as all accidents occurred in below freezing weather. All accidents also occurred at the negative peak of wave.

Research has shown that in the presence of ice and salt contamination, negative streamers have a higher streamer propagation velocity and positive streamers propagate slower [47]. Breakdown voltages and time to breakdown, under negative polarity, are still higher than for positive polarity. Under light contamination, with an ESDD (equivalent to salt deposit density) of 2.5 μS/cm, the streamer inception voltage is lower for negative polarity than for positive. At higher contamination levels of 80 μS/cm the positive polarity inception voltage tended to be lower.

Investigation in [48] showed that while streamers can propagate in air alone at approximately 5 kV/cm, lower electric fields were able to produce stable streamer propagation with ice on the surface of an insulator. Under a lower contamination of 2.5 μS/cm, the effect of temperature was more significant. Both increasing surface conductivity and increasing temperature, lower the required electric field for stable streamer propagation.

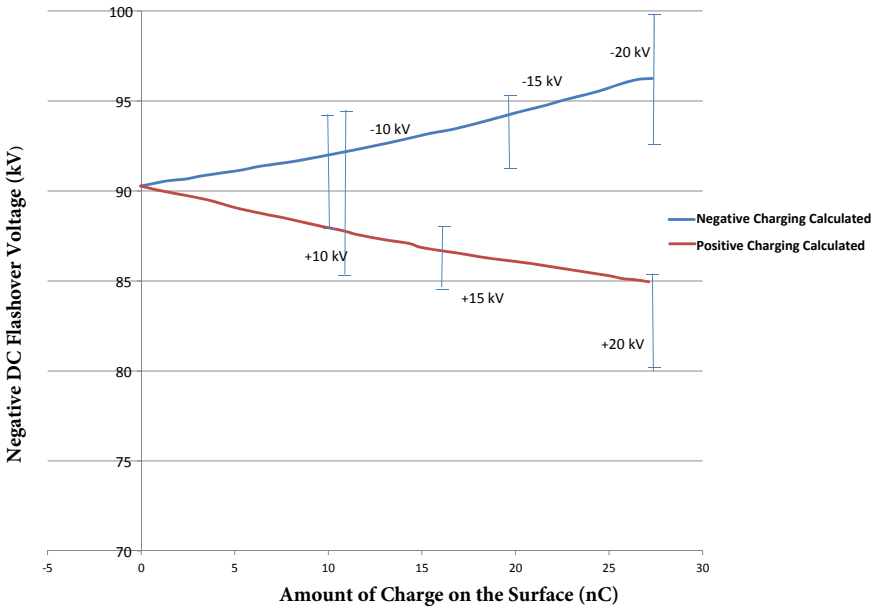

Fig. 2.4: Negative DC flashover voltage, experimental (error bars) and calculated, with positive and negative charge on the surface [2].

2.3 Flashover of Insulators under DC Voltage

The research on the impact of surface charge on flashovers has mainly focused on impulse voltages and non-FRP flat materials. Darveniza *et al.* [49] determined that surface charges had an influence on the impulse flashover voltage for polymer insulators. An increase in flashover strength was noted in their experiments.

Kumara *et al.* [2] studied the effect of surface charges on the negative DC flashover voltages of a cylindrical SIR insulator, both experimentally and theoretically. This paper is a continuation of the work in [12]. It was determined through experimentation and theoretical finite element simulation that for a negative DC flashover voltage, positive charges decreased the flashover voltage, where as negative charge increased the flashover voltage. The results of the work can be found in Figure 2.4

In [50], the results of an experimental study completed in [51] are discussed. The ex-

Table 2.1: Experimental CFO flashover voltages as reported in [51] and discussed in [50].

Voltage Polarity	Charge Polarity	Experimental CFO (kV)
Positive	None	58.9
Positive	Positive	56.1
Positive	Negative	63.8
Negative	None	-57.9
Negative	Positive	-55.9
Negative	Negative	-60.2

perimental study focused on flat samples of EPDM and SIR with electrodes made of half cylindrical brass rods on either side. The experiments, using impulse voltages, revealed that the positive flashover voltage for a sample with no charge is slightly higher than when a negative polarity voltage is applied. When positive charge is present on the surface, both the positive and negative flashover voltages decrease. When negative charge is applied to the surface the flashover voltage for positive and negative polarity both increase. The lowest flashover voltage is experienced with positive charge located on the surface and negative voltage is applied until flashover (Table 2.1). The results in [51] agree with the flashover voltages and conditions presented in [2], as the results correlate for negative flashover voltage, with positive and negative surface charge on a cylindrical SIR sample.

In [52], lightning impulse tests are carried out on a 15 kV HDPE insulator. Under all test conditions that were applied to the insulator, a 50 % flashover voltage (CFO) that was higher for negative polarity than positive polarity resulted. This was attributed to the presence of negative charge on the surface for negative flashover voltages which slows the progress of streamers and the presence of a lesser amount of positive charge on the surface in the case of positive flashover.

Computer simulations in [53], on 35 kV post insulators to determine the effect of deposited charges under impulse flashover voltage (IFV) proved that when the insulator is far removed from the ground plane, positive charges decrease the IFV while negative charges

increase the IFV for both polarities of applied impulse voltage. Conversely when the ground plane is closer (*i.e.* touching) the post insulator, the opposite effect is observed, compared to when the ground plane is far away. For positive IFV, positive surface charge increases the IFV, while negative surface charge causes a decrease. For negative IFV, negative surface charge causes a decrease in the IFV and positive charge also causes a slight lowering of the IFV.

Du and Xiao [23] studied the impact of surface charge on the DC flashover voltages of flat Epoxy/BN (boron nitride) Nanocomposites. With no charge on the surface, the negative flashover voltage was shown to be lower than the positive one. With positive charge present on the surface, the flashover voltage was shown to be the lowest for a positive applied voltage. When negative charge was present on the surface, the negative flashover voltage was shown to be the lowest for a 2 cm gap. Charge accumulation is noted as being the main driver behind decreased flashover voltages.

In a recent paper [54] it is shown that for air gap flashovers without the presence of an insulator, needle and rod type flashovers occur at lower voltages under positive polarity than negative polarity. For a sphere gap flashover, the voltages are more similar with negative polarity flashovers actually occurring at a slightly lower flashover level. When a flat PMMA (polymethyl methacrylate) insulator sample is introduced, the positive polarity flashovers are much higher than negative polarity flashovers. Flashover voltages were higher with an insulator present versus an air gap only.

In [55], the effect of surface charge under AC and DC applied voltage is studied for a disc insulator in SF_6. It was determined that with increased charges the AC or DC flashover voltage would decrease but under DC voltage the largest decrease would be seen with a 23% decrease vs 10% for AC.

2.3.1 Fast Flashovers

Manitoba Hydro experienced two flashovers in 1997 and 2002 at 550 kV AC [3] which were determined to be due to light pollution. Since Manitoba Hydro also has 500 kV DC HVDC lines, additional tests were carried out to study direct voltage. During this test a "fast flashover" phenomenon was discovered. Fast flashovers occurred at voltages less than the system operating voltage, lower humidities than pollution type (as low as 67%), negative DC polarity, clean FRP tools and aerial booms, and at leakage currents less than 2 mA(detection limit of the monitoring equipment at IREQ). In more recent testing on a 3 m hot stick a fast flashover occured at a relative humidity of 53% [5]. Fast flashovers were found to occur both for 32 mm diameter FRP hot sticks of 3.0 m length and a 44 cm diameter 4.72 m aerial device boom. Fast flashovers were completely mitigated by the use of 2 polymer sheds on the FRP hot sticks and only one shed had a considerable impact in raising the flashover voltage. Fast flashovers are of particular significance for aerial device booms and ladders as normally the leakage current is monitored during live-line work but if no prior current is noticed, workers are particularly vulnerable to fast flashovers.

Fast flashovers are repeatably produced on FRP hot sticks by McDermid, in [4] . It is suggested that the high voltage electrode under negative DC polarity produces a negative space charge which leads to a positive streamer from the ground electrode. A large double toroid electrode at the ground end wrapped with metal fabric (Figure 4.24) was used to increase the flash over voltage from below system operating voltages to greater than 600 kV. The thin wire acts to increase the corona inception field and suppresses positive streamers [56]. Although this may not be practical to apply to hot sticks, it may be effective to prevent fast flashovers on aerial devices.

In this chapter, the existing literature on surface charging of insulators, streamer propagation, and flashover of insulators under DC conditions is summarized. An understanding is gained on the behavior of surface charge, streamer propagation, and how surface charge

impacts the DC flashover voltage for various insulating material types. As discussed in 1.2 the surface charging characteristics of FRP samples could not be successfully investigated in existing research and the fast flashovers were not successfully produced at the Manitoba Hydro high voltage laboratory.

The following chapter will summarize the experimental setup and methodology for characterizing the surface charging and DC flashover voltage characteristics for an FRP sample.

Chapter 3

Experimental Setup and Methodology

This chapter of the thesis discusses the experimental setup and methodology used for studying the DC surface charging and flashover characteristics of FRP insulator samples.

3.1 Surface Charging Characteristics

3.1.1 Experimental Setup

FRP, SIR, and wood insulator samples were used in the experiments. The samples were all 13 cm long. Details of each sample are shown in Table 3.1.

The larger FRP sample is from a strain type tool (*i.e.* used to change insulators) while the smaller is from a universal hot stick tool (*i.e.* used by lineman with various tools at

Table 3.1: Details of insulators samples used for surface charging characteristic experiments.

Insulator Type	Outer material	Core Material	Total Diameter	Outer Material Thickness
FRP large	fibre glass reinforced epoxy resin	hollow/foam filled	3.81 cm	3.6 mm
FRP small	fibre glass reinforced epoxy resin	hollow/foam filled	3.2 cm	3.0 mm
SIR large	silicone rubber	fibre glass reinforced epoxy resin	4.3 cm	3.5 mm
SIR small	silicone rubber	fibre glass reinforced epoxy resin	3.0 cm	3.0 mm
Wood	varnished wood	solid wood	3.2 cm	NA

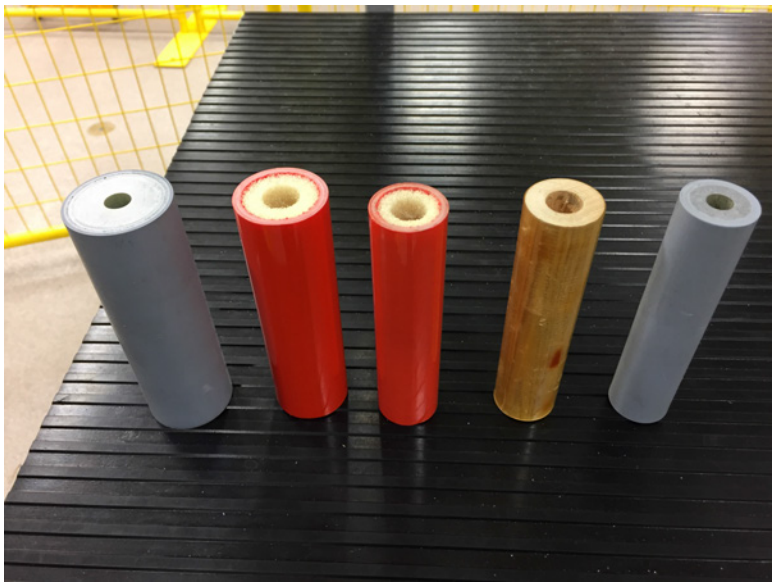

Fig. 3.1: Samples, of 13 cm length, used in surface charging experiments, from left to right: Silicone Rubber (SIR) large, Fiberglass Reinforced Plastic(FRP) large, FRP small, Wood, SIR small.

the end). The silicone samples are from silicone covered FRP rods for use as a modular system of suspension type insulators. The wood sample is from a vintage 1950's hot stick tool. The relative permittivity (dielectric constant) of the FRP, the silicone rubber, and the wood sample insulators (surface) were assumed to be 4.0, 3.5 [12], and 2.6 in dry conditions respectively. The relative permittivity of wood, however, can range from 1.4 to 2.9 [57]. It should be noted that for the FRP tools some have assumed permittivities as high as 5.0 [43]. In Figure 3.1 a picture of the samples used is shown.

The effective length of each sample is 11 cm, as 1 cm on each side is inserted into the grooves of two metallic, smoothed, round electrodes mounted on a wooden setup. The work of Kumara *et al.* [12] on SIR materials was used as a benchmark for this investigation of FRP tools and thus a similar length was chosen for our samples. Figure 3.2 shows the experimental equipment used for measuring surface potential distributions. Two 150

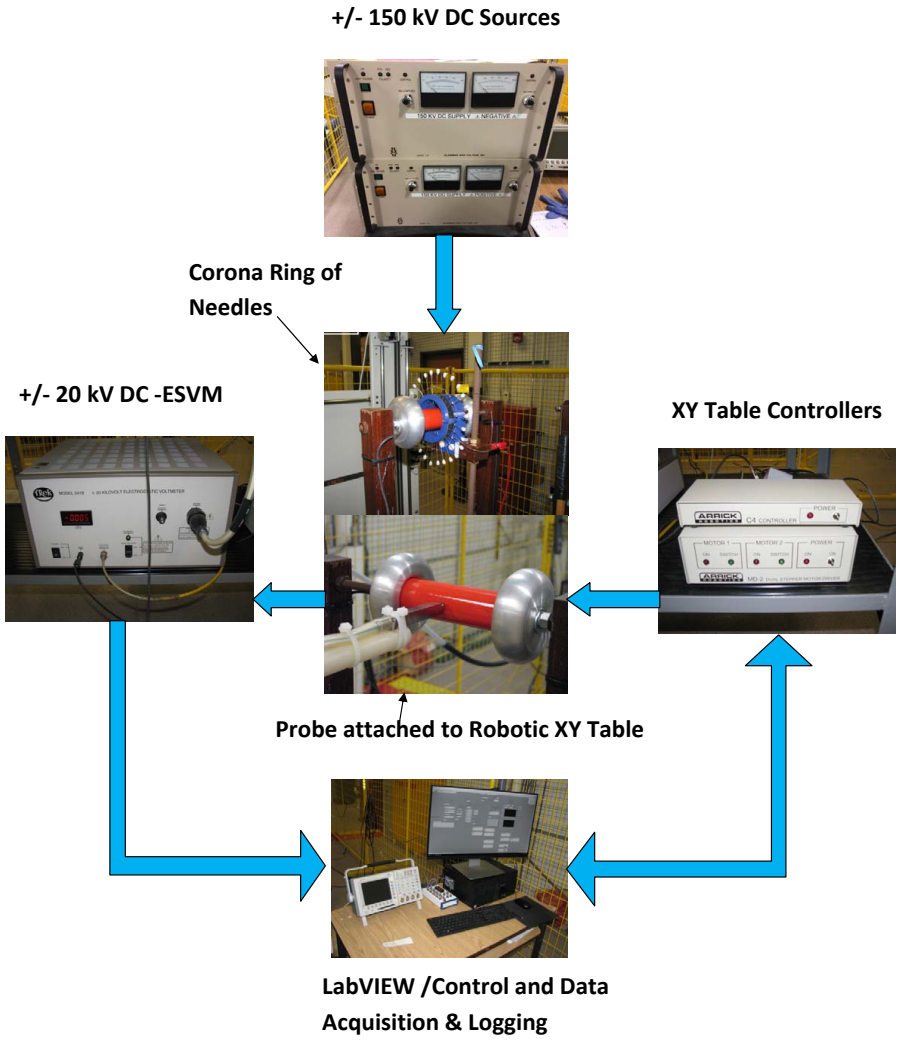

Fig. 3.2: Experimental setup for surface charging characteristics. The DC sources supply voltage to the corona ring of needles or the pre-stressing electrode. The potential along the surface of the insulator sample is measured by the vibrating Kelvin probe connected to the DC-ESVM. The measured potential at each location is recorded by the data acquisition and logging equipment. The location of the probe is controlled by the XY table controllers using LabVIEW.

kV, 12 mA Glassman (Model LX150P12 for positive polarity and LX150N12 for negative polarity) HVDC sources are used separately for positive and negative energization. A ±20 kV electrostatic voltmeter, Trek model 341B, is used for surface potential measurement through a vibrating Kelvin probe (Trek Model 3455ET). For high accuracy, the probe-to-surface distance is kept at 2 mm during surface potential measurements. The positioning of the probe is achieved by using an XY table, Arrick Robotics XY30, traveling in two directions. A LabVIEW program is used for controlling the positioning system, collecting, and recording the experimental data through a data acquisition card. The potential from the DC-ESVM was provided to the DAQ unit and scaled by 1000. The positioning was provided to the DAQ unit from the Arrick Robotics controllers as a digital signal. The potential and digital signal were interfaced to the computer and LabVIEW via a National Instruments BNC-2110 which could accept BNC cables and digital signals.

LabVIEW software was used to create a virtual instrument with 3 different loops. One loop was for the movement and control of the probe location. The probe is moved to its initial position and stepped in 0.5 cm increments. The measurement is delayed for 1 second after the movement, due to vibrations of Kelvin probe after each movement. The probe is held for one second for the measurement of the potential. After the measurement is complete the probe is moved to a safe position away from the high voltage source. The second loop was for the position of the probe. The position of probe was determined by starting at an initial position and incrementing the position by sending a digital signal to LabVIEW from the motor controls after every move. The last loop was for recording the potential and position of the probe at each location to an Excel file for plotting and data analysis in MATLAB. The recorded potential is the average of 10 samples per second of the DC RMS average of the ESVM voltage signal. The ESVM BNC voltage monitor output is a modulated signal (due to the Kelvin probe being sinusoidally modulated) where the DC RMS average of the signal is the surface potential. Using this method we were able to

exactly match the LabVIEW calculated potential with that displayed digitally on the front of the ESVM.

3.1.2 Methodology Used for Surface Charging

Three different charging methods were employed to study surface charge characteristics of the insulator samples. The first method was to induce space charges in the surrounding air through a non-contact corona discharge source, referred to as a corona ring of needles. The ring of needles consists of a 3D printed polyethylene frame on which 27 connected needles are mounted. The 6.4 cm long needles are distributed around the frame periphery with 1 cm spacing between two adjacent needle tips. The needles are symmetrically distributed around the sample surface and the separation distance between the needle tips and the sample's surface is maintained at 5 mm during charging (see Figure 3.3). The ring of needles is energized with both polarities of different DC voltages ranging from 7 kV up to 20 kV, while the two electrodes are kept grounded as per Figure 3.4. The ring of needles was hinged such that it could easily be opened for installation and removal. The ring of needles is displayed in Figure 3.5 in both a closed and open configuration. The results of the experiments are presented in Section 4.1.2.

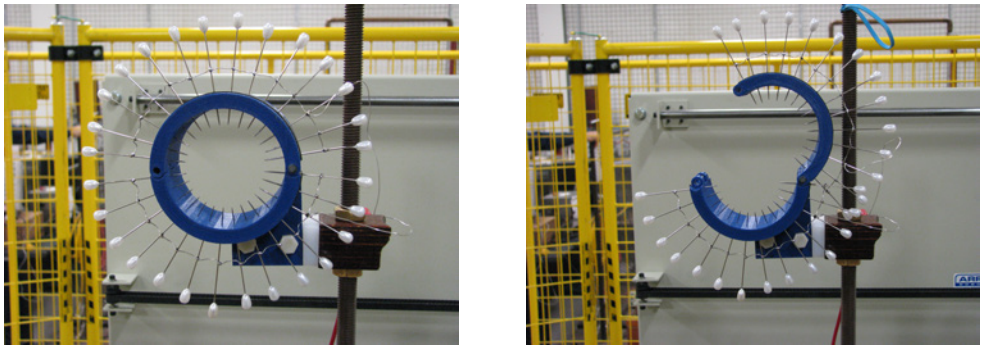

(a) Ring of needles closed **(b)** Ring of needles open

Fig. 3.5: Corona ring of needles used for applying non-contact space charge.

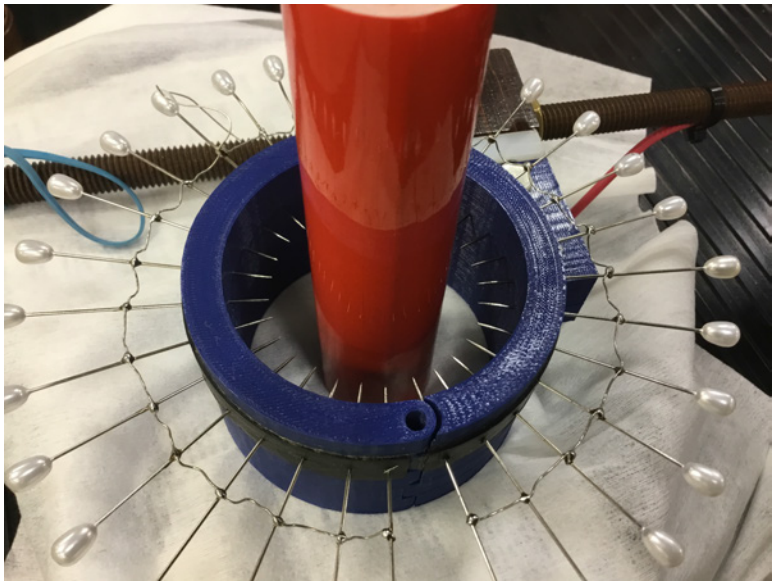

Fig. 3.3: Closeup view of corona ring of needles.

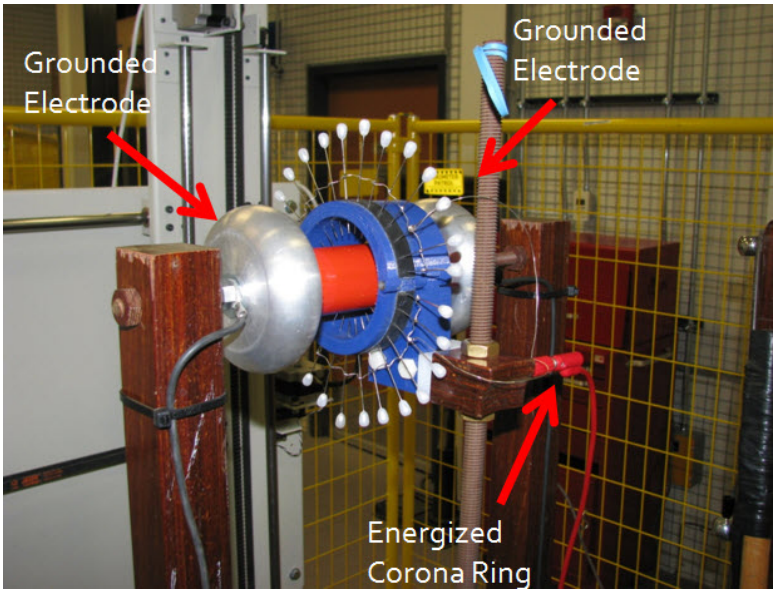

Fig. 3.4: Corona ring of needles with both electrodes grounded.

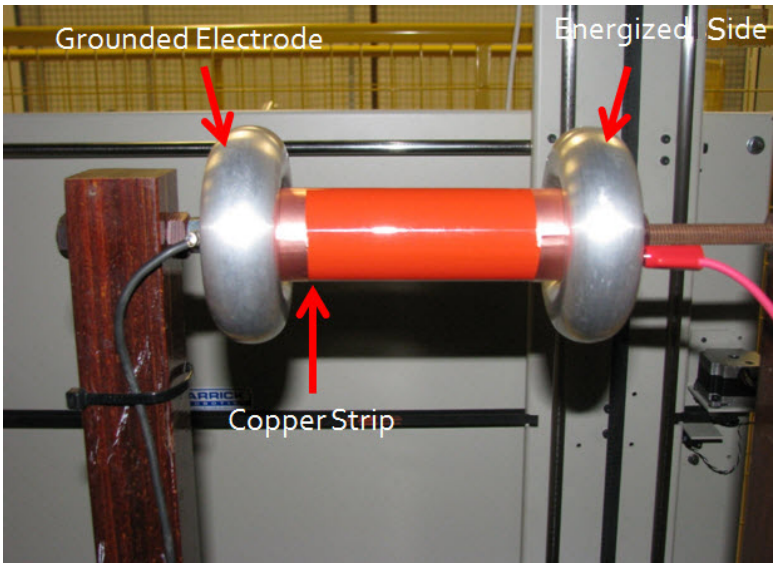

Fig. 3.6: Pre-stressing from one electrode with the other electrode grounded and use of copper strips.

The second charging method is to create space charges along the sample surface through direct contact between the sample and the DC voltage source, which is known as pre-stressing [12]. Pre-stressing is achieved by energizing one of the electrodes with a DC voltage, while the other electrode is kept grounded. Charging the FRP surface by corona discharge, from energized nearby objects or from direct contact with energized objects, allows for controlling charge deposition on the FRP surface [16]. Our original electrodes were too large and corona free to produce significant space charges. Copper strips were introduced to create triple point junctions between air, the insulator, and the electrodes. Tests were carried out without copper strips, with copper strips at both ends, and with copper only at the ground or energized side. The results of the experiments are presented in Section 4.1.3.

The third charging method allows for uncontrolled charging, by wiping the insulator surface, which produces space charges by friction action. Wiping FRP hot sticks, using cot-

ton and/or silicon wiping clothes, is a daily routine done before live-line maintenance work, to be sure that the surface is contaminant free and has excellent hydrophobic properties. This was found to induce significant charge on the FRP sample, as presented in Section 4.1.4.

3.1.3 Experimental Procedure

All samples must be free of surface charges before running the experiments. This can be achieved through removing any deposited residual charges by wrapping the sample with a wetted (tap water) piece of cloth for 2 minutes, then cleaning the surface with isopropyl alcohol. Extra care is given to not rub the surface as the friction from wiping can cause significant surface charge, therefore the surface is rinsed and the dabbed lightly. The insulator surface was scanned prior to tests to ensure there was no significant charge on the surface. The ring of needles is mounted symmetrically around the sample at the desired location, then the needles are energized with different values of both polarities of DC voltage (7, 10, 15, and 20 kV). The duration of applying any voltage to the needles is 2 minutes. This time is chosen based on an experimental investigation for studying the affect of charging time. It was discovered that more than 80% of the charges are deposited during the first 2 minutes. Next, the voltage source is turned off and grounded and the ring of needles is carefully removed while the probe is brought to the starting measuring point in about 30 to 45 seconds. The scanning span contains 19 measuring points of a 5-mm separation each and takes around 90 sec to complete the measurement.

During the pre-stressing method of depositing charges, the DC voltage is applied to one of the two electrodes for 2 minutes while the other electrode is grounded. The DC source is then turned off and grounded at the energized electrode side. The probe is brought to the starting measuring point in about 40 seconds and the electrostatic voltage measurement as described above is repeated.

The charging by wiping of samples is done in the same way as the live-line maintenance procedure. First, the FRP sample is wiped by using cotton cloth for contamination removal. Then a silicone cloth is used to produce a hydrophobic layer on its surface. Unlike the two other charging methods, there is no need to a voltage source but still the two electrodes are grounded during the wiping as well as during the measurement. After wiping, the probe is brought to its starting point and the measurement starts in about 40 seconds, similar to that described above.

The laboratory conditions were monitored daily during the experiments using a Vaisala HM70 humidity meter. The temperature was constant in the laboratory at approximately 23 °C and the average atmospheric pressure was 99 kPa. The humidity was very low at the beginning of the experiments. In the first half of the experiments, the humidity was between 8% and 23% with an average of 13% while in second half of the experiments, the humidity was in the range of 10% to 28% with an average of 20%. The variation of the humidity and temperature is displayed in Figure 3.7.

3.2 DC Flashover Tests on Insulator Samples

The experimental setup and methodology used to characterize the DC flashover performance, with surface charge, of FRP samples is discussed below.

3.2.1 Experimental Setup

Figures 3.8a and 3.8b shows the schematic of the circuit used for laboratory tests and a photograph of the laboratory setup.

The high voltage sources used for the experimentation were again the 150 kV/12 mA Glassman DC sources which provided both negative and positive polarities. The sample was charged, with positive or negative voltage, using the ring of needles and then negative or positive voltage was applied and raised until flashover. The DC source was protected by

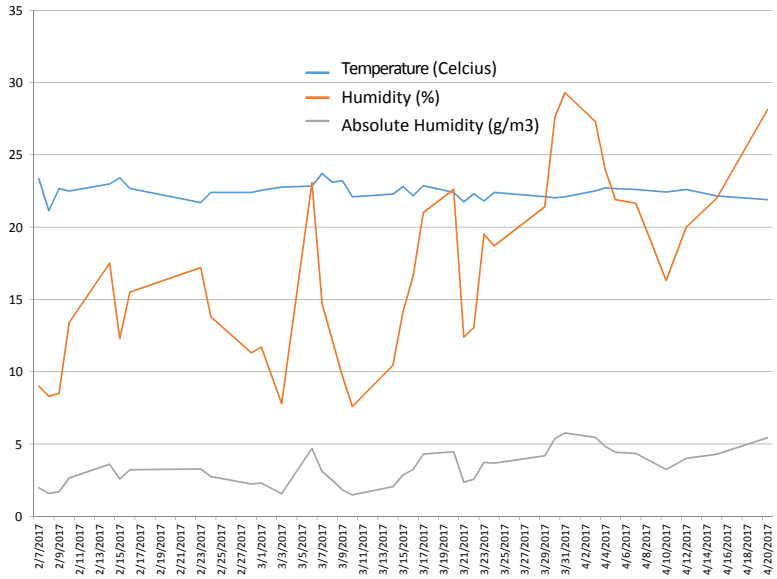

Fig. 3.7: Laboratory environmental conditions during surface charging experiments.

placing a 100-MΩ resistor in series with the source to ensure that the maximum capability of 12 mA was not exceeded during the flashovers. Next, two 100-kV 0.25-μF capacitors were placed in series to the ground. The capacitors were installed in series to allow the voltage to be increased above the single unit rating of 100 kV. The capacitors smoothed the output of the DC sources as we did not have a controller and this allowed us to consistently ramp the DC voltage at a rate of 2-kV/s manually. High Voltage Testing Standards recommend an approximate rate of rise of 2% per second of the withstand voltage [58], [59]. Since the flashover voltage for these experiments is in the order 100 kV, a raise of 2-kV/s is appropriate. A 300-kΩ ohm resistor was then installed in series with the insulator sample to limit the current output of the capacitors and across the insulator sample during flashover. The flashover voltage was monitored by an oscilloscope connected to a 1000:1, Ross Eng. Corp., 225 kV voltage divider. A multimeter was connected in series with the ground side of the insulator sample and ground to monitor leakage current of the insulator. Since

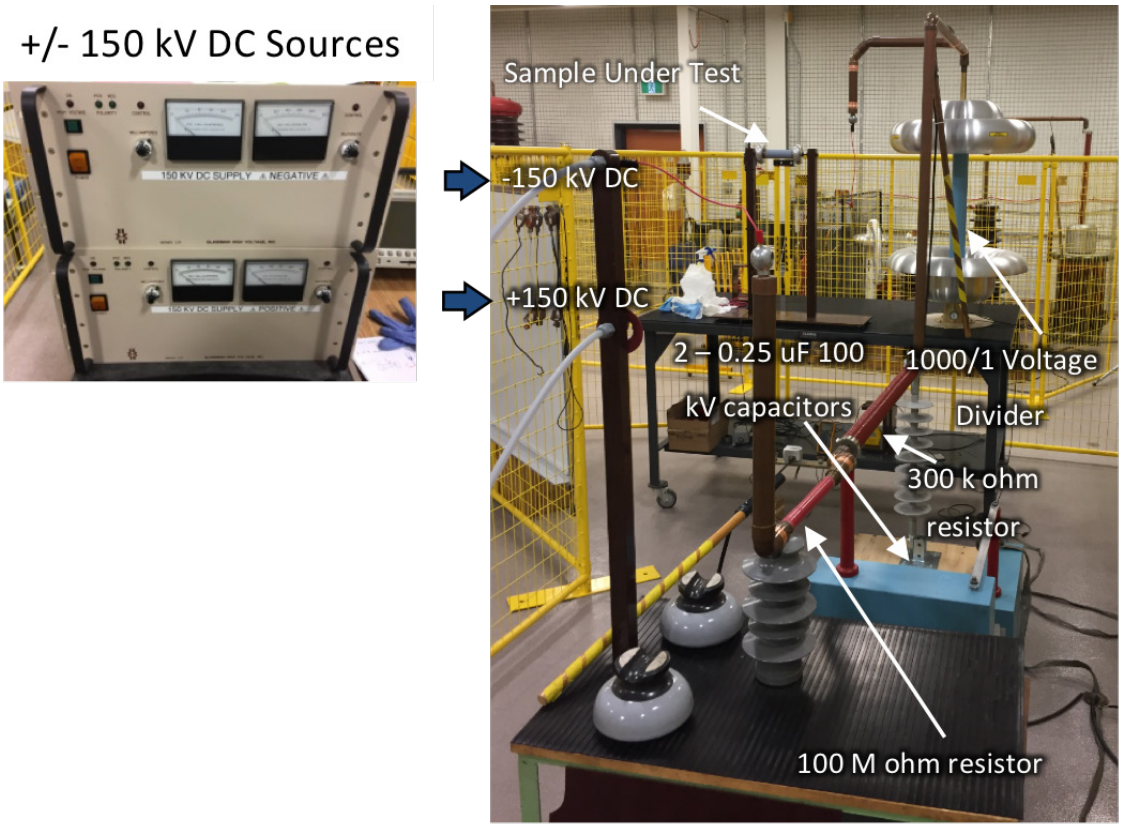

(a) Labratory setup for DC flashover tests of insulator samples

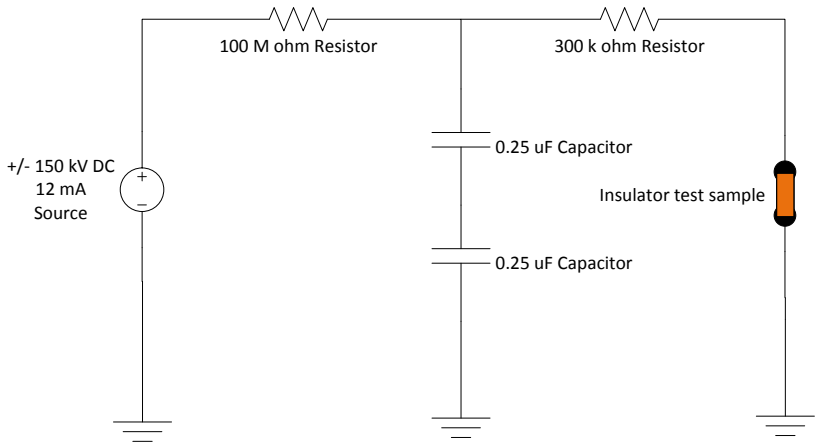

(b) DC flashover circuit diagram

Fig. 3.8: a) DC flashover test equipment and, b) the equivalent circuit

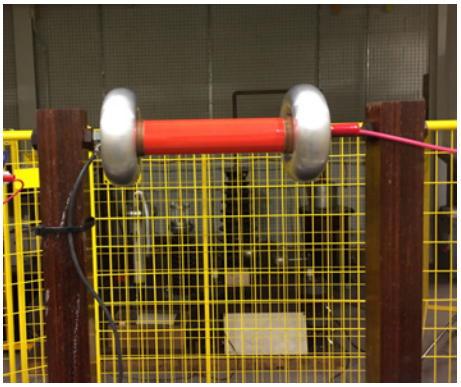

(a) FRP - copper rings

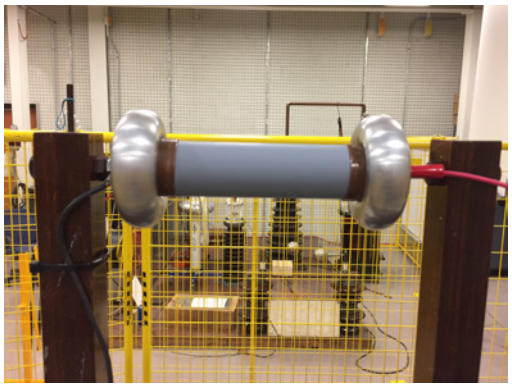

(b) SIR - copper rings

Fig. 3.9: a) FRP and b) SIR insulator samples with copper rings at each end to create triple point junctions.

in the previous testing for pre-stressing, the copper tape strips caused flashovers at lower voltages than desired under positive polarity due to the overlap of tape and the associated imperfection, an improvement was made for the flashover testing. Perfectly uniform and symmetrical copper rings, 15 mm in length, were placed at each end, between the larger, rounded, corona-free aluminum electrodes and the sample to create a triple point junction between air, the insulator surface, and the electrode. This is the most effective method to produce significant surface space charge and was also found to lower the flashover voltages to levels within the specifications of our DC sources. If only the larger round aluminum electrodes were used, flashovers could not be achieved with the high voltage sources. For all flashover tests there was a distance of 13 cm between the edges of the copper rings as displayed in Figure 3.9. Surface charge was induced, with the ring of needles, on the large FRP and SIR sample for the DC flashover testing as in Figure 3.4, and in the case of pre-stressing the small FRP sample was used. Given our effective source capacitance of 0.125-μF and that the flashovers occur at approximately 100 kV, the capacitive source can supply 12.5-mC of charge during the flashover.

3.2.2 Methods of Charging for DC Flashover Tests

As discussed in Section 3.1.2 two different charging methods were applied to produce space charge on the insulator samples prior to raising the DC voltage to flashover. The first method to create space charge was by using a ring of needles. The ring of needles was used to charge the FRP sample with either 20 kV positive or negative voltage with both electrode ends grounded. The second method to create space charge was to pre-stress the FRP sample from one end while the other end was grounded. This would be very similar to real case scenario of a lineman contacting energized apparatus with an FRP tool while they are standing on a grounded structure. The wiping method was attempted but since the laboratory humidity had risen significantly from the time of the previous surface charging tests, it was difficult to create surface charge and relevant flashover results.

3.2.3 Experimental Procedure

Prior to each of the DC flashover tests, the sample was cleaned prior to testing to ensure that the surface is clean, dry and neutralized from any charge as per Section 3.1.3. The most effective method, as mentioned previously, that was found to neutralize charges is to take a damp cloth saturated in tap water and wrap it around the sample for 2 minutes. The FRP sample is then rinsed with isopropyl alcohol to clean the surface and ensure there are no contaminants or conductive residue left behind. The surface is only ever dabbed to remove moisture as rubbing and wiping of the surface can leave behind significant positive charge that could impact the results. In the previous surface charging tests, the surface was always scanned prior to the next test. Since we developed a method that was able to repeatably neutralize charge, to insignificant levels, the insulator surfaces did not need to be scanned for charge prior to flashover tests.

To induce space charges using the ring of needles, the needles were energized by a 20 kV positive or negative voltage for 2 minutes. To do this the flashover circuit was bypassed

and the needles were directly connected to the DC sources as in Section 3.1.3. The ring of needles was then removed from around the sample after charging. Next, the flashover circuit (Figure 3.8a) was ungrounded and the voltage was raised at a rate of approximately 2-kV/s until flashover occurred. The flashover voltage was recorded on an oscilloscope while the leakage current to ground through the sample was monitored at all times on a multimeter. Samples were replaced if any significant changes in leakage current or flashover voltage was observed. Degradation of the FRP samples was experienced after 8-10 flashovers. SIR samples were noted to be able to withstand flashovers better than the FRP samples. No burn marks were evident on the samples after flashovers and more tests could be carried out on each SIR sample before replacement. For pre-stressing the FRP sample, the voltage was raised to 72 kV positive and negative and held for 2 minutes. The same voltage, of either positive or negative polarity, was then ramped at a rate of 2 kV/s until flashover occured. The laboratory conditions at the time of testing were an average temperature of 22.5 °C, 33.4% of relative humidity, and an absolute humidity of 6.6 g/m^3. The average atmospheric pressure was 98 kPa during the period of testing.

The experimental setup and methodology used for the DC surface charging and flashover characteristics have been explained. In the following chapter of the thesis, the experimental results are presented and discussed.

Chapter 4

Results and Discussion

In this chapter the results of testing for the DC surface charging and flashover characteristics are presented and discussed.

4.1 DC Charging Characteristics

In the section of the chapter, the results of the experiments for DC charging characteristics, of the insulator samples, are presented and discussed. The ϕ-matrix method used to convert the measured surface potential to charge density is also presented.

4.1.1 Probe Response Matrix

Since the DC-ESVM only provides a surface potential on the surface of the insulator, a method is required to translate the potential to a surface charge density. To find the surface charge density distribution, it is assumed that the electrostatic voltage on the surface of insulator and the surface charge density are related by [12]:

$$[V]_{n\times 1} = [\phi]_{n\times n}\,[\sigma]_{n\times 1} \tag{4.1}$$

or

$$[\sigma]_{n\times 1} = [\phi]^{-1}_{n\times n}\,[V]_{n\times 1} \tag{4.2}$$

where, σ $[\mu C/m^2]$ is a vector containing the calculated values of surface charge density distribution, V [volts] is a vector containing the measured values of surface potential, and ϕ is the probe response matrix. This method is known as the ϕ-matrix method, presented in [60] and used in [12]. As discussed in [12], since the electrodes, the cylindrical insulator, and the ring of needles all have axial symmetry, the measured surface potentials are also assumed to be rotationally symmetrical on each segment. A finite element method (FEM) based software, (Comsol Multiphysics), solving Poisson's equation for the rotationally symmetric model, is used to calculate the probe response matrix [16]. When space charge exists, the electrostatic Poisson's equation:

$$\nabla^2 V = \frac{-\rho}{\varepsilon} \tag{4.3}$$

is solved where, ρ is the charge density and ε is the permittivity.

In the absence of charge (4.3) becomes Laplace's equation:

$$\nabla^2 V = 0 \tag{4.4}$$

The boundary conditions of the electrostatic simulation can be described across any boundary (region) as:

$$D_{n2} - D_{n1} = \rho_s \tag{4.5}$$

where D_{n1} and D_{n2} are the normal components of the electric flux and ρ_s is the surface charge at the boundary,

$$E_{tan1} = E_{tan2} \tag{4.6}$$

where E_{tan1} and E_{tan2} are the tangential components of the electric field.

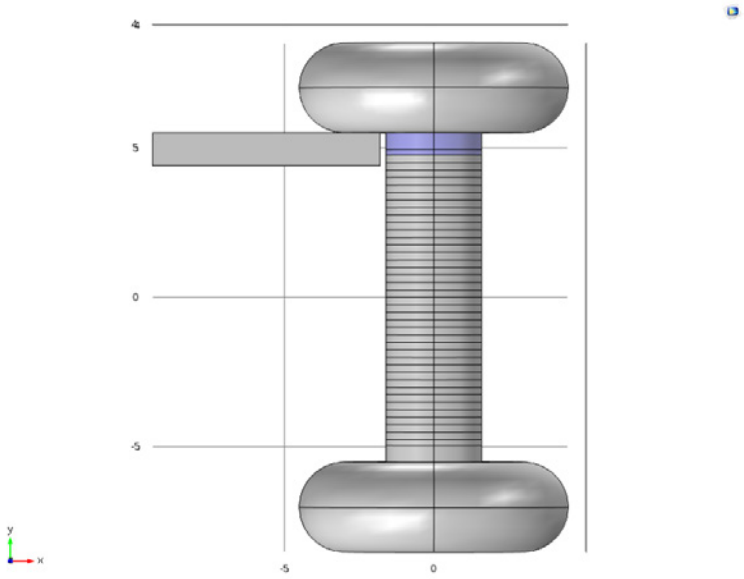

Fig. 4.1: 3D Comsol Multiphysics model of electrodes, insulator and probe. A surface charge density of 1 $\mu C/m^2$ is assigned to one of the rings and zero for other rings.

The boundary conditions for the electrostatic model are such that the electrodes have a voltage of zero assigned, the probe/electrode/insulator model is inside a grounded box and surrounded by air, one segment of the insulator sample has a charge density assigned while the others have zero charge density, and the probe potential is varied through a range of voltages.

The simulation model can be seen in Figure 4.1. The sample surface is divided into 19 rings, each of 5 mm width. The 5 mm width was determined by the chosen measurement step, using the vibrating Kelvin probe and was found to provide sufficient resolution. Potentials, for those rings, are measured experimentally with the vibrating Kelvin probe. Two extra rings, one at each end, are added between the last point that the probe can reach and the two grounded electrodes. Potentials of those two rings are interpolated between the nearest rings potential and the electrodes potential, which is zero.

This results in a square matrix (21 by 21), containing 441 elements. Since symmetry

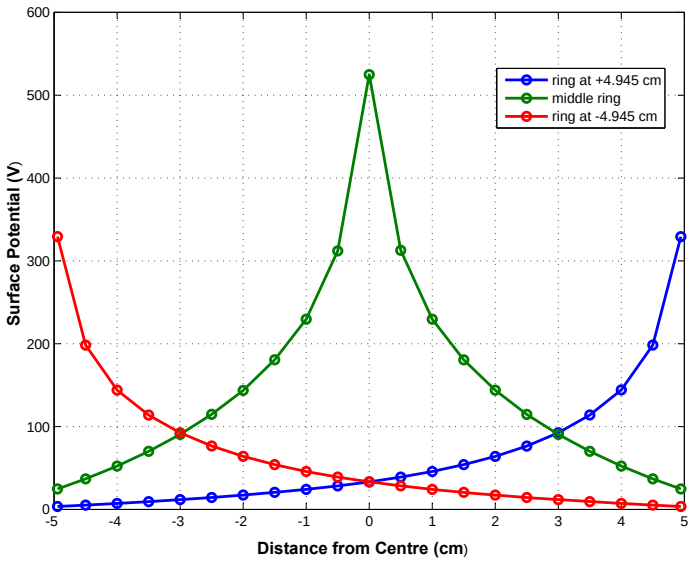

Fig. 4.2: Three columns of the probe response matrix of large diameter FRP sample.

can be assumed, the calculations were only carried out for 11x21 elements. The values of each column of $[\sigma]$ represent the surface potential induced at each ring due to a surface charge density of 1 $\mu C/m^2$ assigned to one of the rings and zero for other rings. Figure 4.2 represents surface potentials induced by a 1 $\mu C/m^2$ charge density assigned to the middle as well as the two extremely right and left rings.

For each of the probes locations, the potential on the point directly beneath the probe surface is calculated. The value of the matrix element is obtained when the probes potential is equal to the calculated potential of the ring element at which the probe is located. Two sweep functions were used in Comsol Multiphysics, one for moving the probe to face the middle point of each ring to reduce the number of runs, and one for achieving "the field nullifying effect" of the vibrating Kelvin probe, by initially setting the probes potential to a certain value (0 V) and letting it change through a range. The potential of the probe was swept from 0 to 200 V at each location along the surface of the insulator. The potential at

the point directly under the probe is calculated and the potential of the probe is determined by solving a linear equation. Since the probe voltage is varied through a range and we know the induced voltage on the surface for these values, and we know the potential of the probe is equal to the potential on the surface, we have a linear equation representing the potential on the surface in the form:

$$Ps = m \cdot Pp + b \tag{4.7}$$

and since

$$Pp = Ps \tag{4.8}$$

therefore,

$$Pp = \frac{b}{1 - m} \tag{4.9}$$

where, Ps is the potential on the surface, Pp is the potential on the probe, m is the slope of the linear equation for the range of potentials induced on the surface by the probe, and b is the y-intercept of the linear equation for the range of potentials induced on the surface by the probe. This equation is solved for all 21 locations along the surface for each charge condition, and as previously mentioned results in a 21x21 matrix. Five models were completed to extract the probe response matrix for each material sample.

4.1.2 Corona Ring of Needles Charging Method

4.1.2.1 Charging Time

Experimental investigation for the charging time proved that more than 80% of the charges are deposited during the first two minutes compared to 10 minutes using the corona ring of needles. This is shown in Figure 4.3, with the ring of needles located at the centre of

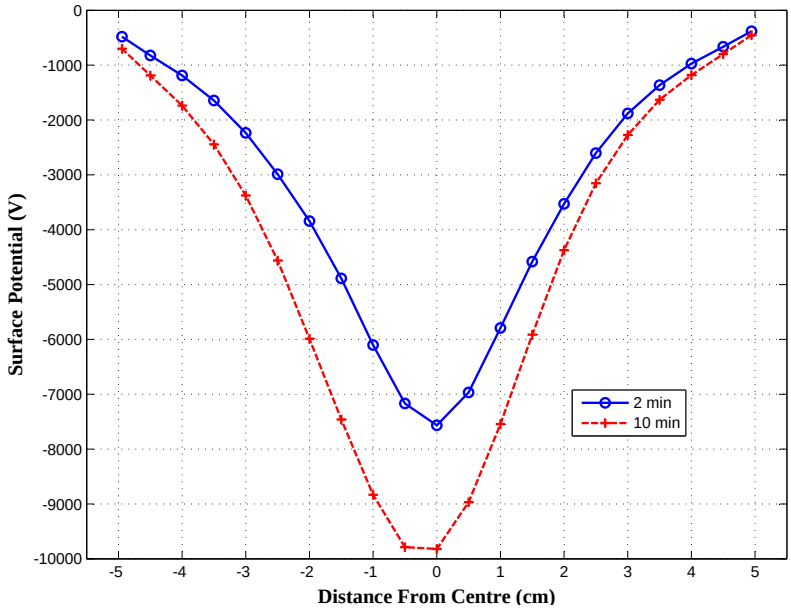

Fig. 4.3: Effect of corona charging time on surface potential distribution with applied voltage of -20 kV on the large FRP sample.

the sample, and explains why 2 minutes was chosen as the default charging time for the remaining experiments. Using 2 minutes resulted in a repeatable test that could be carried out consistently and efficiently.

4.1.2.2 Location of the Corona Ring of Needles

The effect of moving the location of the ring of needles was tested by moving the needles 2.5 cm to the left. It has been noticed that there is no significant change in the voltage distribution when the ring is moved from the middle to the left for both DC polarities other than a spatial shift. The position of the ring of needles is chosen to be at sample mid-point for the remaining corona charging studies. Having the sample in the middle is also the safest as locating the needles to close to the ground electrodes could result in arcing. Figure 4.4 shows the results of the study on the location sensitivity of the ring of needles for the small

FRP sample.

4.1.2.3 Charging Voltage

Next, the impact of the charging voltage was carried out. Repeatable tests were possible with the ring of needles charging method at each charging voltage. Each plot displayed in the following figures of this chapter for the charging characteristics are the average plots of 5 tests done at each operating condition where the sample is cleaned prior to the test and scanned to ensure no significant remaining space charge existed. Figure 4.5a and 4.5b show an example of the average data with error bars for a positive and negative charging condition ($\pm$20 kV). The results show that the surface charge profiles can be repeatably produced. As will be seen in the testing, negative charge tended to have a higher surface potential than positive polarity. Negative charge also tends to be more widely spread over the surface of the insulator, while positive charge is more narrowly distributed on the surface. The error is noted to be less on the left side of the sample than the right. This may be do to the asymmetry of the ring of needles, as the needles are not located exactly at the center (located at left of center) of the ring.

Th surface potential and the corresponding charge distributions are plotted in Figure 4.6 for two study cases (large FRP sample energized by ring of needles at $\pm$20 kV), to clearly show the consistency between the calculated surface charge distribution pattern using the, ϕ - matrix method, and the measured induced surface potential pattern. Again it is noted that negative charging results in the highest surface potential at the middle. In the case of both positive and negative charging, hetero-charges (charges of the opposite polarity) are observed near the electrodes. The charge density is actually slightly higher at the middle for positive polarity charging, due to the fact the charge is concentrated more in a narrow band at the center of the sample, where as the negative charge is more spread out over the surface.

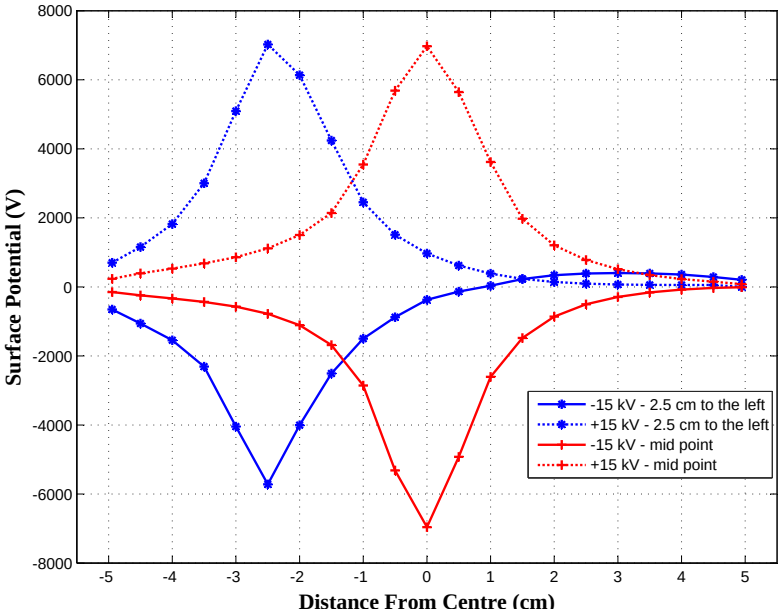

(a) Surface potential distribution

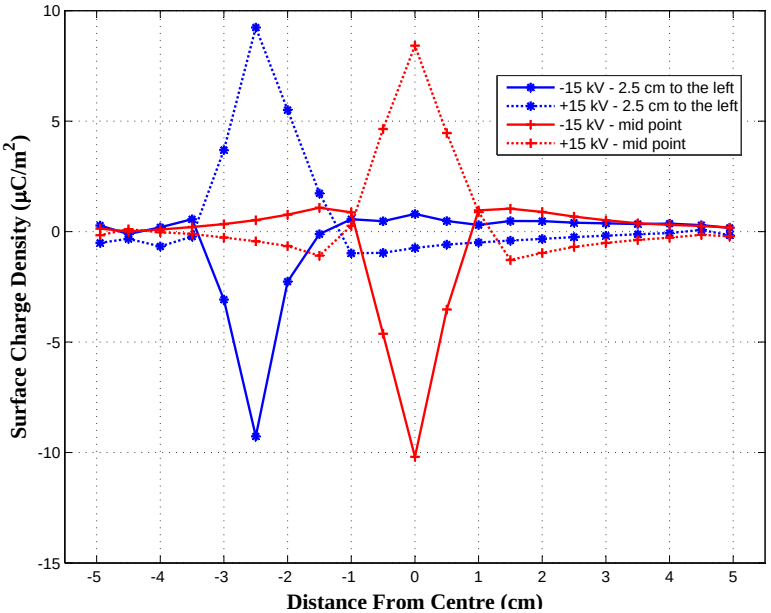

(b) Surface charge distribution

Fig. 4.4: Position effect of the ring of needles on a) the surface potential and b) charge density distribution for the FRP small sample surface at ±15 kV for 2 minutes.

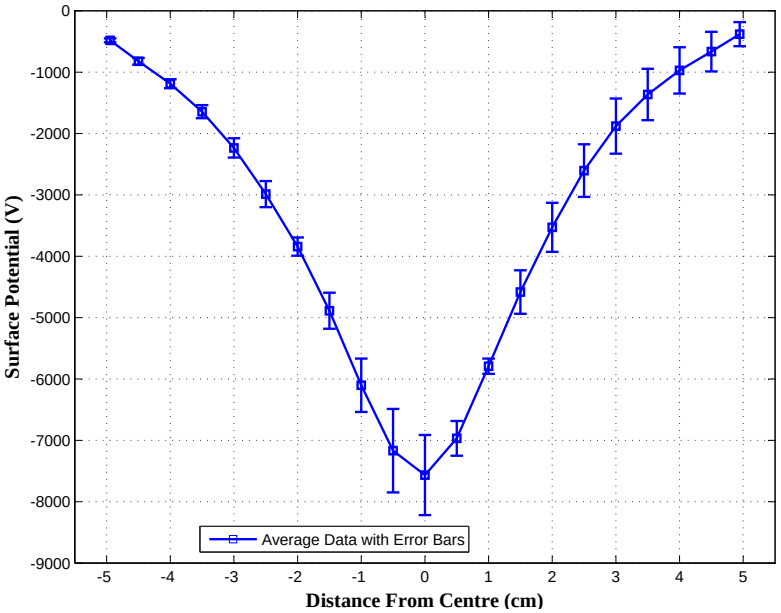

(a) -20 kV for 2 min

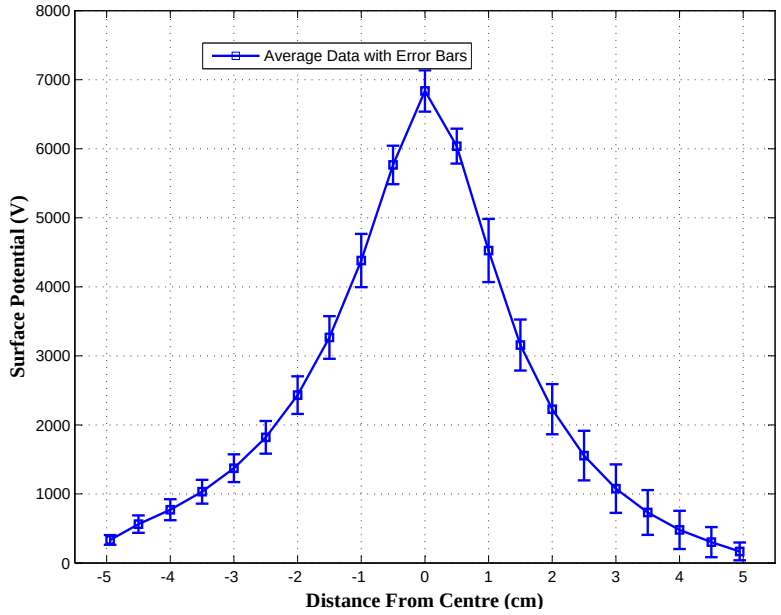

(b) 20 kV for 2 min

Fig. 4.5: Surface potential distribution of the large FRP sample with error bars when charged at a) -20 kV and b) +20 kV for 2 minutes using the ring of needles.

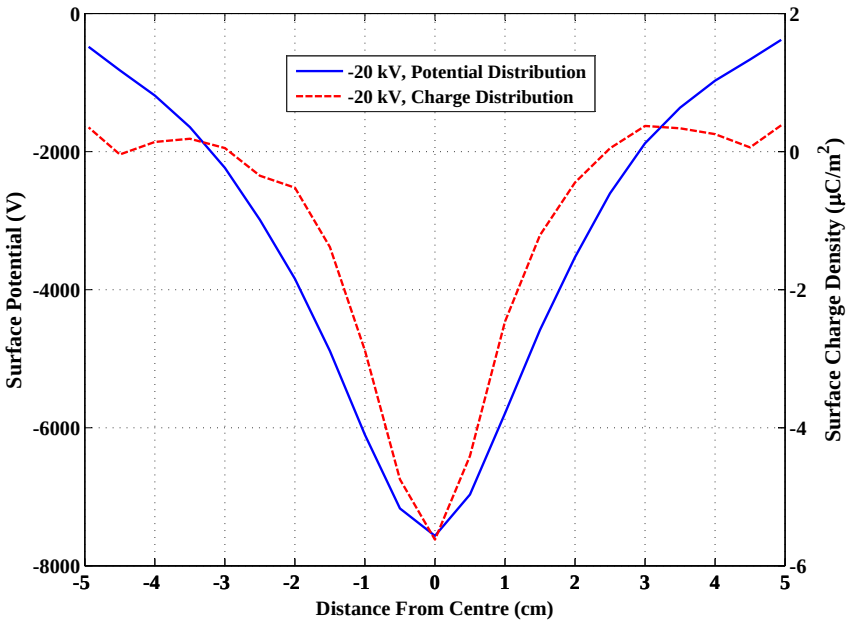

(a) -20 kV for 2 minutes

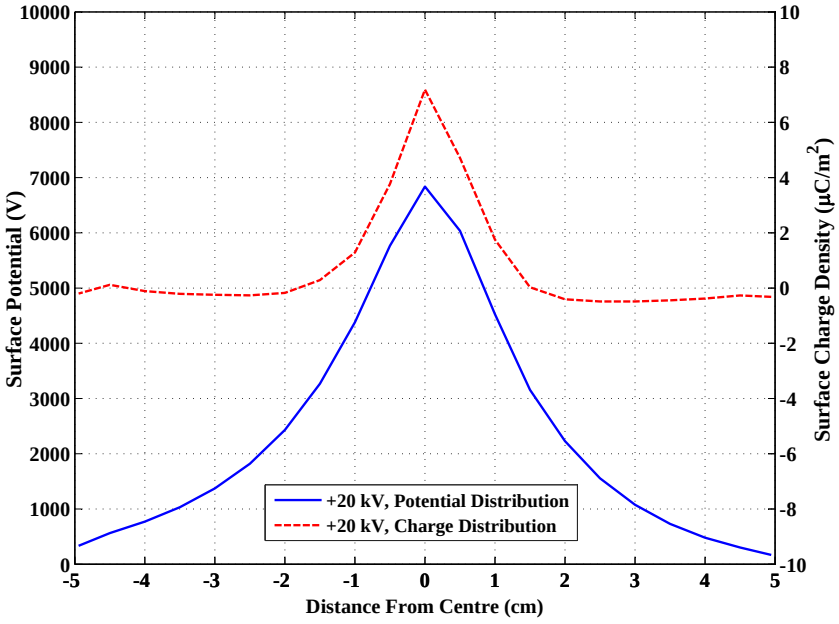

(b) 20 kV for 2 minutes

Fig. 4.6: The surface potential and charge distribution for the large FRP sample for a) -20 kV and b) +20 kV for 2 minutes.

The surface potential distributions were measured for each insulator sample when voltages (±7 kV, ± 10 kV,± 15 kV, and ± 20 kV) were applied to the corona ring of needles. These tests were to determine the effects of charging voltage magnitude and polarity on each insulator sample for comparison. In Figure 4.7 the effect of the corona ring of needles charging voltage, with different polarities and magnitudes, on the surface charge and potential distributions is shown for the large FRP sample. It is observed that for the higher values of applied voltages, ± 15 kV and ± 20 kV, the profiles of surface potential distribution have a bell shape. The measured surface potential values for low applied voltages, ± 7 kV and ± 10 kV, are significantly low as compared to higher voltages. The measured surface potentials give an indication of the amount and polarity of charges deposited on sample surface during the charging process. Negative charging voltages result in higher surface potential values, measured over the sample surface, as compared to the positive charging voltages, as seen in Figure 4.7a. This can be related to the nature of electrons and positive ions, as electrons are much faster and more diffusible than the positive ions [61]. For the same applied voltage, more electrons can reach the sample surface resulting in higher surface potential. The calculated values of surface charge density distribution for both polarities of different magnitudes of applied corona charging voltage are shown in Figure 4.7b. It is clear that surface charge profiles follow their corresponding surface potential profiles. In the case of negative charging voltages, homo-charges (having the same polarity as charging voltage) are more widely extended over the insulator surface (from the ring location) as compared to that produced by positive charging voltages. The positive charges are more centralized to the location of the ring of needles, pointing to the higher mobility of electrons compared to positive ions. Low values of hetero-charges (having the opposite polarity of charging voltage) are observed closer to the electrodes. Similar observations and mechanisms explaining the reasons were reported in [12].

The surface potentials and charge distributions were measured and calculated for all

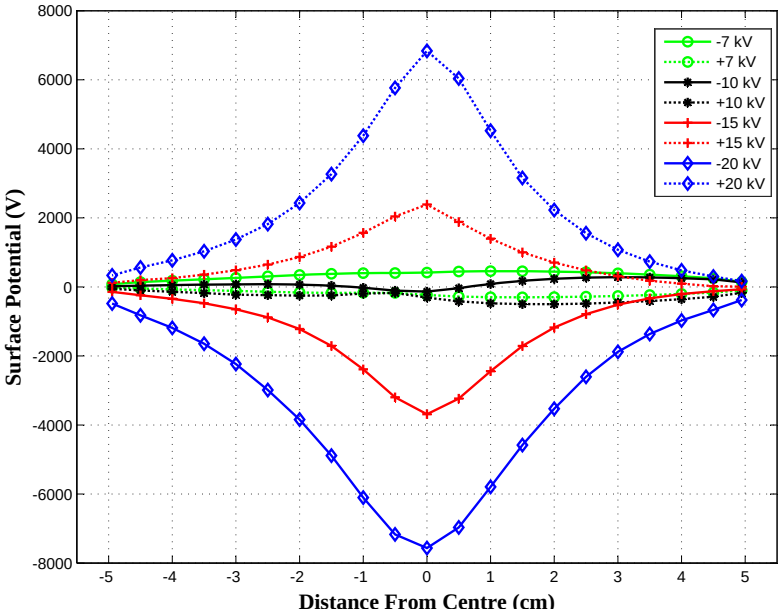

(a) Surface potential distribution

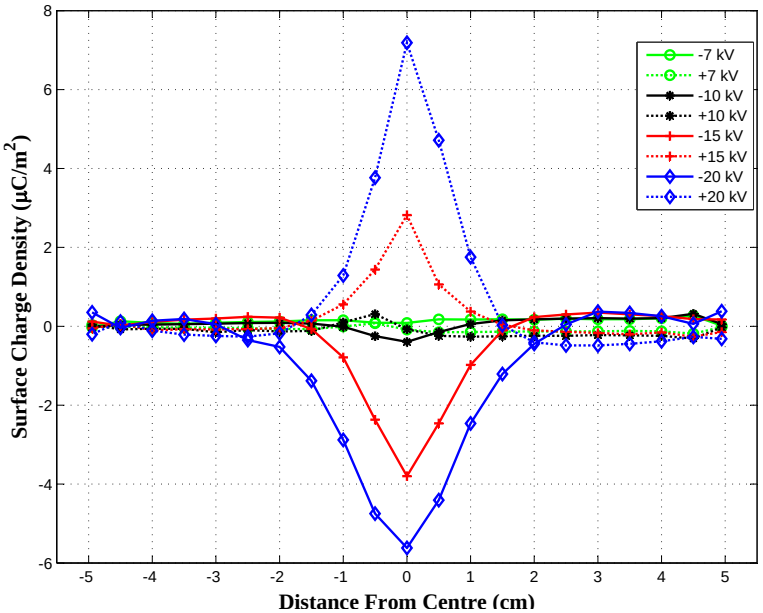

(b) Surface charge density distribution

Fig. 4.7: The large FRP sample a) surface potential and b) charge density distribution for ±7 kV, ± 10 kV,± 15 kV, and ± 20 kV.

of the FRP, SIR and the wood samples as described in Table 3.1, for the same charging conditions as illustrated in Figure 4.7. The results can be found in Appendix B. These results were used to calculate the total charge on all of insulator samples, for each charging voltage magnitude and polarity, as discussed below.

The total amount of charge deposited on the sample surfaces for each corona charging voltage is shown in Figure 4.8. The total charge values were calculated using a surface integral of the obtained charge densities. The main observation is that increasing the magnitude of applied corona charging voltage is accompanied by an increases in the total amount of charges injected to the surface. The net charge injected to the surface during negative charging is significantly higher than that induced by positive charging. In addition, it is noted that, for lower charging voltages, ($\pm$7 and $\pm$10 kV), hetero-charges are observed on the surface for both polarities. Under negative charging polarity at -20 kV the large FRP and large SIR had the largest total charge accumulation. Under positive charging, all samples had similar total charge on the surface at 20 kV except for the wood sample. It is observed that the total surface charge on the samples increases linearly with charging voltage as was observed in [12].

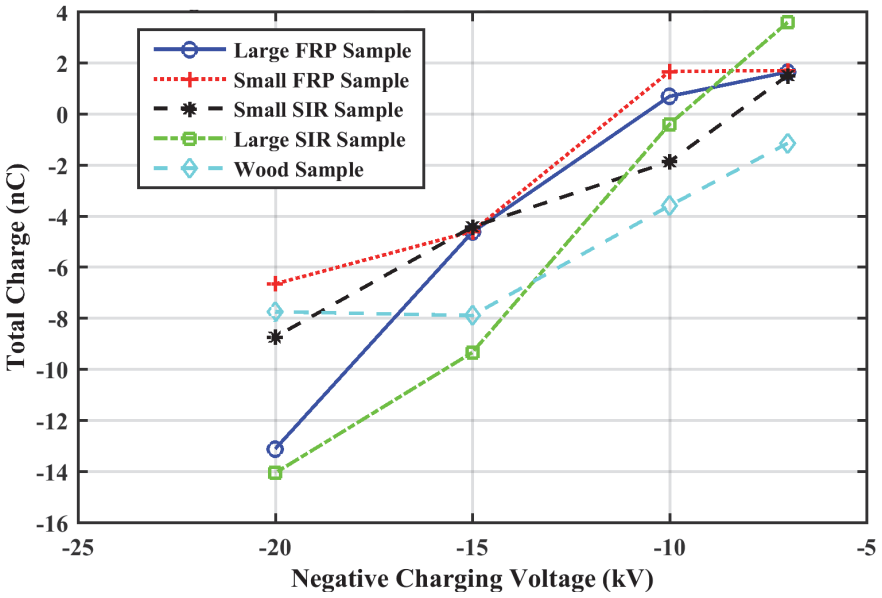

(a) Total charge induced on samples when charged with a negative voltage

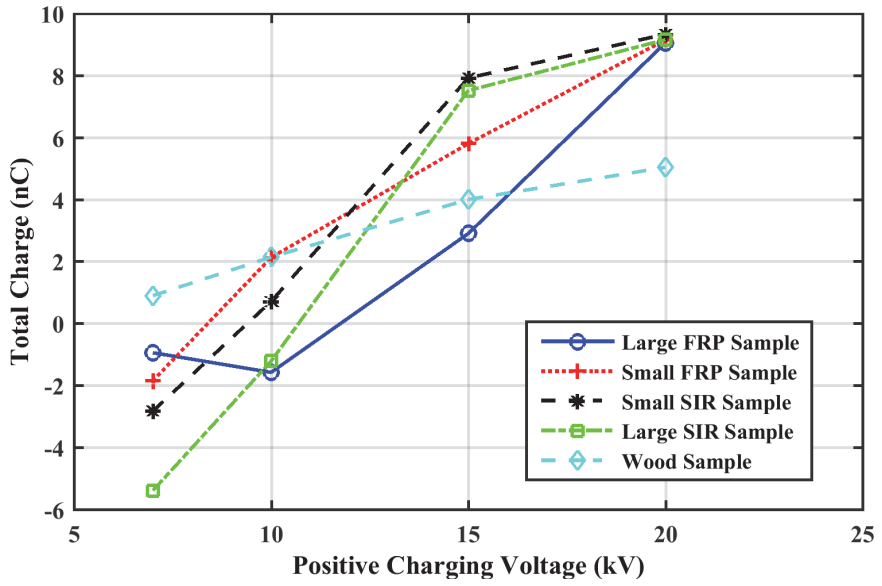

(b) Total charge induced on samples when charged with a positive voltage

Fig. 4.8: Effect of a) negative and b) positive charging voltage on the total charge accumulation on the insulator samples.

Fig. 4.9: Adjustment of needles using a caliper for investigating the effects of the needle-to-surface separation distance.

4.1.2.4 Needle to Surface Separation Distance

This study is conducted to investigate the effect of the distance of energized nearby objects on surface charge distribution on insulating materials (FRP and SIR). The needles were adjusted one by one using a caliper, as displayed in Figure 4.9 to accurately obtain the desired needle-to-surface distance for each sample. The tests carried out throughout the rest of this thesis with the ring of needles was at a distance of 5 mm from the needles to the surface.

Testing was completed at ±20 kV on the small FRP and SIR samples and the following conclusions were observed. In Figure 4.10 it is shown by the measured values that increasing the distance between the surface and needles increases the surface potential for both polarities and for both materials. The so called back discharges are noted which will be discussed in Section 4.1.2.5 and were also noted in [12].

The surface potentials shown in Figure 4.10 were converted to their corresponding surface charge densities and integrated over the surface to determine the total charge.

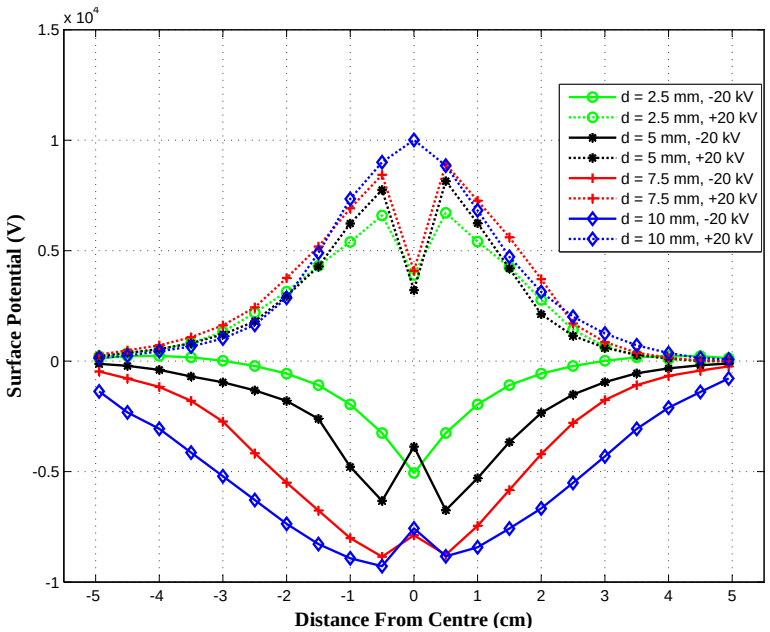

(a) Small FRP sample, ±20 kV applied voltage

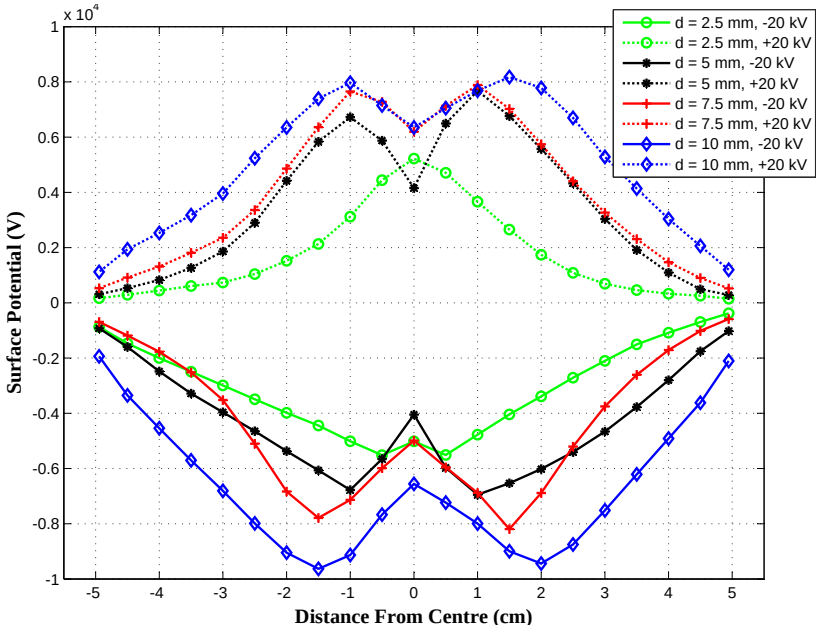

(b) Small SIR sample, ±20 kV applied voltage

Fig. 4.10: Effect of needle-to-surface separation distance on the surface potential distribution for a) the small FRP sample and b) small SIR sample for ±20 kV charging voltages.

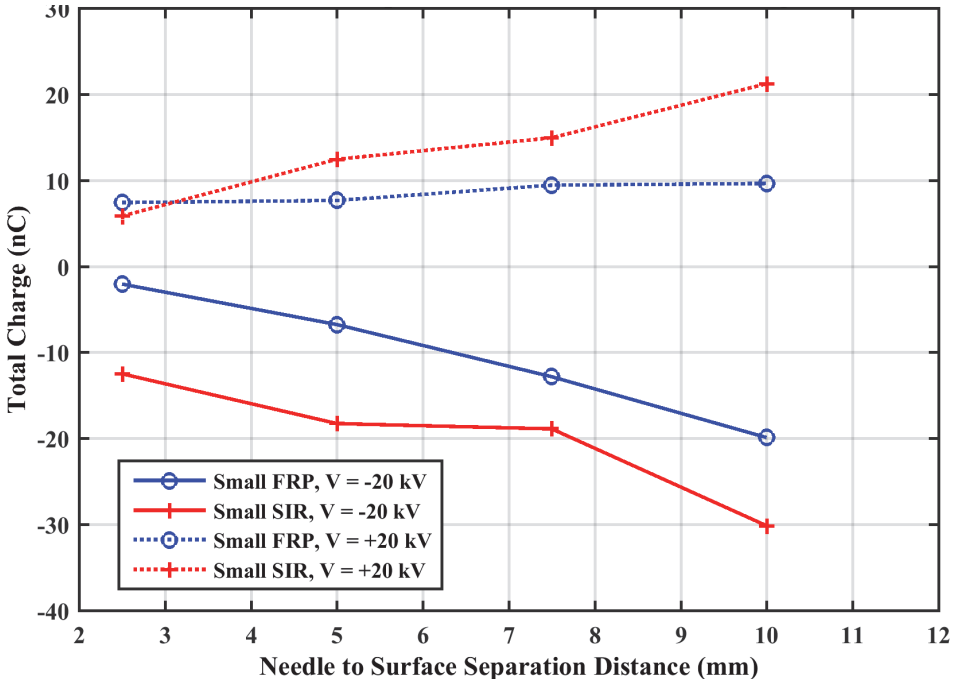

Fig. 4.11: Effect of needle-to-surface separation distance on surface charge accumulation for positive and negative charging voltages.

Figure 4.11 shows that increasing the needle-to-surface separation distance for both DC polarities increases the total amount of charges accumulated on the surface for both SIR and FRP linearly. For negative DC charging voltage, however, the total charge accumulated on the surface is higher than that of positive DC for both SIR and FRP. SIR insulating material is noticed to attract more charges than FRP hot sticks. It also verifies the results shown in Figure 4.8 that for positive charging of 20 kV at 5 mm the results are almost the equal, for the small FRP and small SIR, and for negative charging of -20 kV at 5 mm the charge on the small FRP is noticeably smaller than the small SIR.

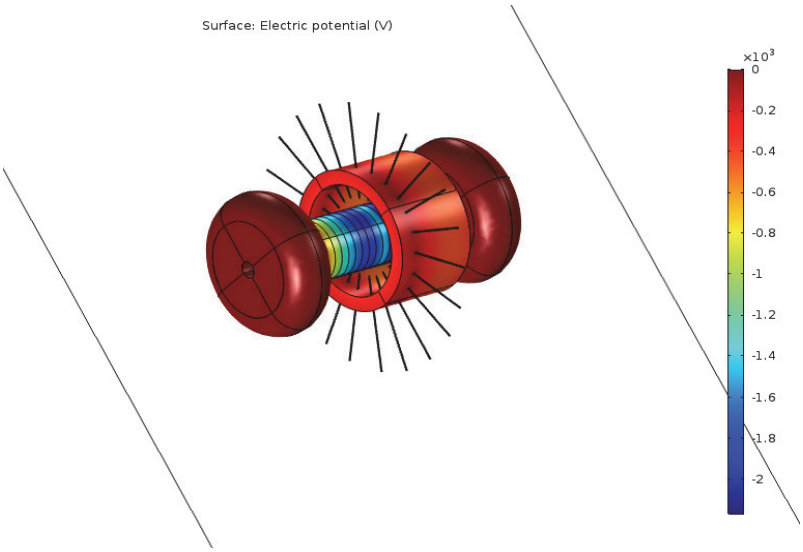

Fig. 4.12: Electrostatic simulation model of FRP sample, corona ring of needles and electrodes to investigate back discharge.

4.1.2.5 Back Discharge

It was noted that for all samples we were experiencing back discharges during the ring-of-needles-distance study of (Section 4.1.2.4) which lowered the measured potentials in the middle of the sample. This was not common at the beginning of our testing and had only been noticeable on the wood sample at that time. Back discharges happen between the charged surface and needles after switching off the voltage supply and grounding the ring of needles. This can be attributed to higher electric field strength between the needles and charged surface and also higher humidity in the laboratory, which was lowering the inception voltage for air ionization [62]. An electrostatic study was completed to calculate the electric field strength between the charged surface and the needles using the electrostatic model as discussed in Section 4.1.1. In the model the probe was replaced with a grounded corona ring of needles as illustrated in Figure 4.12.

The calculated surface charge density distributions for two study cases were specified as boundary conditions. The case used was the -20 kV and -15 kV result as shown in Appendix Figure B.4 and in Figure 4.13a. It has been found that for the study case with back discharge the electric field strength, between the surface and the needle tip, is higher than the air ionization threshold (> 30 kV/cm) and lower than that value for the study case without back discharge. As seen in the study in Section 4.1.2.4 humidity can lower the air ionization threshold and result in more frequent back discharges.

4.1.2.6 Surface Charge Decay

Surface charge decay tests were carried on all the insulator samples for a charging voltage of -20 kV. As discussed earlier in Section 2.1.1, there is not a significant difference in the decay time of positive or negative charges. All samples were charged using the ring of needles with a 5 mm needle to surface distance for 2 minutes. After charging, the samples were scanned at different times for a period up to 4 hours and the humidity conditions were similar for all tests. In Figure 4.14, an example of measured surface potentials and calculated charge densities can be found for the small SIR sample. The total surface charge was calculated for each sample surface at each measurement time and plotted. The surface charge was nominalized by dividing each total charge value by its initial charge value. The resulting data is displayed in Figure 4.15. During the first 45 minutes, the SIR material lost 50% of its initial surface charge while, the FRP material still held around 70-80% of its initial surface charge. Also, it has been noticed that, the SIR and the wood materials can neutralize their surface charges approximately, 1.6 faster than the FRP material. The remaining plots, of surface charge decay, for all materials showing the surface potentials and charge densities are shown in Appendix C.

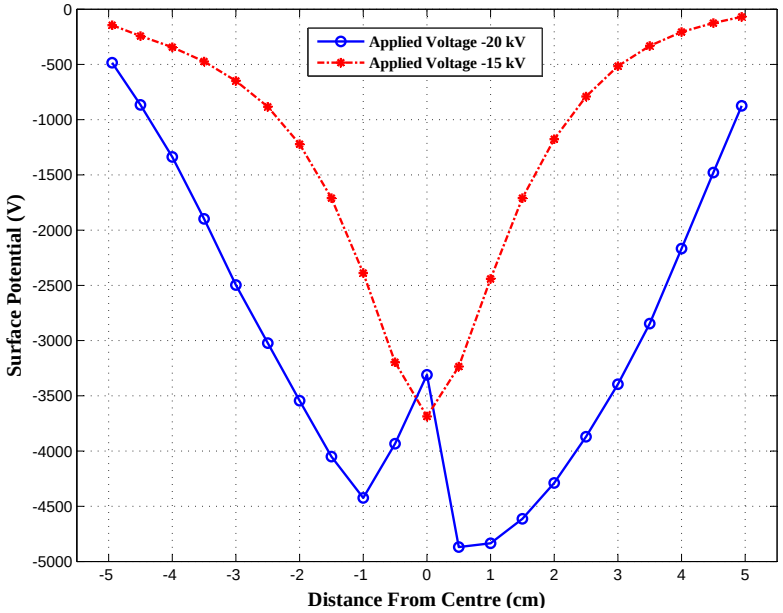

(a) Small FRP surface potentials for -15 kV and -20 kV

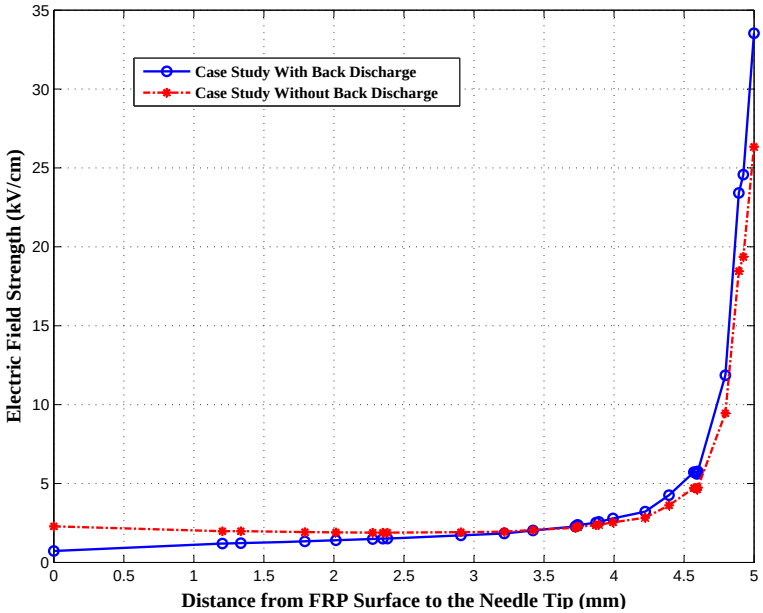

(b) Magnitude of electric field strength between tip of needle and surface of small FRP sample

Fig. 4.13: Case study results for a) negative surface potentials with and without back discharge and b) electric field strength, between surface and needle tip, due to surface charges for needle to surface distances.

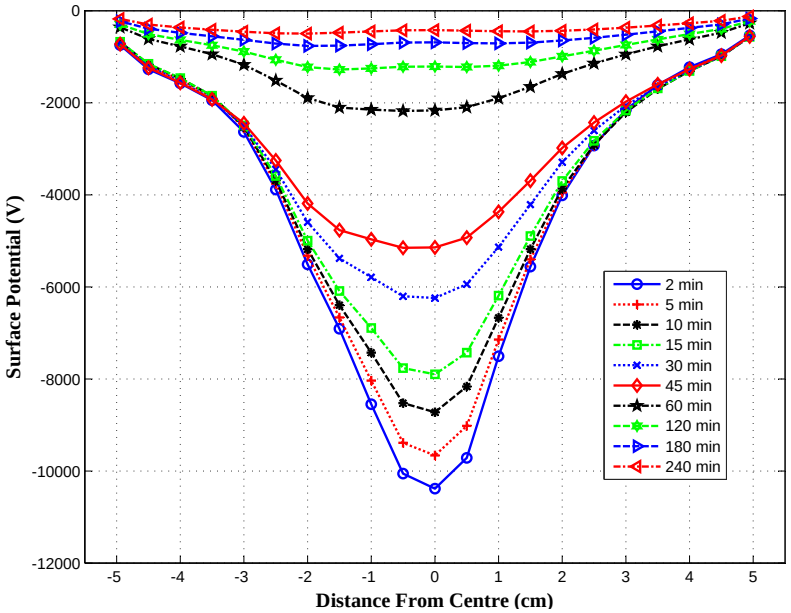

(a) Measured surface potential for charge decay test

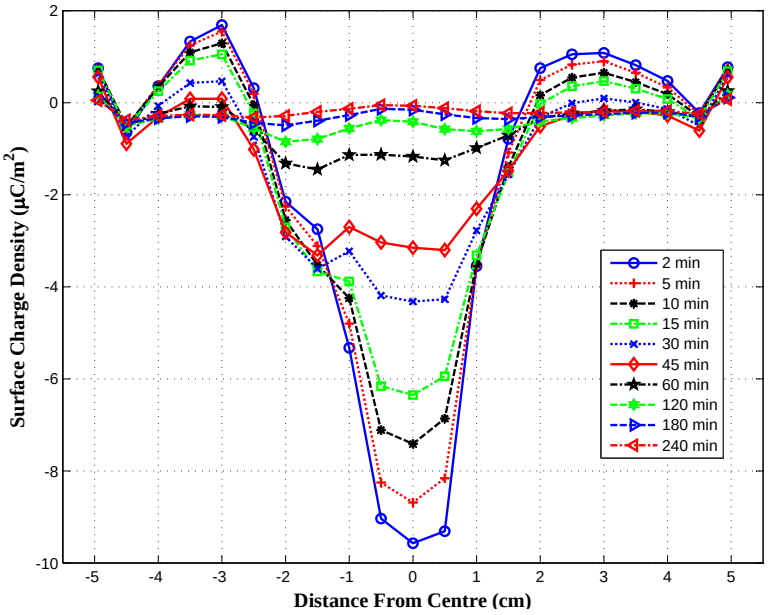

(b) Calculated charge density for charge decay test

Fig. 4.14: Surface charge decay test for the small SIR sample showing a) surface potential decay and b) surface charge density decay for -20 kV charging voltage.

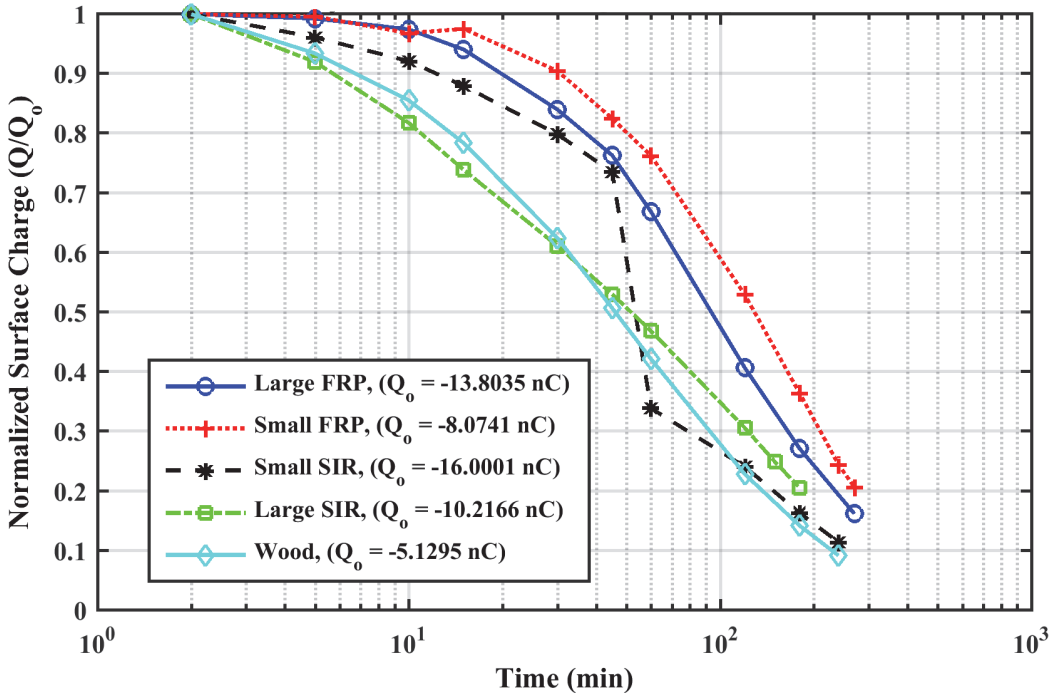

Fig. 4.15: Decay of normalized total charge on the surface of samples.

4.1.3 Pre-stressing Charging Method

The work done by Kumara *et al.* [2] (as discussed in Section 2.3) showed that, pre-stressing one electrode with -72 kV while the other electrode grounded will produce positive surface charge over the cylindrical SIR insulator sample. Also they demonstrated that, if positive charges exist on insulator surface, the flashover voltage will be lower (than if negative charge existed) for negative DC applied voltage.This is interesting from the perspective of the fast flashover [3], [4] as these flashovers also occurred under negative polarity on clean surfaces. The electrodes used in [2], [12] were smaller than the electrodes used in our experiments and also had a sharper edge right at the surface of the insulator which would create a triple junction point and high electric fields. The electrodes we used in the testing were large and

without triple junction. They were relatively corona free and only created surface charge of the same polarity as the charging voltage. For producing more surface charges on the FRP surface, copper strips (conductive copper tape) were used at both electrode sides (as shown in Figure 3.6). These copper strips create a triple junction point between air, surface, and electrodes which in turn produces more corona discharge at the FRP surface.

4.1.3.1 Charging Time

The large FRP sample was pre-stressed with voltage at -72 kV for durations of 2,4, and 6 minutes. It is noticed that in the first two minutes of pre-stressing, about 90% (Figure 4.16) of the charge is deposited on the surface. Therefore, a duration of 2 minutes was chosen for the remaining pre-stressing tests.

4.1.3.2 Charging Voltage

The large FRP sample was pre-stressed with voltages of -66, -69 and -72 kV. As mentioned in [12], negative pre-stressing "with corona discharge" produces more positive charges. Also, for pre-stressing at voltages lower than -66 kV it was observed that no significant corona discharge initiated at the electrodes and the surface was negatively charged. There was not a significant difference in the amount of surface charge on the surface for the three charging voltages and increasing the voltage any higher could risk a possible flashover for which our equipment was not protected from at the time. Figure 4.17 shows the surface potential and charge density for the different negative pre-stressing voltages. In Figure 4.18, the results are shown for different positive pre-stressing voltages, where the large FRP sample was stressed for 2 minutes. It is noticed that the positive pre-stressing with "corona discharge" produces more negative surface charges. It can also be seen that the amount of charge from positive pre-stressing is considerably less than negative pre-stressing. This speaks to the higher mobility of electrons compared to positive ions. For positive pre-stressing the voltage

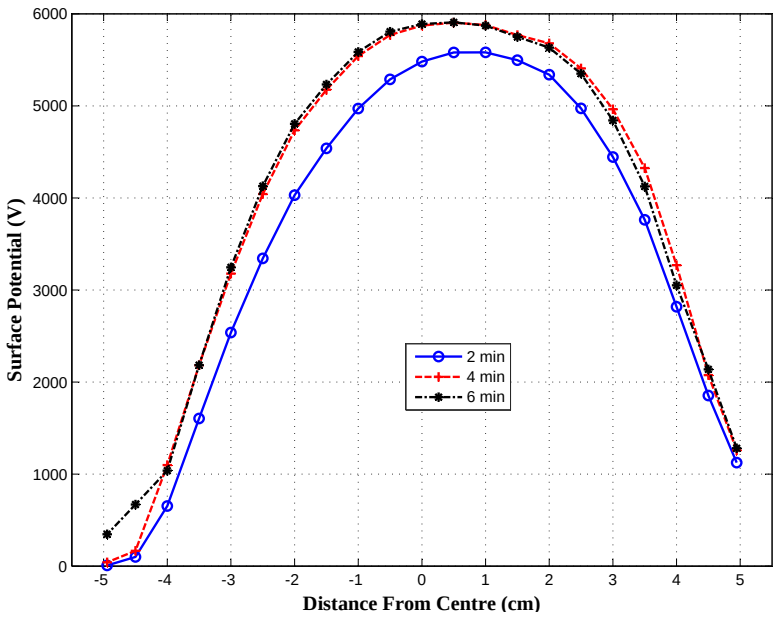

(a) Pre-stressing surface potential

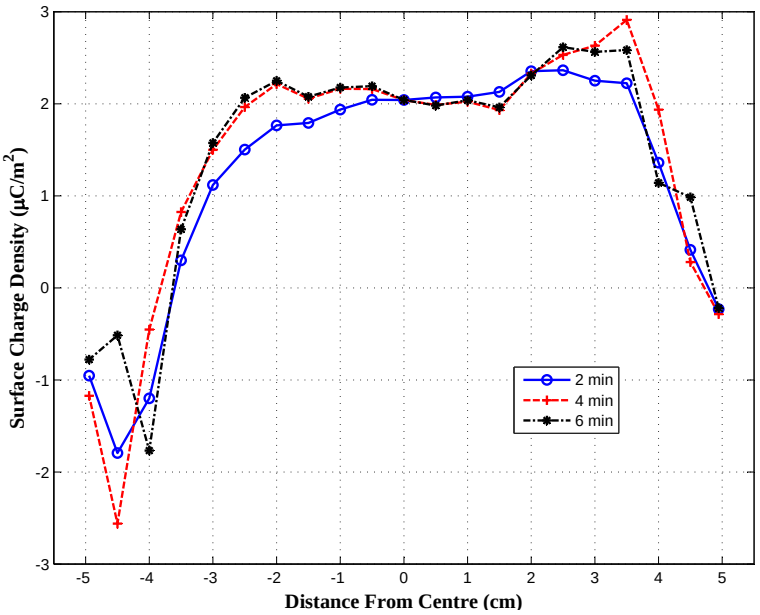

(b) Pre-stressing surface charge density

Fig. 4.16: Pre-stressing results for an applied voltage of -72 kV on the large FRP sample showing a) measured surface potential and b) calculated surface charge density.(-5 cm is grounded side and +5 cm is the energized side)

could not be increased as high due to the non-uniform tape which had an overlap on one side that would initiate positive streamer activity and there was a risk of flashover.

4.1.3.3 Electrode Configuration

This study is done to investigate the effect of sharp edged electrodes (triple junction point) on charging of the sample surface through four different electrode configurations. For both DC polarities, electrodes with copper strips at both ends are noticed to inject hetero-charges to the FRP surface. Further investigation is required into why this occurs. On the other hand, the FRP surface is charged with homo-charges if copper strips existed at only one electrode end or both electrode ends without copper strips. It is also noticed that, if one electrode end with a copper strip can initiate corona discharge (in the case of positive voltage, visually seen with a corona camera), it will inject hetero-charges to the surface. The results for this investigation are displayed in Figure 4.20.

During testing for positive and negative corona discharge with pre-stressing and the use of the copper strip for creating a triple point junction at both ends of the sample, observations were made using a corona camera on the differences between negative and positive corona discharge. The corona camera was a Syntronics CoronaFinder which was connected to a camera for capturing corona activity. Negative corona appears like small pulsating spheres covering the whole edge around the copper strips (Figure 4.19a). Positive corona appears like a streamer discharge with many branches (Figure 4.19b) coming out from a point on copper strip and propagates along the surface to the ground electrode. Positive streamers occur at a lower voltage than the negative voltage for the point discharge. Negative corona pulses are referred to as trichel pulses and the positive streamers are known in literature to be severe [63] as they occur at lower electric fields.

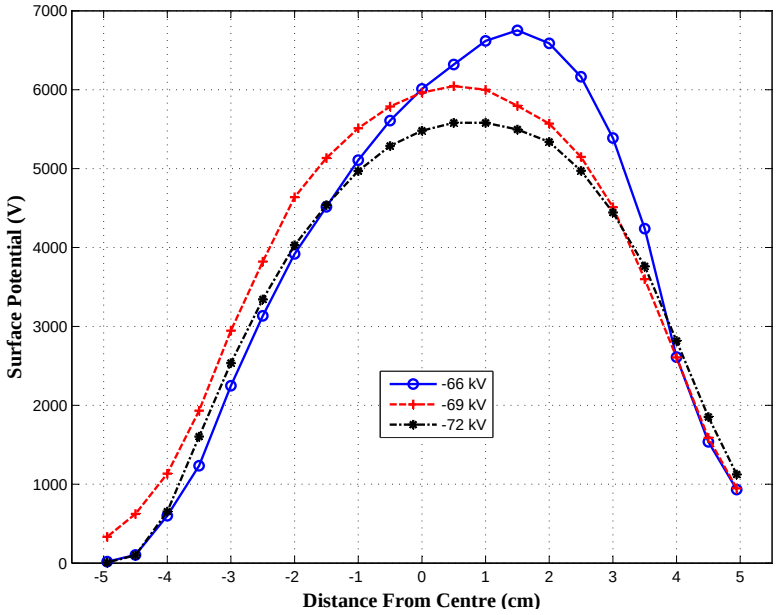

(a) Pre-stressing surface potential

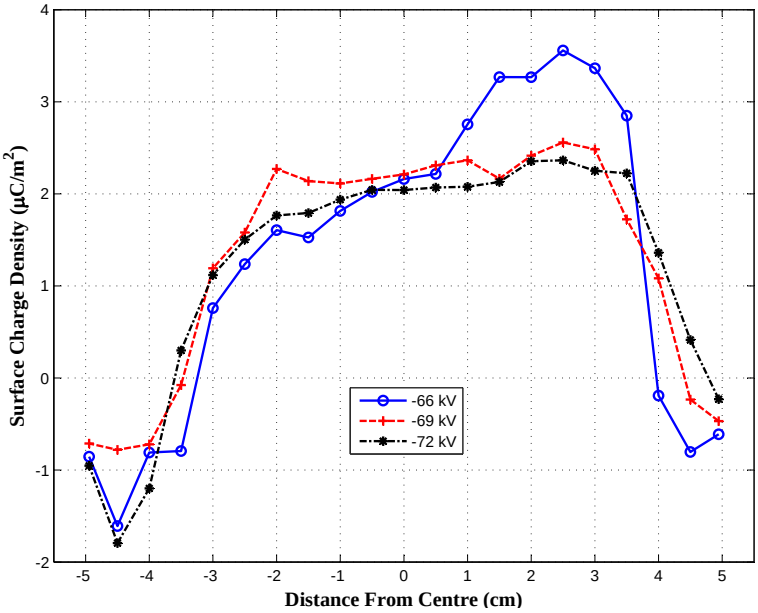

(b) Pre-stressing surface charge density

Fig. 4.17: Pre-stressing results for an applied voltages of -66,-69,-72 kV on the large FRP sample showing a) measured surface potential and b) calculated surface charge density. (-5 cm is grounded side and +5 cm is the energized side.)

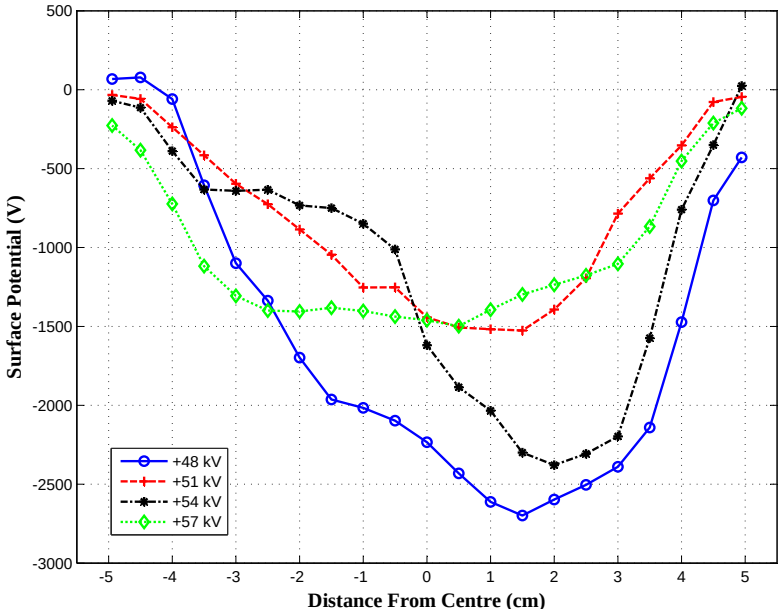

(a) Pre-stressing surface potential

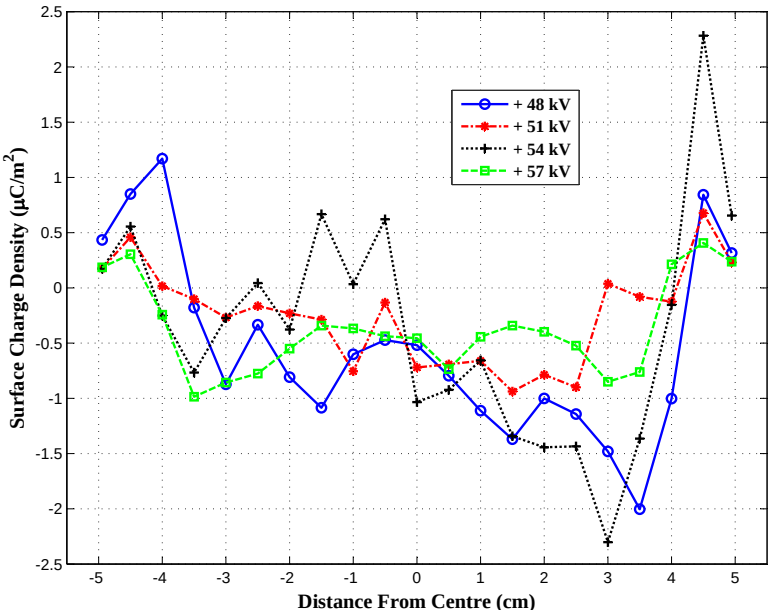

(b) Pre-stressing surface charge density

Fig. 4.18: Pre-stressing results for applied voltages of +48,+51,+54, and +57 kV on the large FRP sample showing a) measured surface potential and b) calculated surface charge density.(-5 cm is grounded side and +5 cm is the energized side.)

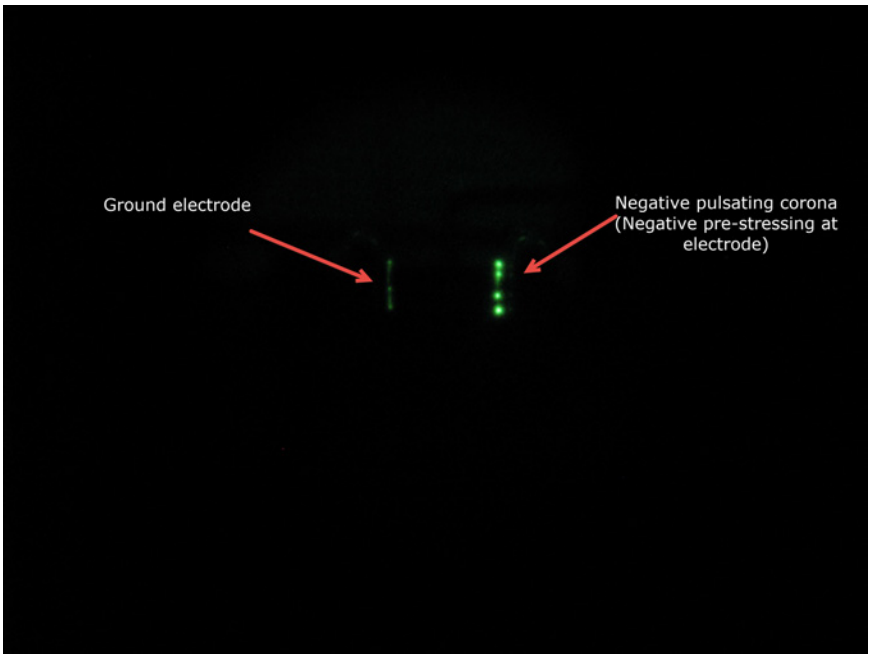

(a) Negative corona

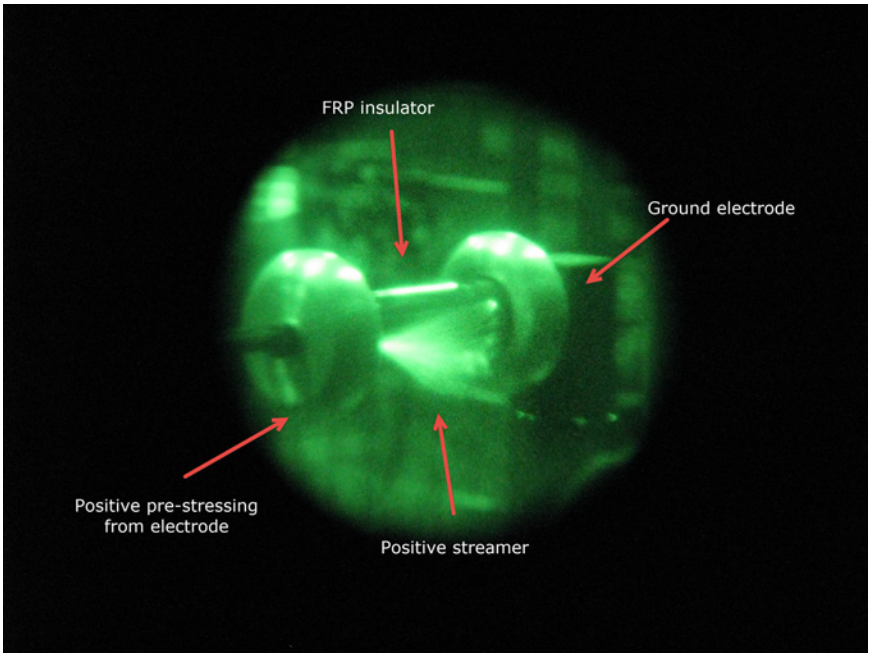

(b) Postive corona

Fig. 4.19: Photos of negative and positive corona taken using a corona camera.

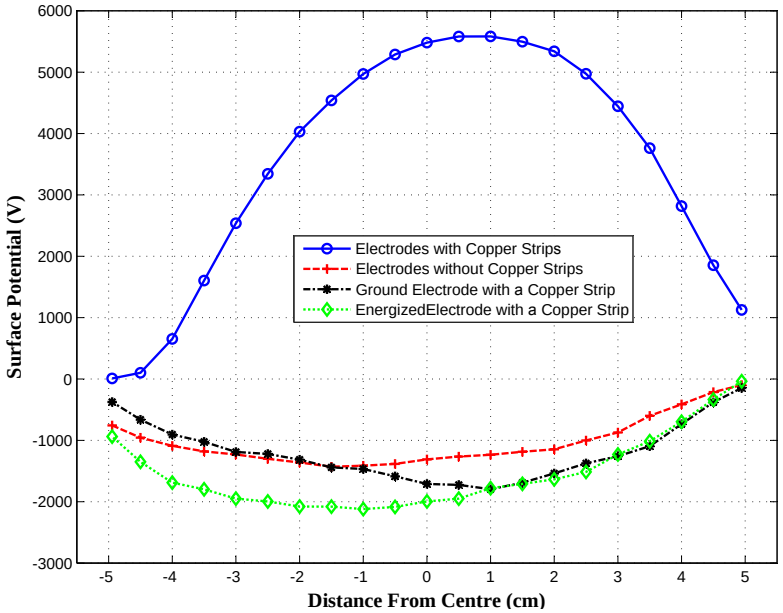

(a) Negative pre-stressing

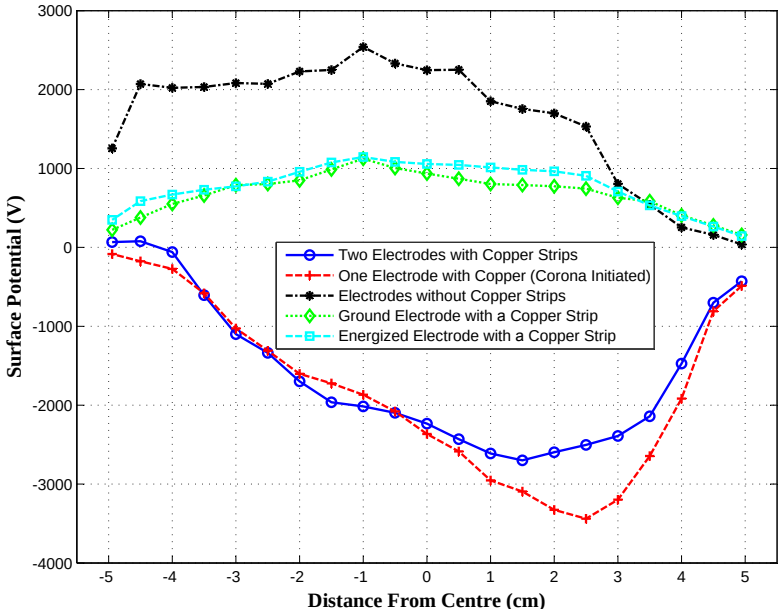

(b) Positive pre-stressing

Fig. 4.20: Pre-stressing results for a) negative and b) positive applied polarity, showing surface potential for different electrode configurations.

4.1.4 Charging by Wiping with Cloth

Wiping hot sticks with a cotton cloth and then by a silicone wiping cloth is a daily routine done in the field before live-line work to be sure that there is no pollution contaminates on the stick surface and to improve the tools hydrophobicity. Figure 4.21 shows the amount charge that can be induced on an FRP tool from wiping with cotton clothes and silicone clothes. The surface potential induced on the FRP surface was higher than what the DC-ESVM was rated for and exceeded 20 kV at the center of the sample. Figure 4.21 shows a comparison between all charging methods that were introduced in this study as well. It is noticed from this figure that the maintenance practice on hot sticks of wiping should be given special consideration prior to live-line work, especially during the dry/winter months for HVDC live-line work. More charge was deposited on the surface compared to the other methods used in this study. Methods may need to be adapted such that tools are cleaned, wiped and prepared the day prior to live line work so that significant charge does not exist. Surface charge on FRP tools has been shown to decay at a slow rate.

4.2 Determination of DC Flashovers

The results of the DC flashover testing on the tested insulator samples is presented and discussed below. To present the flashover results, box plots are used. A box plot shows the range of flashover voltages which include the maximum, minimum, and median of the data (red line). The bottom and top of the blue box represent the first and third quantiles, respectively.

4.2.1 FRP Insulator Sample

Figure 4.22 shows box plots for the flashover voltages under negative and positive voltages for three conditions: i) a clean and charge free large FRP sample (strain pole-type/38.1

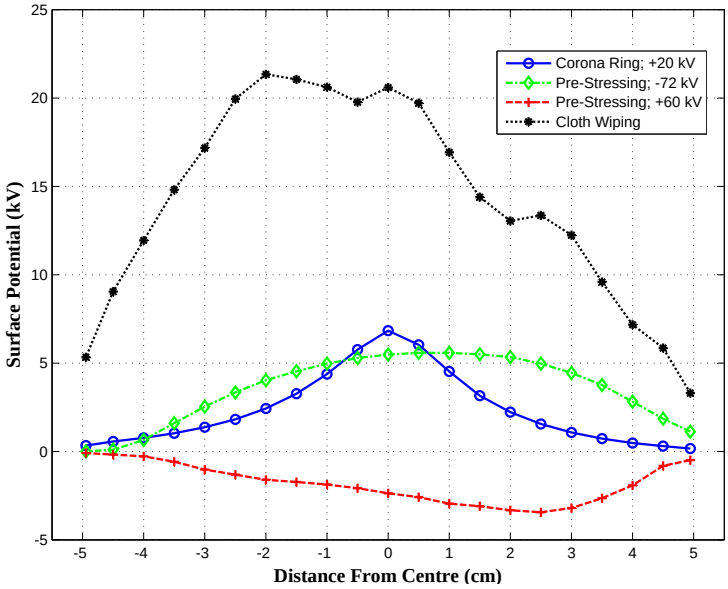

Fig. 4.21: A comparison of the surface potential distributions for a FRP insulator sample charged using different methods.

mm diameter), ii) same sample charged using a positive voltage from the ring of needles at +20 kV, and iii) with negative charging from the ring of needles at 20kV. Each test was repeated approximately 5 times.

It can be seen that the negative flashover voltage for a clean sample is lower than that of a positive flashover. Under negative and positive applied voltages (Figures 4.22a and 4.22b), an FRP sample with positive charge on the surface will flashover at a lower voltage than a clean sample whereas with the presence of negative charges it will flashover at a higher voltage. The majority of all the flashovers occurred with no leakage current on a μA scale. The largest measured leakage current prior to flashover was 115 μA. Small current discharges could be noticed on the micrometer in the range of 0.1 to 0.3 μA of the same polarity of the applied voltage, but mostly they occurred with absolutely no prior warning. Evidence of the arc burns was always seen on the negative electrodes indicating that flashovers were always positive streamers from the positive to negative electrode.

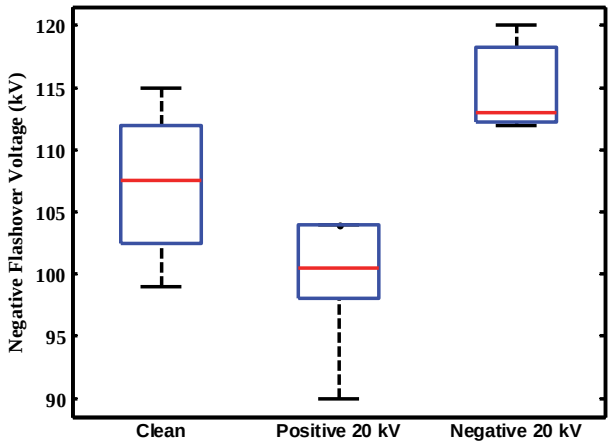

(a) Negative flashover voltage

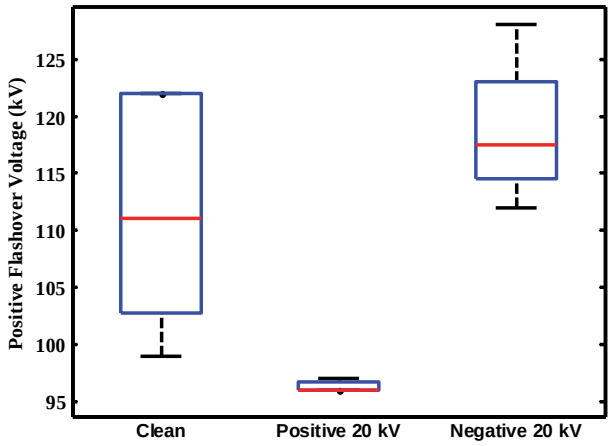

(b) Positive flashover voltage

Fig. 4.22: Flashover voltage of the large FRP (38.1 in mm diameter) sample for the 3 cases of clean FRP, charged using the ring of needles at +20kV, and charged using the ring of needles at -20kV when the applied DC flashover voltage is a) negative, and b) positive.

The results shown in Figure 4.22a also follow the pattern of the results for an SIR sample with negative applied polarity as presented in [2]. The results in Figures 4.22a 4.22b also correlate with data presented in Table 2.1. The results also confirm the conclusions of Meng *et al.* [34] whom concluded that negative charge on the surface of an insulator weakens positive streamers. It would seem that positive charge on the surface enhances the positive streamers.

Figure 4.23 shows the results for pre-stressing the sample for 2 minutes by applying a DC voltage at one electrode while the other electrode is grounded, and then performing a flashover test.

In this case, the smaller hot stick type FRP sample (32 mm in diameter) was used. Figure 4.23a shows that when the sample is pre-stressed at -72 kV for 2 minutes, the flashover voltage is reduced compared to the clean sample. This is similar to the results of Figure 4.22a, and with the discussion presented in Section 4.1.3.2. This confirms that under pre-stressing with a negative voltage, the surface will have a positive charge on the surface, thus it is expected that the flashover voltage will be reduced. In Figure 4.23b, it is demonstrated that when pre-stressing with a positive voltage and then raising the voltage to flashover, there was a rise in the median flashover voltage. This is also expected, and consistent with the results shown in Section 4.1.3.2, that when pre-stressing the sample with a positive voltage, a negative surface charge will be developed on the insulator surface thus increasing the flashover voltage as shown in Figure 4.22b. As it has been shown in Section 4.1.3.2, positive pre-stressing does not create as significant amount of negative charge as using the ring of needles or negative pre-stressing, therefore there is not a considerable difference between a clean FRP sample or positive pre-stressing.

The results for pre-stressing presented in Figure 4.23 support the work of Manitoba Hydro [3], [4] as the negative polarity fast flashovers were observed at voltages less than system operating, low humidity, with leakage current less than 2 mA, and negative pre-

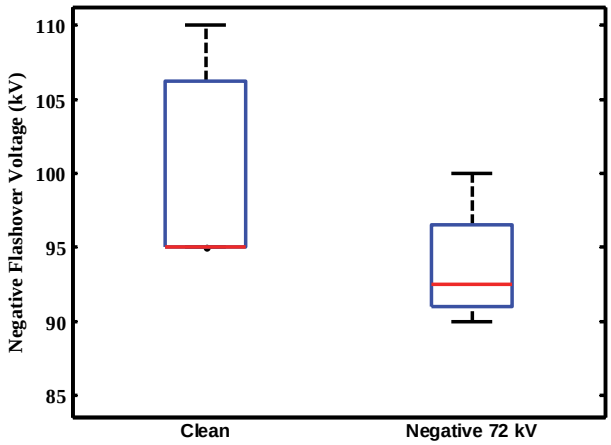

(a) Negative flashover voltage

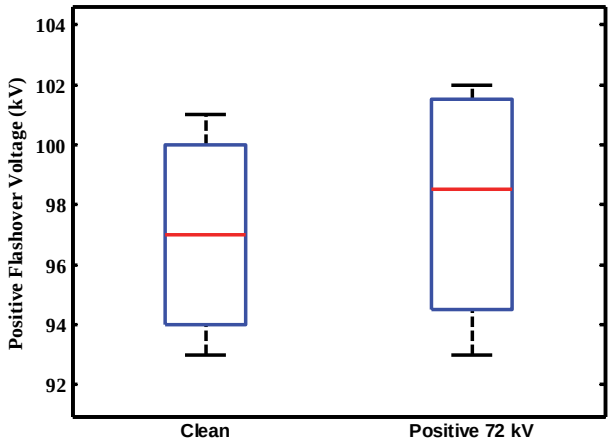

(b) Positive flashover voltage

Fig. 4.23: A comparison of the flashover voltage of a clean FRP (32 mm in diameter) sample with the cases of a) pre-stressing at -72 kV and negative applied voltage, and b) prestressing at +72 kV and positive applied voltage.

stressed voltage. In this research flashovers occurred on a 3-m FRP hot stick under applied negative voltage. Under negative pre-stressing voltage, a positive surface charge is formed along the surface of the tool which would decrease the flashover voltage. Under positive applied voltage, a negative surface charge along the tool surface and an increase in the flashover voltages are seen. This is a possible explanation for why no positive polarity fast flashovers were observed and only occurred under negative polarity.

A test was also carried out for the large FRP sample where the ground side copper ring was removed. The sample was clean prior to the test and the voltage was raised to flashover. The maximum output voltage at the energized electrode was 130 kV, due to voltage drop across 100 MΩ resistor. The sample was able to withhold the applied stress of 130 kV for 20 seconds before flashover. This rise in flashover voltage corresponds well with the previous surface charge studies. When a corona ring is removed only charges of the same polarity (negative in this case) will be produced along the surface of the insulator sample. Also by eliminating the copper ring we have removed the triple point junction where a positive streamer would have propagated from. Thus is this case we were able to cause the flashover voltage to rise above what we obtained previously with a negative voltage applied to a clean sample with corona rings at both ends. This would be similar in theory to the streamer inhibitor which has been developed to suppress positive streamers from the ground electrode under DC conditions and can prevent fast flashovers [4], [64]. They are composed of double toroid electrodes and wrapped with a thin fabric layer of stainless steel cloth. The streamer inhibitor is designed to operate in a corona glow mode such that positive streamers are inhibited from forming. The thin wires used on the electrode cause a increase in the electric field required for corona inception and increases the rate of rise of voltage for which below this critical value streamers will be suppressed [56]. They can be used to protect aerial devices or could be used on transmission structures. A photograph of the streamer inhibitor installed over the collector band of an aerial device boom is shown in Figure 4.24.

In our case, the removal of the triple point junction was an effective way to inhibit positive streamers at lower voltages. In the case of the aerial device boom, the installation of the inhibitor device over the sharp edges of the collector band is a good solution.

Flashovers have been show to occur on FRP samples at stresses as low as 700 kV/m (7 kV/cm). This compares well with the work of Allen *et al.* [28] whom suggested that electric fields stresses of 700 kV/m and higher are very likely to cause flashovers across the gap. Stable propagation of positive streamers occurs at electric field stresses of 500 kV/m [42].

4.2.2 FRP Insulator Sample with Sheds

As described earlier in Sections 2.2 and 2.3.1, sheds have proven to be successful in increasing the voltages required for the flashover of insulator samples and 3-m hot sticks. They were shown to mitigate the fast flashovers under negative polarity and aid in the blocking and weakening of the surface streamer component known as "fast" [3, 36].

Polymer, heat-shrinkable sheds were installed on the large 38.1 mm FRP sample. The sheds had an overhang, from the surface, of 30 mm. Although a larger diameter of shed would be more effective at streamer mitigation, it could impact the ability of a live-line worker to see the end of the tool during the work procedure. Flashovers were carried out on clean samples with the shed located at the ground end, energized side and in the middle of the sample. Figure 4.25 shows the FRP insulator sample with the polymer sheds installed. For the shed at the grounded side the sample was reversed.

The testing revealed that for the negative applied voltage polarity with the shed at the energized side (negative), as shown in Figure 4.25b, a flashover could not be achieved. The voltage was held at 130 kV for over one minute in the absence of flashover as revealed in Figure 4.26a. When the shed was located in the middle the flashover voltage was reduced and the lowest flashover voltages were seen when the shed was located at the ground side. In Figure 4.26b it is illustrated that for positive flashover voltage, the flashover voltage was

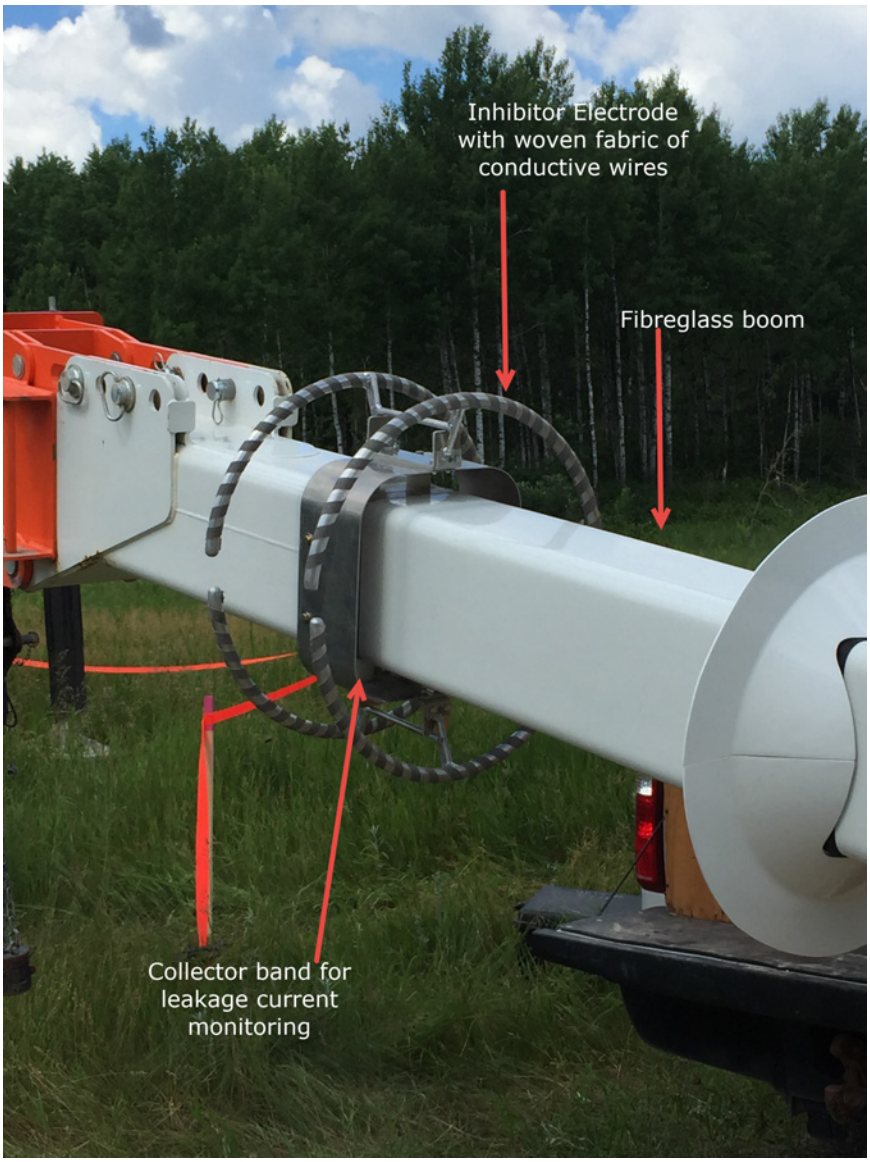

Fig. 4.24: Streamer inhibitor electrode installed on ground side of boom of an aerial device. Photograph courtesy of Manitoba Hydro.

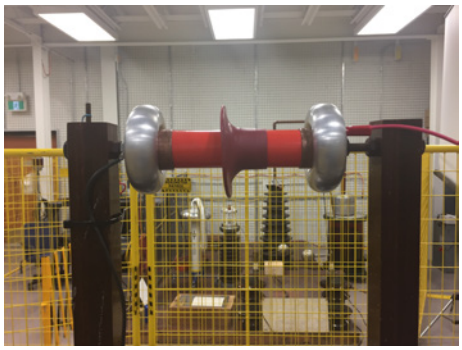

(a) FRP sample with the shed in middle middle

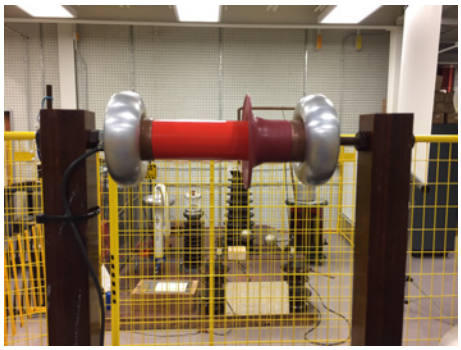

(b) FRP sample with the shed at the energized side (right)

Fig. 4.25: FRP insulator sample with polymer shed located at a) middle of sample and at b) energized side.

lowest when the shed was located at the energized side (positive). The flashover voltage slightly increased with the shed located at the middle but was the highest when the shed was located at the ground side. Based on this study it appears the best locations for sheds would be a shed located at both the energized and ground side of a FRP tool. For workers this would mean a shed could be installed as a marker for their minimum approach distance and a shed can be installed further up the stick near the end but no so close as to hamper their visual sight of the end of the tool. Earlier research had shown the best placement of a shed was near the ground side with negative applied DC voltage at the source side. In this case a positive pulsed needle located at the ground initiated streamers [36]. Other research also showed the best location for the shed was at the source of streamer initiation [30]. These were under very different electrode configurations however. In [3] it is discussed that two sheds on a hot stick completely eliminated fast flashovers. They were located at 1/3 and 2/3 of the FRP hot stick's 3 m length. With one shed in the middle, the flashovers were greatly reduced but not completely eliminated. The range and error of flashover values is noted to decrease as well with the sheds. Based on this research the preferred location for

the shed is always at the negative cathode.

One can visually observe the impact of the sheds on the streamer as Figure 4.27 shows how the streamer/arc travels over the shed compared to along the surface when no shed exists.

4.2.3 SIR Insulator Sample

Additional flashover testing was performed on the large SIR sample to compare with the results of Kumara *et al.* [2]. In this paper, the SIR sample had a 30 mm diameter and was of 10.8 cm length. Due to the electrode design the actual length is 10.2 cm between the electrodes. The sample was tested under negative DC voltage until flashover and the average was determined to be about 88 kV. The standard deviation of the flashover voltages was noted to decrease with charge present on the surface as compared to with charge.

The results of the testing on the large SIR sample under negative DC is shown in Figure 4.28. Similar to [2], the range of flashover values decreased for SIR with charges present on the surface. The flashover voltage decreased with positive charge present on the surface and increased with negative charge on the surface when comparing the 50 % median flashover value. The flashover values are higher in this study due to the longer length of the sample. For the SIR material, more cases of higher leakage current were noted than for the FRP samples. Although many flashovers occured with no prior leakage current, and some in the 0.1 μA range, others occured with leakage currents as high as 300 μA.

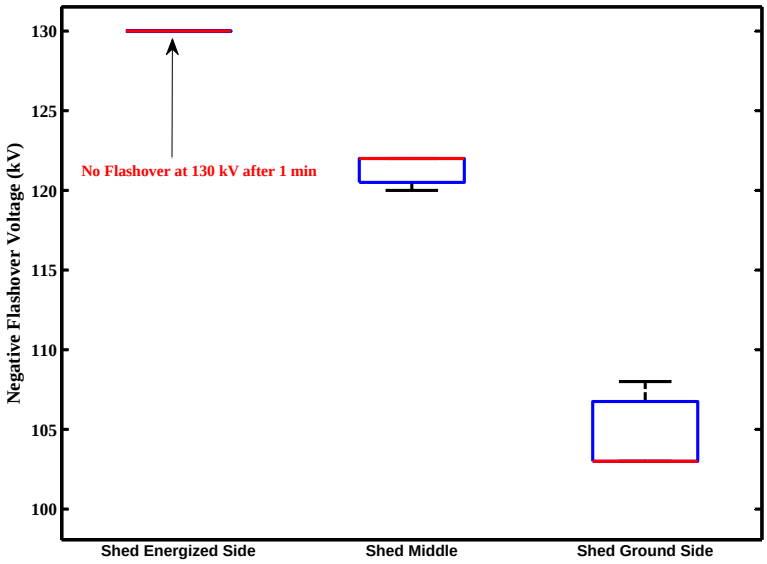

(a) Negative flashover voltage for shed location

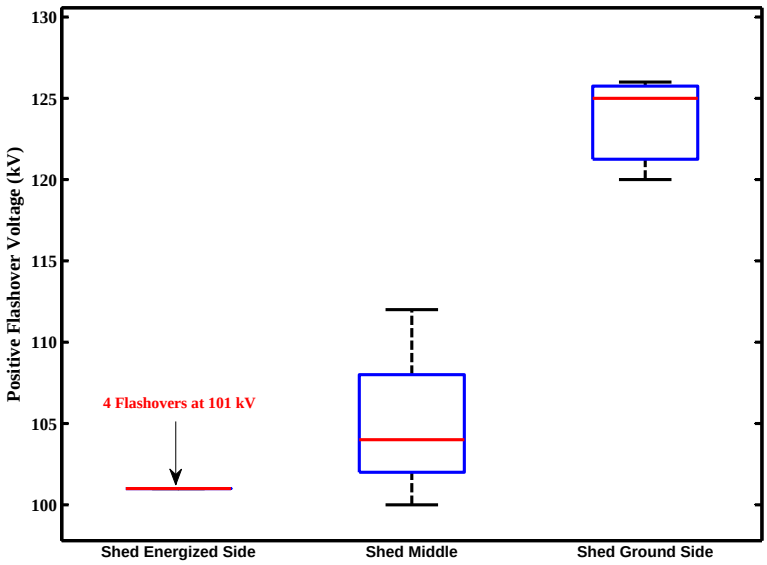

(b) Positive flashover voltage for shed location

Fig. 4.26: DC Flashover voltage of the FRP (38.1 mm diameter) sample for the 3 cases of shed located at energized side (right), middle and grounded side (left) when the applied DC voltage is a) negative, and b) positive.

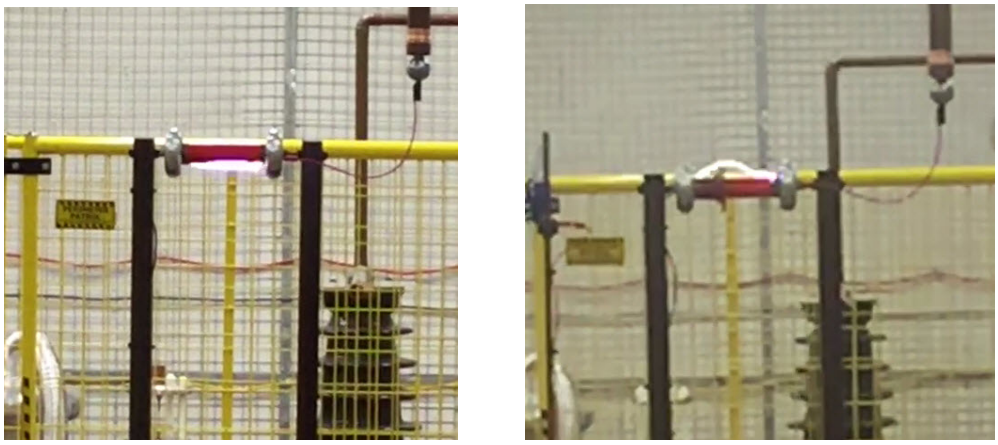

(a) FRP - no shed **(b)** FRP - shed grounded side

Fig. 4.27: Screenshot captured from videos of flashovers for a) no shed on an FRP insulator b) shed located at ground side of FRP insulator.

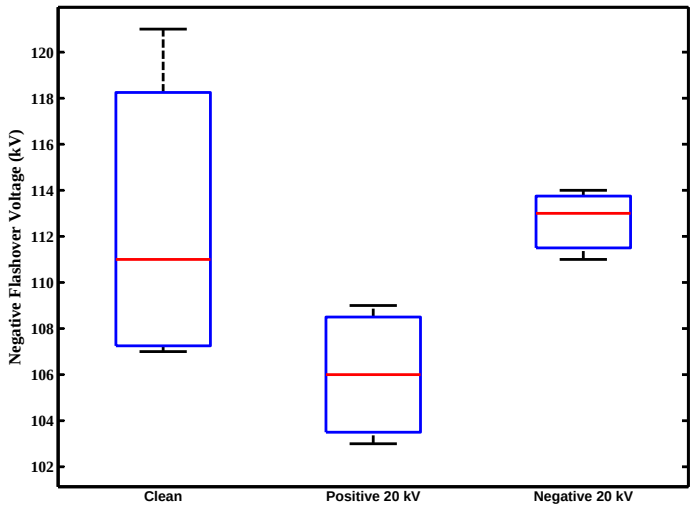

Fig. 4.28: DC Flashover voltage of the large SIR (43 mm diameter) under negative DC applied voltage.

The results of testing for the DC surface charging and flashover characteristics have been presented and discussed. In the following chapter the conclusions will be summarized

for the thesis based on the results obtained in this chapter.

Chapter 5

Conclusions

The thesis has investigated the effects of DC corona on the surface charge and flashover characteristics of an FRP hot stick. An understanding has been provided, of the impact of surface charges and their characteristics on the DC flashover voltage of FRP tools, which is essential to consider in live-line working standards, live-line methods, and flashover prevention.

Three different charging techniques were used for surface charging of FRP, SIR and wood cylindrical insulator samples. The measured surface potentials are used to calculate charge density distributions using the probe response matrix. A negative charging voltage used with the ring of needles produces higher surface potentials than that produced with a positive charging voltage. The profiles of both measured surface potentials and calculated surface charge densities have bell shapes, and clearly show the consistency between measurements and numerical calculations. The total amount of charges deposited on the surfaces increases linearly as the magnitude of the applied corona charging voltage increases. Under negative DC charging voltage (-20 kV) the larger FRP and SIR sample had the most charge on the surface while under positive charging (+20 kV) all samples (except wood) had similar total charge on the surface. The deposited charges are widely spread on the sample surface

as the applied corona charging voltage increases. Most of the charges (80%) are deposited on the surface during the first 2 minutes. Charging the FRP sample by pre-stressing with different values of positive or negative DC voltages for 2 minutes, results in deposition of hetero-charges along the entire sample surface with a smaller amount of homo-charges close to the electrodes. Both electrodes should have corona discharge to allow for hetero-charge deposition on the surface. Otherwise, the entire surface will be charged with homo-charges. Wiping hot sticks with a cotton cloth and then by a silicone wiping cloth is a routine done in the field, before live-line work, to be sure that there is no pollution contaminates on the surface of the hot stick. Wiping FRP samples results in high accumulation of positive charges on the surface and should be given special consideration before live line work. The decay of charge is faster on wood and SIR materials than FRP materials. SIR and wood have a higher rate of decay and are faster to neutralize. Back discharges were experienced with increasing humidity, due to the lowered inception voltage, and are found to occur if the electric field strength between the surface and the tip of the needle is larger than 30 kV/cm. It was determined that increasing the tip of needle (ring of needles) to surface distance increases the total amount of charge on the surface of the insulator. During this testing it is noted that SIR material collects more total charge than FRP material on the surface. The observed differences between negative and positive corona are presented as well.

In the DC flashover tests of the study, two different charging techniques were used for depositing surface charges on the FRP samples and flashover voltages under DC conditions were measured. It was demonstrated that for the given electrode configuration, the negative flashover voltage is lower than the positive flashover voltage for a clean sample. For both positive and negative voltages, the flashover voltage is reduced when positive charge is present on the insulator surface while it is conversely increased with negative charge on the surface. Under positive pre-stressing conditions, the positive flashover voltage is slightly

increased while under negative pre-stressing the negative flashover voltages decreases for the FRP insulator as compared to the clean case. Removal of the ground side copper ring raised the flashover value for the FRP sample.

Sheds were installed on the FRP tools at different locations and it was determined that under negative polarity the sheds should be installed at the energized side and for positive polarity the sheds should be located at the ground side. From a live-line working perspective, sheds should be installed as a marker for the minimum approach distance and at the energized side. Flashover profiles were found for SIR under negative voltage and were in agreement with the research in [2]. Flashovers were repeatedly produced with no noteworthy leakage current prior to discharge and in a low humidity environment.

It has been demonstrated that wiping hot sticks prior to live-line work can produce substantial positive charges on the surface of an FRP tool prior to live-line work and surface charges on FRP tools will reside for a significant period of time. Changes in this FRP tool maintenance practice prior to live-line work should be given consideration, especially during dry/winter months, before HVDC live-line work as the flashover voltage may be reduced with the presence of positive charges on the surface of the tool. The solution for DC flashover prevention under normal working conditions may not be to increase the length (leakage distance) of the tool as for pollution type flashovers, but instead, consideration should be given to the use of sheds or inhibitor electrodes for the FRP tools and aerial devices under DC operating conditions to increase the flashover voltage as it has been proven that the presence of charges on the surface of an insulator can influence and reduce the flashover voltage. Leakage current monitoring itself can not be considered a satisfactory protection scheme for booms and ladders for HVDC live-line work due to the absence of leakage current prior to flashovers. Consideration should also be given to ensure corona free tools and equipment as well as materials with increased surface charge decay times and less charge accumulation developed for DC live-line work. Standards for HVDC live-line

working should give consideration to the effects of space charge on FRP tools.

5.1 Future Work

- Future work should be carried out to determine the effects of light pollution (salt contamination) and icing on the surface charge profiles and flashover characteristics of FRP tools.
- Further studies should also be developed to investigate the impact of humidity in conjunction with the above scenarios and also for clean samples with pre-existing charge.
- Testing should also be carried on longer samples at higher DC voltages (actual length of FRP tools used for live-line work) to develop repeatable laboratory tests with the absence of leakage current. Verify if results for short samples can be linearized.
- Larger diameter insulators should be investigated to determine if there is truly an impact.
- The role of a closed space versus an outdoor environment should be given consideration for DC testing and how that may impact space charge and flashover characteristics.
- Investigate the possibility of positive streamer based flashovers on glass insulators to better gain an understanding of anomalous flashovers.
- Electrode design should also be further studied for optimum space charge production.
- Perform positive flashover tests on SIR insulator sample.
- Test the performance of sheds under positive and negative applied voltage with pre-existing surface charge until flashover.
- Simulation models should be developed to produce time varying dynamic simulations of the research to date for clean insulators and then for lightly polluted insulators. The impact of linear versus non-linear contamination should be investigated.

- An inhibitor type electrode should be tested in the laboratory for flashover mitigation.
- Further testing should be completed with partial discharge monitoring to understand if a protective safety tool could be developed to warn of possible flashovers under DC conditions.
- The above work should be repeated also for AC conditions.
- Determine if the material used for live-line tools could be improved such that the surface charge decay is faster and the surface accumulates less charge.
- Investigate the flashover performance of an FRP tool, with pre-existing charge, for a transient impulse voltage superimposed on the steady-state DC voltage.
- Determine if back discharges occur during turning off of the power supply or when it is grounded. Develop a method to mitigate or correct the back discharge.

References

[1] G. Asplund, "Sustainable energy systems with HVDC transmission," in *IEEE Power Engineering Society General Meeting, 2004*, June 2004, pp. 2299–2303 Vol.2.

[2] S. Kumara, S. Alam, I. R. Hoque, Y. V. Serdyuk, and S. M. Gubanski, "Dc flashover characteristics of a polymeric insulator in presence of surface charges," *IEEE Transactions on Dielectrics and Electrical Insulation*, vol. 19, no. 3, pp. 1084–1090, June 2012.

[3] W. Mcdermid and D. R. Swatek, "Experience with dielectric surfaces of FRP tools used in live line work," *IEEE Transactions on Dielectrics and Electrical Insulation*, vol. 21, no. 6, pp. 2415–2427, December 2014.

[4] W. McDermid, "Characterization of fast flashover of external insulation," in *Conference Record of the 2008 IEEE International Symposium on Electrical Insulation*, June 2008, pp. 510–513.

[5] ——, "Experience with electrical testing of aerial devices for use at 69-500 kv," in *2013 IEEE Electrical Insulation Conference (EIC)*, June 2013, pp. 402–403.

[6] M. Ghassemi and M. Farzaneh, "Calculation of minimum approach distances for tools for live-line working under freezing conditions," *IEEE Transactions on Dielectrics and Electrical Insulation*, vol. 23, no. 2, pp. 987–994, 2016.

[7] W. Mcdermid, D. Swatek, and J. Laninga, "Observation of and Response to Fast Flashover of FRP surfaces," in *CIGRÉ D1-097 - Submitted*, 2017.

[8] "IEEE guide for maintenance methods on energized power lines." IEEE 519-2009.

[9] "Live working minimum approach distances for ac systems in the voltage range 72.5 kv to 800 kv a method of calculation." IEC 61472-2013.

[10] "Standard specification for fiberglass-reinforced plastic (FRP) rod and tube used in live line tools." ASTM F711-02(2013).

[11] "500 kV Flashover 2002 03 20 Interim Report," Manitoba Hydro, Tech. Rep.

[12] S. Kumara, I. R. Hoque, S. Alam, Y. V. Serdyuk, and S. M. Gubanski, "Surface charges on cylindrical polymeric insulators," *IEEE Transactions on Dielectrics and Electrical Insulation*, vol. 19, no. 3, pp. 1076–1083, June 2012.

[13] J. Kindersberger and C. Lederle, "Surface charge decay on insulators in air and sulfurhexafluorid - part II: measurements," *IEEE Transactions on Dielectrics and Electrical Insulation*, vol. 15, no. 4, pp. 949–957, August 2008.

[14] "Performance requirements for tools for live line work on HVDC systems - intial full-scale testing," EPRI Report 3002000856, Dec. 2013.

[15] "Space Charge and dc Bias effects on HVDC Live Line Working Tools," EPRI Report 3002007637, Dec. 2016.

[16] M. Amer, J. Laninga, D. Swatek, W. Mcdermid, and B. Kordi, "Surface charging characteristics of fiberglass reinforced plastic (FRP) hot sticks under HVDC operating conditions," *accepted for presentation at 2017 IEEE Conf. Electrical Insulation and Dielectric Phenomenon (CEIDP)*, Oct.,2017.

[17] J. Laninga, M. Amer, D. Swatek, W. Mcdermid, and B. Kordi, "HVDC flashover performance of fibreglass reinforced (FRP) hot sticks considering space charges," *accepted for presentation at 2017 IEEE Conf. Electrical Insulation and Dielectric Phenomenon (CEIDP)*, Oct.,2017.

[18] F. Wang, Q. Zhang, Y. Qiu, and E. Kuffel, "Insulator surface charge accumulation under dc voltage," in *Conference Record of the the 2002 IEEE International Symposium on Electrical Insulation*, Apr 2002, pp. 426–429.

[19] Y. Yamano, A. Ohashi, K. Kato, H. Okubo, and Y. Hakamata, "Charging characteristics on dielectric surface by different charging processes in vacuum," *IEEE Transactions on Dielectrics and Electrical Insulation*, vol. 6, no. 4, pp. 464–468, Aug 1999.

[20] G. Q. Su, H. B. Mu, W. W. Shen, B. P. Song, Y. Lang, and G. J. Zhang, "Surface charge accumulation on silicon rubber material under DC voltage in atmosphere," in *Annual Report - Conference on Electrical Insulation and Dielectric Phenomena, CEIDP*, 2013, pp. 456–459.

[21] S. Kumara, Y. V. Serdyuk, and S. M. Gubanski, "Surface charge decay on polymeric materials under different neutralization modes in air," in *IEEE Transactions on Dielectrics and Electrical Insulation*, vol. 18, no. 5, 2011, pp. 1779–1788.

[22] H. Sjöstedt, S. M. Gubanski, and Y. V. Serdyuk, "Charging characteristics of EDPM and silicone rubbers deduced from surface potential measurements," in *IEEE Transactions on Dielectrics and Electrical Insulation*, vol. 16, no. 3, 2009, pp. 696–703.

[23] B. Du and M. Xiao, "Influence of surface charge on DC flashover characteristics of epoxy/BN nanocomposites," *IEEE Transactions on Dielectrics and Electrical Insulation*, vol. 21, no. 2, pp. 529–536, 2014.

[24] N. L. Allen and A. Ghaffar, "The conditions required for the propagation of a cathode-directed positive streamer in air," *Journal of Physics D: Applied Physics*, vol. 28, no. 2, pp. 331–337, 1995.

[25] N. Allen and A. Ghaffar, "Propagation of positive streamers over insulating surfaces in air," in *Proceedings of 1995 Conference on Electrical Insulation and Dielectric Phenomena*, 1995, pp. 447–450.

[26] N. L. Allen and P. N. Mikropoulos, "Dynamics of streamer propagation in air," *Journal of Physics D: Applied Physics*, vol. 32, no. 8, pp. 913–919, 1999.

[27] M. Akyuz, L. Gao, V. Cooray, T. G. Gustavsson, S. M. Gubanski, and A. Larsson, "Positive streamer discharges along insulating surfaces," *IEEE Transactions on Dielectrics and Electrical Insulation*, vol. 8, no. 6, pp. 902–910, 2001.

[28] N. Allen, A. Hashem, H. Rodrigo, and B. Tan, "Streamer development on silicone-rubber insulator surfaces," *IEE Proc.-Sci. Meas. Technol*, vol. 151, no. 1, pp. 31–38, 2004.

[29] B. Tan, H. Rodrigo, and N. Allen, "Positive corona progression over profiled insulator surfaces near the breakdown condition," *Science Measurement Technology IET*, vol. 2, no. 4, pp. 196–207, 2008.

[30] N. L. Allen, B. H. Tan, and H. Rodrigo, "Progression of positive corona on cylindrical insulating surfaces part II: Effects of profile on corona," *IEEE Transactions on Dielectrics and Electrical Insulation*, vol. 15, no. 2, pp. 390–398, 2008.

[31] P. N. Mikropoulos, "Streamer propagation along room-temperature-vulcanised silicon-rubber-coated cylindrical insulators," *IET Science, Measurement Technology*, vol. 2, no. 4, pp. 187–195, July 2008.

[32] P. N. Mikropoulos, C. A. Stassinopoulos, and B. C. Sarigiannidou, "Positive streamer propagation and breakdown in air: The influence of humidity," *IEEE Transactions on Dielectrics and Electrical Insulation*, vol. 15, no. 2, pp. 416–424, 2008.

[33] J. Hui, Z. Guan, L. Wang, and Q. Li, "Variation of the dynamics of positive streamer with pressure and humidity in air," *IEEE Transactions on Dielectrics and Electrical Insulation*, vol. 15, no. 2, pp. 382–388, 2008.

[34] X. Meng, H. Mei, L. Wang, Z. Guan, and J. Zhou, "Characteristics of streamer propagation along insulation surface: quantitative influence of permittivity and surface properties," *IEEE Transactions on Dielectrics and Electrical Insulation*, vol. 23, no. 5, pp. 2867–2874, October 2016.

[35] X. Meng, H. Mei, C. Chen, L. Wang, Z. Guan, and J. Zhou, "Characteristics of streamer propagation along the insulation surface: Influence of dielectric material," *IEEE Transactions on Dielectrics and Electrical Insulation*, vol. 22, no. 2, pp. 1193–1203, 2015.

[36] X. Meng, H. Mei, L. Wang, and Z. Guan, "Characteristics of Streamer Propagation along Insulation Surface: Influence of Shed Configuration," *IEEE Transactions on Dielectrics and Electrical Insulation*, vol. 23, no. 4, pp. 2145–2155, 2016.

[37] Y. V. Serdyuk, a. Larsson, S. M. Gubanski, and M. Akyuz, "The propagation of positive streamers in a weak and uniform background electric field," *Journal of Physics D: Applied Physics*, vol. 34, no. 4, pp. 614–623, 2001.

[38] M. Farzaneh and W. Chisholm, *Insulators for Icing and Polluted Environments*, ser. IEEE Press Series on Power Engineering. Wiley, 2009.

[39] N. L. Allen and P. N. Mikropoulos, "Streamer propagation along insulating surfaces," *IEEE Transactions on Dielectrics and Electrical Insulation*, vol. 6, no. 3, pp. 357–362, 1999.

[40] A. Luque, V. Ratushnaya, and U. Ebert, "Positive and negative streamers in ambient air: modelling evolution and velocities," *Journal of Physics D: Applied Physics*, vol. 41, no. 23, p. 234005, 2008.

[41] T. M. P. Briels, J. Kos, G. J. J. Winands, E. M. van Veldhuizen, and U. Ebert, "Positive and negative streamers in ambient air: measuring diameter, velocity and dissipated energy," *Journal of Physics D: Applied Physics*, vol. 41, p. 234004, 2008.

[42] J. Qin and V. P. Pasko, "On the propagation of streamers in electrical discharges," *Journal of Physics D: Applied Physics*, vol. 47, no. 43, p. 435202, 2014.

[43] M. Ghassemi, M. Farzaneh, and W. A. Chisholm, "Three-dimensional FEM electrical field calculation for FRP hot stick during EHV live-line work," *IEEE Transactions on Dielectrics and Electrical Insulation*, vol. 21, no. 6, pp. 2531–2540, 2014.

[44] M. Ghassemi, M. Farzaneh, W. A. Chisholm, and J. Beattie, "Potential and electric field calculation along a FRP live-line tool under cold and icing conditions," *EIC 2014 - Proceedings of the 32nd Electrical Insulation Conference*, no. June, pp. 218–222, 2014.

[45] M. Ghassemi and M. Farzaneh, "Effects of tower, phase conductors and shield wires on the electrical field around a tower window during live-line work," *IEEE Transactions on Dielectrics and Electrical Insulation*, vol. 22, no. 6, pp. 3413–3420, 2015.

[46] M. Ghassemi and M. Farzaneh, "Coupled Computational Fluid Dynamics and Heat Transfer Modeling of the Effects of Wind Speed and Direction on Temperature Increase of an Ice-Covered FRP Live-Line Tool," *IEEE Transactions on Power Delivery*, vol. 30, no. 5, pp. 2268–2275, 2015.

[47] I. Ndiaye, M. Farzaneh, and I. Fofana, "A Comparative Study of Positive and Negative Streamer Development along an Ice Surface," *Electrical Insulation and Dielectric Phenomena, 2008. CEIDP 2008. Annual Report Conference on*, pp. 650–653, 2008.

[48] I. Ndiaye, M. Farzaneh, and K. D. Srivastava, "On the streamer stability field for a positive discharge propagating along an ice surface," *2008 International Conference on High Voltage Engineering and Application, ICHVE 2008*, pp. 40–44, 2008.

[49] M. Darveniza, T. K. Saha, S. Wright, and M. A. Leijon, "Effects of deposited charge on impulse test techniques for polymer insulators," *CIGRE Symposium on Behaviour of Electrical Equipment and Components in Tropical Environments*, vol. 4, no. 200-11, pp. 1–4, 2001.

[50] R. Montano, Sjo, X, H. Stedt, Y. Serdyuk, and S. Gubanski, "Effect of surface charges on the flashover voltage characteristics of polymeric materials: Comparison between theory and practice," *Electrical Insulation and Dielectric Phenomena, 2007. CEIDP 2007. Annual Report - Conference on*, pp. 368–371, 2007.

[51] J. Blennow and T. Sörqvist, "Effect of Surface Charge on Flashover Voltage of Polymer Materials," in *Proceedings of the 19th Nordic Insulation Symposium*, Trondheim,Norway, June 2005.

[52] M. S. A. A. Hamam, S. Ochiai, and C. Burns, "Effect on 50% flashover voltage due to accumulated charges on the surface of polymer insulators," *Proceedings of the 3rd International Conference on Properties and Applications of Dielectric Materials*, pp. 4–7, 1991.

[53] S. Kumara, Y. Serdyuk, and S. Gubanski, "Simulation of surface charge effect on impulse flashover characteristics of outdoor polymeric insulators," *IEEE Transactions on Dielectrics and Electrical Insulation*, vol. 17, no. 6, pp. 1754–1763, 2010.

[54] K. Takabayashi, T. Furuyashiki, T. Sakai, and H. Okubo, "DC partial discharge and flashover characteristics and charging activity on solid insulator in air," in *2016 IEEE Conference on Electrical Insulation and Dielectric Phenomena (CEIDP)*, Oct 2016, pp. 352–355.

[55] B. Qi, C. Gao, C. Li, L. Zhao, and X. Sun, "Effect of surface charge accumulation on flashover voltage of GIS insulator in SF6 under DC and AC voltages," in *2015 IEEE Conference on Electrical Insulation and Dielectric Phenomena (CEIDP)*, Oct 2015, pp. 848–851.

[56] F. Rizk and G. Trinh, *High Voltage Engineering.* Taylor & Francis, 2014. [Online]. Available: https://books.google.ca/books?id=XTcyAwAAQBAJ

[57] T. Gilles, *Advances in the Formulations and Accuracy of the Method of Moments Applied to Electromagnetics*, ser. Thèses de l'École polytechnique de

Louvain. Presses universitaires de Louvain, 2011. [Online]. Available: https://books.google.ca/books?id=hho-DSIlUNIC

[58] "IEEE standard for high-voltage testing techniques," *IEEE Std 4-2013 (Revision of IEEE Std 4-1995)*.

[59] "High-voltage test techniques - Part 1: General defintions and test requirements," *IEC 60060-1, Edition 3.0 2010-09*.

[60] D. Faircloth and N. Allen, "High resolution measurements of surface charge densities on insulator surfaces," *IEEE Transactions on Dielectrics and Electrical Insulation*, vol. 10, no. 2, pp. 285–290, 2003.

[61] J. Chen and J. H. Davidson, "Model of the Negative DC Corona Plasma: Comparison to the Positive DC Corona Plasma," *Plasma Chemistry and Plasma Processing*, vol. 23, no. 1, pp. 83–102, 2003.

[62] Arshad, A. Nekahi, S. McMeekin, and M. Farzaneh, "Flashover Characteristics of Silicone Rubber Sheets under Various Environmental Conditions," *Energies*, vol. 9, no. 9, p. 683, 2016. [Online]. Available: http://www.mdpi.com/1996-1073/9/9/683

[63] D. J. Holtzhausen and D. W. Vosloo, "High Voltage Engineering Practice and Theory," 2003. [Online]. Available: http://www.dbc.wroc.pl/Content/3458/high_voltage_engineering.pdf

[64] F. A. Rizk and A. Rizk, "Flashover protection device: wet/dry glow-based streamer inhibitor," United States Patent Application 11/753,961; Canadian Patent Application 2,590,146;PCT/CA2007/000936.

[65] S. Yamaguchi, M. A. Noras, B. T. Williams, and J. Kieres, "New Surface Electrostatic Potential Measurement Technology," in *Munich, Germany presented at the ESD Forum 2007*, 2007.

[66] W. Feng, Q. Yuchang, L. Xinran, W. Pfeiffer, and E. Kuffel, "Insulator surface charge measurement using an improved capacitive probe," *Plasma Science & Technology*, vol. 8, no. 5, pp. 565–568, 2006.

[67] A. Kumada, Y. Shimizu, M. Chiba, and K. Hidaka, "Pockels surface potential probe and surface charge density measurement," *Journal of Electrostatics*, vol. 58, no. 1-2, pp. 45–58, 2003.

[68] A. Kumada, S. Okabe, and K. Hidaka, "Resolution and signal processing technique of surface charge density measurement with electrostatic probe," *IEEE Transactions on Dielectrics and Electrical Insulation*, vol. 11, no. 1, pp. 122–129, 2004.

[69] M. A. Noras, "Non-contact surface charge/voltage measurements Capacitive probe-principle of operation," pp. 1–8, 2002. [Online]. Available: http://www.trekinc.com/pdf/3001_Vibrating_Probe.PDF

[70] I. D. Baikie, "KP Technology - Introduction to the Kelvin Probe for High Resolution Work Function Measurements," 2009. [Online]. Available: http://kelvinprobe.com/MRSSeminar-Notes.pdf

[71] Trek, "Measurement and Power Solutions Brochure," 2015. [Online]. Available: http://connect.physicsworld.com/Journals//2015/09/11/Trek-Brochure-Amp-ESVM-2015.pdf

[72] M. Noras and A. Pandey, "Evaluation of Surface Charge Density with Electrostatic Voltmeter-Measurement Geometry Considerations," in *2008 IEEE, Industry Applications Society Annual Meeting, IAS '08. IEEE*, 2008, pp. 1–6.

Appendix A

Surface Charge Measurement Techniques

This appendix of the thesis discusses the surface charge measurement technique applied in the thesis.

A.1 Surface Charge Measurement Techniques

The technique used in this thesis for measuring the electrostatic potential before conversion to a charge density is by way of a vibrating Kelvin probe. The vibrating Kelvin probe is a non-contact electrostatic voltage measurement device which is connected to the electrostatic voltmeter (ESVM). A DC-feedback ESVM as used in the thesis has several advantages over electrostatic field meters and AC-feedback ESVM. The DC-feedback ESVM has very good resolution, excellent accuracy at the specified probe to surface distance, and has a lesser chance of arcing due to the body of the probe being at the same potential of the surface that is measured. AC-feedback ESVM and electrostatic fieldmeters have a possibility of arcing during charge measurement as the bodies of the probe are at the same potential as ground. They are not as accurate and do not have as a high a spatial resolution. A fieldmeter is meant more for larger surfaces while the the DC-ESVM can be used on both large and small surfaces [65]. The lack of surface contact with these methods means there

is no charge disturbance. The Kelvin probe, capacitive probe [66], electric fieldmeters, electric field mills, Pockels probe (using optical techniques) [67], [68] and induction probes are examples of non-contact surface charge potential measurement tools. Fieldmeters and electrostatic voltmeters all make use of the vibrating Kelvin probe. Electric field meters and mills provide an electric field measurement. There are also electrometers which come into contact with the surface for measurements and uses a very high input impedance but can only measure in the range of ± 2 kV. The Trek 341 B DC-ESVM electrostatic voltmeter used for this project allows the highest possible surface charge measurements of upto ±20 kV with a non-contact probe which is high speed and very accurate .

A.1.1 Vibrating Kelvin Probe

The Kelvin probe (vibrating capacitive probe) was proposed by Lord Kelvin in the year 1898 in Scotland [69]. It was not vibrating at the time and the plates had to be moved by hand. It was based on the theory that if two plates are brought together, equal but opposite charges will be induced on the surfaces. The contact potential was measured by applying a potential to the plates until the surface charge no longer existed. At that time the externally applied potential would be equal to the contact potential [70].

The vibrating Kelvin probe was invented by in 1932 by William A Zisman in Boston. A vibrating probe was located above the sample surface. The vibrating probe is vibrated sinusoidally. An external voltage is applied to the probe until the voltage on the sample surface is equal to the voltage of the probe and the difference is brought to zero as shown in Figure A.1 [69], [70].

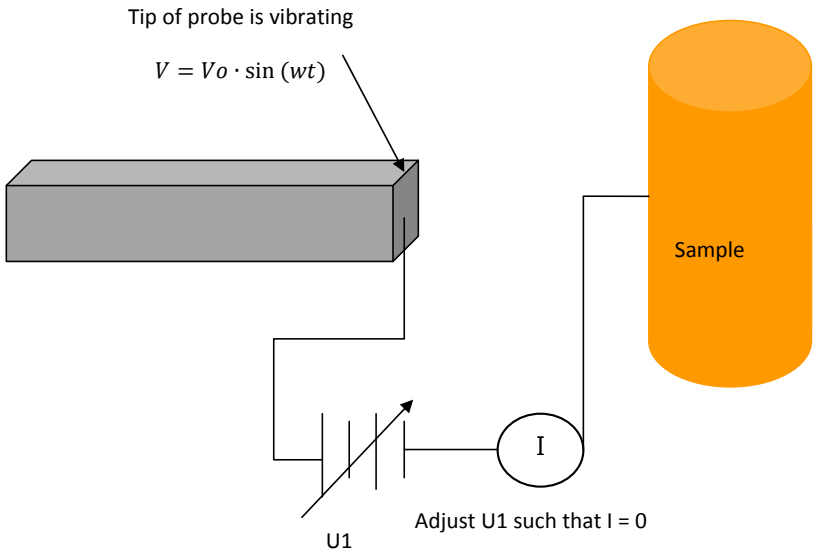

Fig. A.1: Basis of operation for vibrating Kelvin probe.

The principle of operation is based on the below equation where the capacitance C of a capacitor is given by:

$$C = \frac{Q}{U} \quad [F] \tag{A.1}$$

where Q [C] is the charge accumulated by the capacitor and U [V] is the voltage between the two plates of the capacitor.

The capacitance C of a parallel plate capacitor is given by:

$$C = \frac{\epsilon\epsilon_0 A}{D} \quad [F] \tag{A.2}$$

where ϵ is relative permittivity of the air, ϵ_0 is the permittivity of a vacuum, and A [m^2] is the area of the probe surface. ϵ is 1.0 for air and ϵ_0 is $8.854 \cdot 10^{-12}$ [F/m].

Given that the motion of the probe is sinusoidally modulated, the distance between the

probe and the surface being measured can be defined by:

$$D = D_0 + D_1 \cdot sin(\omega t) \quad [m] \tag{A.3}$$

where D_0 [m] is the distance between the probe surface and the surface to be measured when the probe is not vibrating, D_1 [m] is the amplitude of vibrations, ω is the angular frequency of vibrations [rad/s].

The capacitance of the plate to probe configuration then becomes:

$$C = \frac{\epsilon\epsilon_0 A}{D_0 + D_1 \cdot sin(\omega t)} \quad [F/m] \tag{A.4}$$

The current can be then determined by:

$$\begin{aligned} I &= U \cdot \frac{dC}{dt} \\ &= U \cdot \frac{d}{dt}\left(\frac{\epsilon\epsilon_0 A}{D_0 + D_1 \cdot sin(\omega t)}\right) \\ &= -U \cdot \epsilon\epsilon_0 A \cdot \left(\frac{D_1 \omega cos(\omega t)}{[D_0 + D_1 sin(wt)]^2}\right) \quad [A] \end{aligned} \tag{A.5}$$

The field nullifying method that is used by the DC-ESVM, with the vibrating Kelvin probe, adjusts the voltage on the probe such that the voltage U1 is equal to U2 and then U is zero. At this point there is no current flowing to or from the probe. Whenever the probe is sinusoidally modulated and the current becomes zero, the potential of the probe is equal to the potential of the surface. See below Figure A.2 for reference [69].

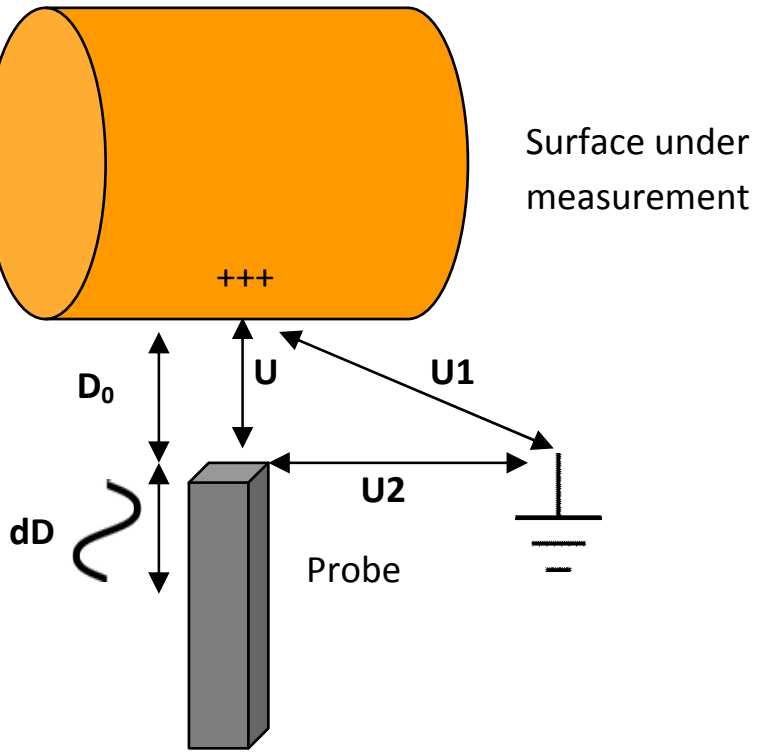

Fig. A.2: Kelvin vibrating capacitive probe reference drawing for equations.

For the most accurate results and for the best spatial resolution the probe to surface distance should be as close as possible and the surface area of the of probe surface should be small. If the distance from the probe to surface, or the probe surface area, is to large the measurements will be affected by other space charges on the surface nearby.

To measure the potential on the test surface, the Kelvin probe is positioned to approximately 3 ± 1 mm. The tip of probe, views the test surface through an aperture at the end of the probe which measures 1.52 mm in diameter as shown in Figure A.3.

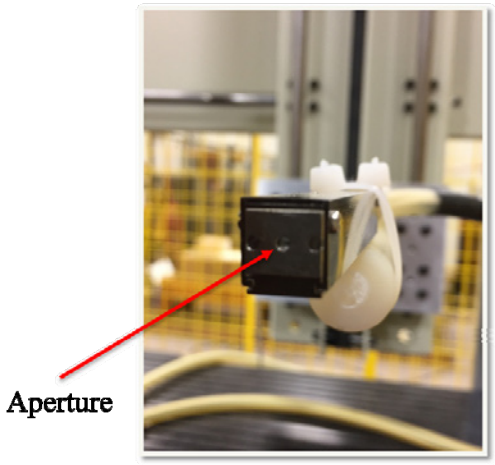

Fig. A.3: Aperture of vibrating capacitive Kelvin probe.

The use of a Kelvin probe with a smaller area and aperture functions to increase the spatial resolution of the probe to a small region on the test surface. This provides a very accurate reading and lessens the impacts of stray capacitance. To explain the basis of operation [71] of the DC-ESVM figure A.4 can be referenced. The vibrating Kelvin probe metallic housing acts as a reference surface and is attached to the output of the high-voltage amplifier (A), which changes the potential applied to the probe reference surface. The probe-end Kelvin sensor is electro-mechanically vibrated to produce capacitive modulation between the tip of the probe and the test surface such that a DC electrostatic charge can be measured due to the time-varying nature. If the potential of the test surface varies from the potential of the reference probe, the change in potential induces an AC waveform on the electrode due to the changing of the capacitance. The current signal is essentially amplified and modulated to produce a potential waveform. The signal induced on the vibrating Kelvin sensor is then provided to a preamplifier (B) in the probe. The amplified Kelvin probe sensor signal and the output potential of the oscillator (M) which drives the electromechanical

modulator are attached to a phase sensitive demodulator whose output signal is a DC potential whose magnitude and polarity correspond to the potential deviation. The signal from the phase sensitive demodulator is attached to the input signal of an integrating DC high-voltage amplifier (A). The output signal of A is the probe reference potential, which is driven, to be equal, to the potential of the surface under testing. The electric field and the current between test surface and probe will thus be brought to zero. With the electric field, potential and current nulled between the probe and test surface, the signal induced on the tip of the electrode is decreased to zero, decreasing the demodulated signal to the integrating DC amplifier to null. The high-voltage amplifier (A) output and the probe reference housing are now kept at the potential of the surface under testing. The output of the high-voltage amplifier (A) is divided down by a ratio of 1000:1 to drive buffer amplifier (C) for precise monitoring and digital display of the measured potential on the test surface, on the front panel of the DC-ESVM [71]. The monitor output is also available as a BNC connection for output to a data acquisition system.

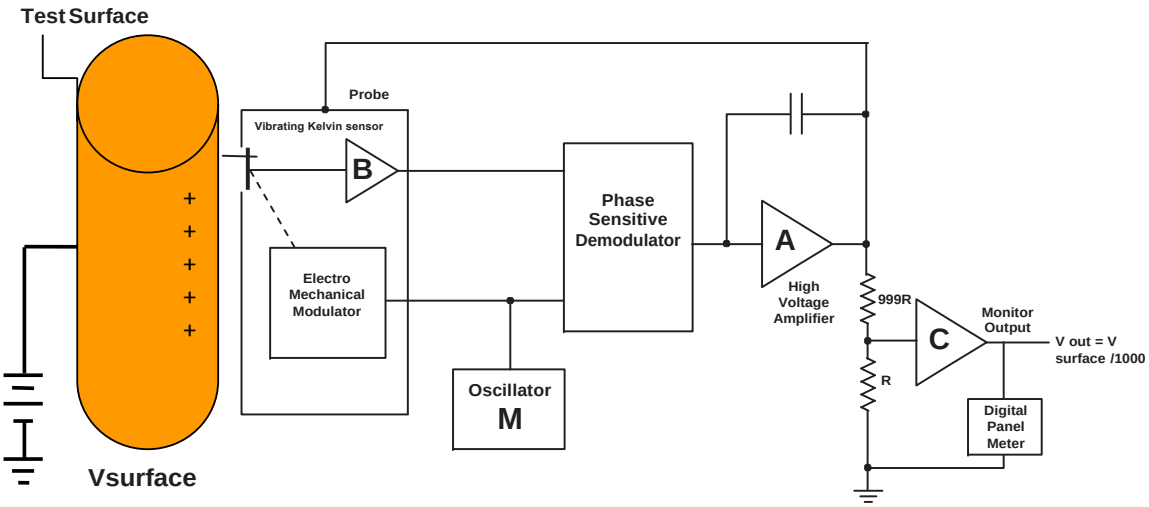

Fig. A.4: Circuit diagram of DC-ESVM [71].

Since the vibrating kelvin sensor and the metallic body of the probe are at the same potential the effects of stray capacitances are less than that of AC feedback ESVM and fieldmeters. The below Figure A.5 illustrates where C1 is the capacitance between the test surface and ground, C2 is the capacitance between the sensor and ground, C3 is the capacitance between the probe body and ground, and Z is the internal impedance of the probe between the sensor and probe housing body. The capacitances between the test surface and sensor/probe body are non-existent due to the field nullifying effect.

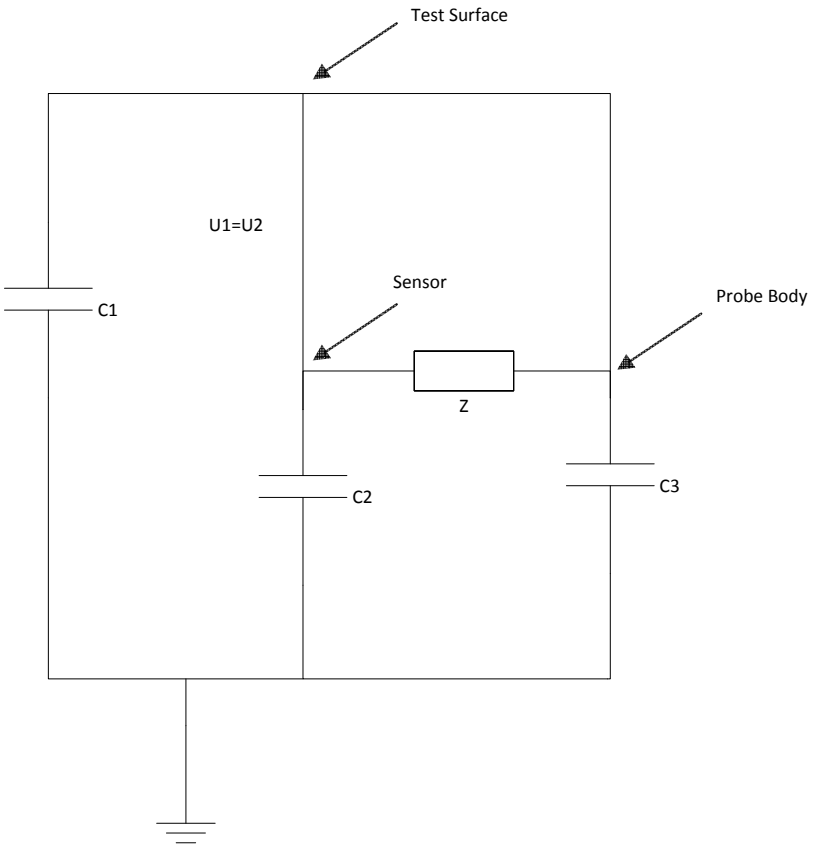

Fig. A.5: Capacitive couplings of DC-ESVM. [72]

Appendix B

Figures of Surface Potential and Charge Distribution of all Insulator Samples

In the below figures the effects of positive and negative charging voltage using the corona ring of needles are shown for all of the insulator samples. All charging is completed with the ring of needles located at the center of the sample and for a 2 minutes charging time. The insulator samples are further described in 3.1.

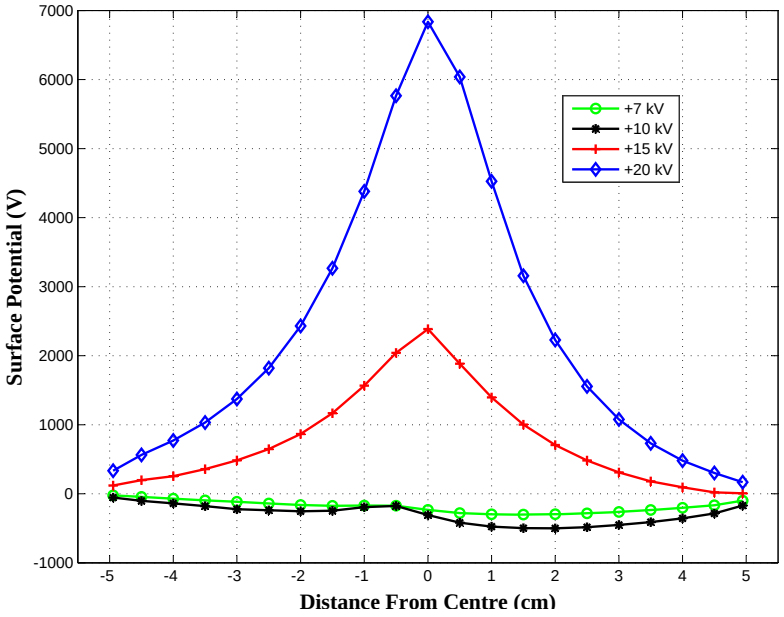

(a) Surface potential distribution, positive charging voltages

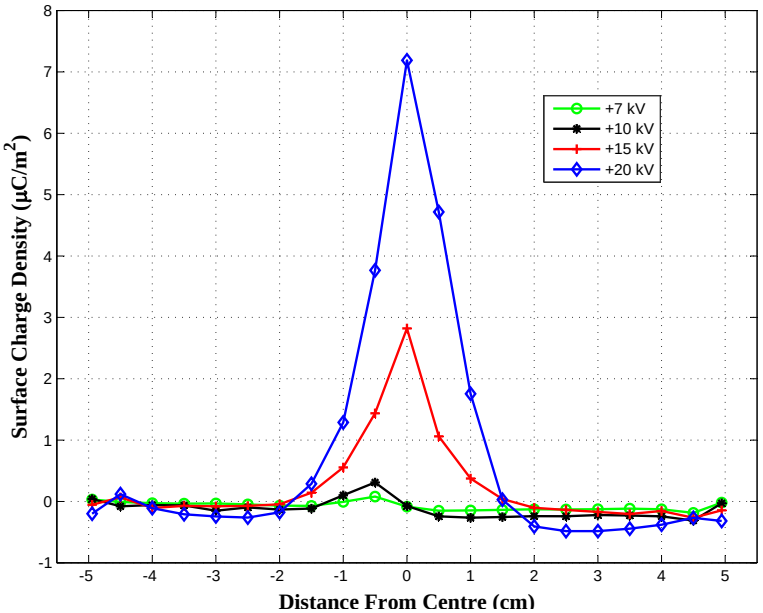

(b) Surface charge distribution, positive charging voltages

Fig. B.1: The large FRP sample a) surface potential and b) charge density distribution for + 7 kV, + 10 kV, +15 kV, and + 20 kV.

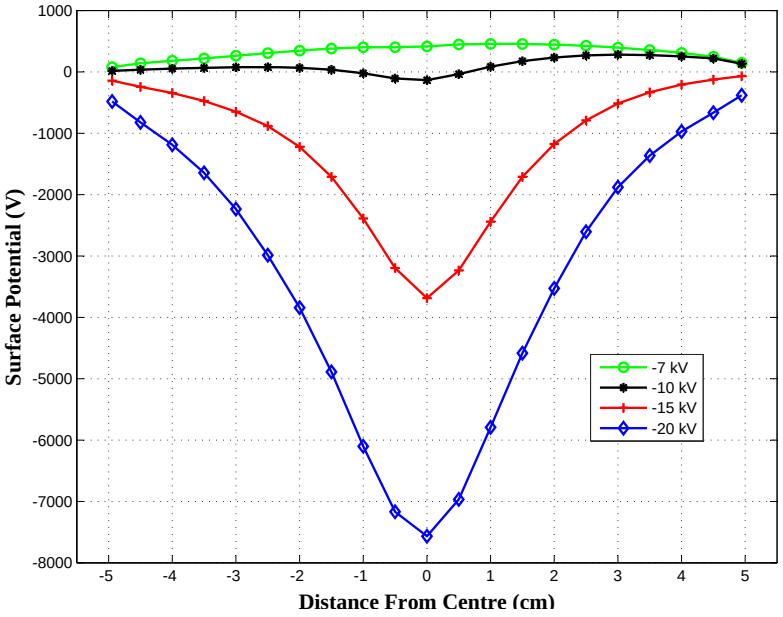

(a) Surface potential distribution, negative charging voltages

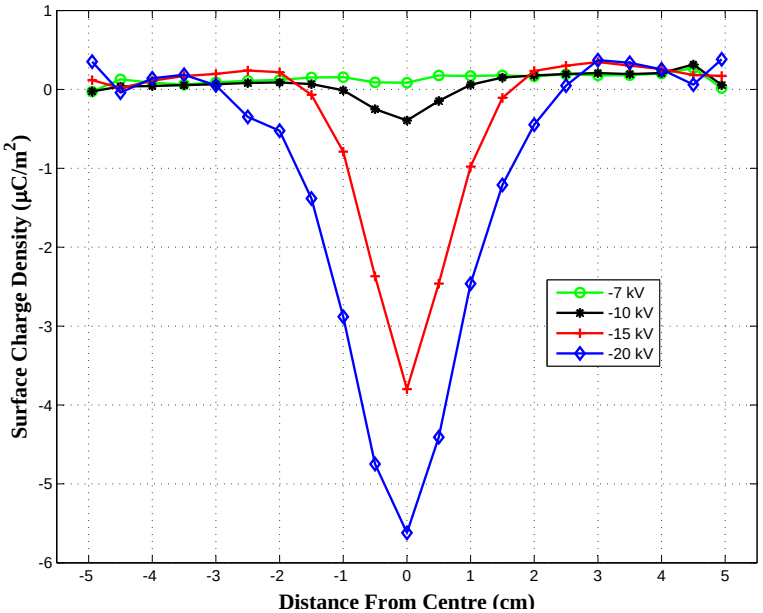

(b) Surface charge distribution, negative charging voltages

Fig. B.2: The large FRP sample a) surface potential and b) charge density distribution for -7 kV, -10 kV, -15 kV, and -20 kV.

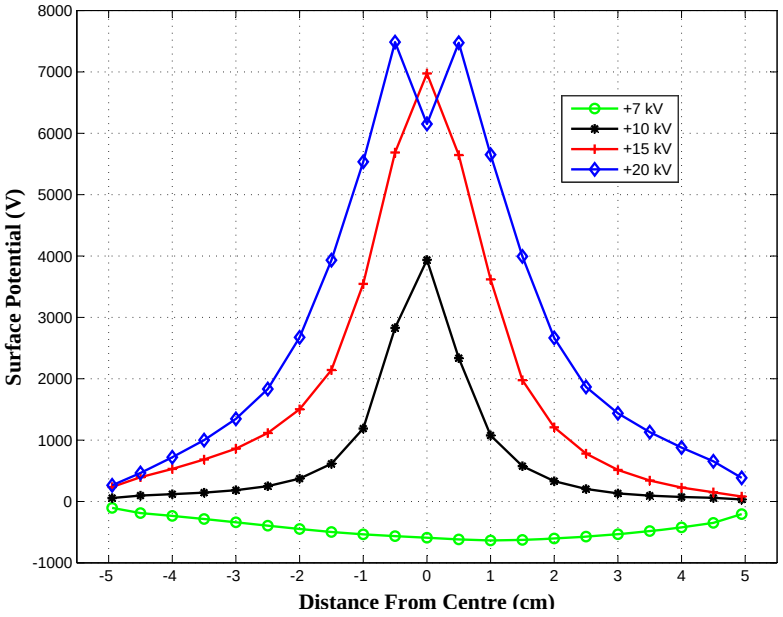

(a) Surface potential distribution, positive charging voltages

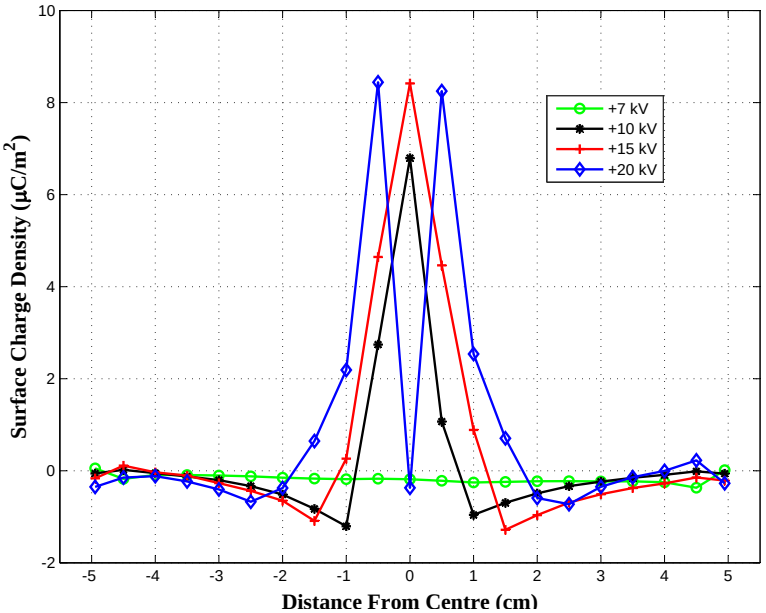

(b) Surface charge distribution, positive charging voltages

Fig. B.3: The small FRP sample a) surface potential and b) charge density distribution for + 7 kV, + 10 kV, +15 kV, and + 20 kV.

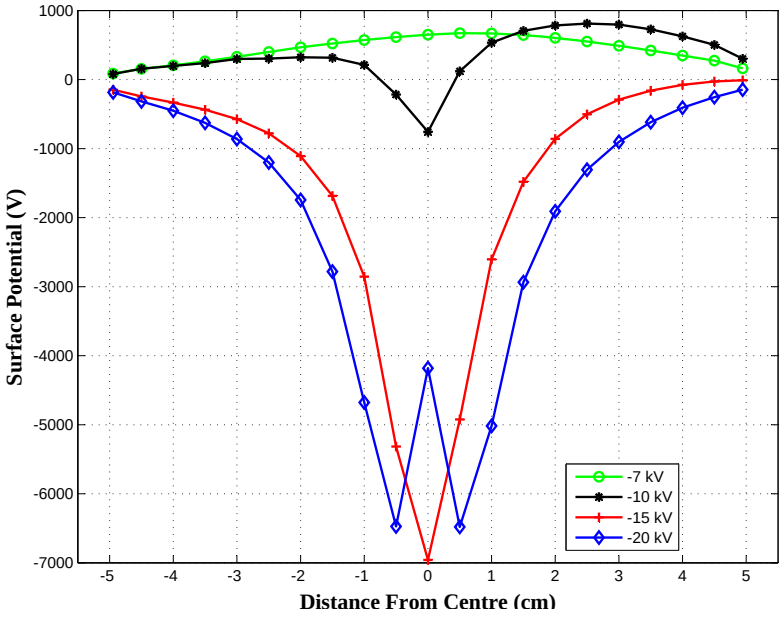

(a) Surface potential distribution, negative charging voltages

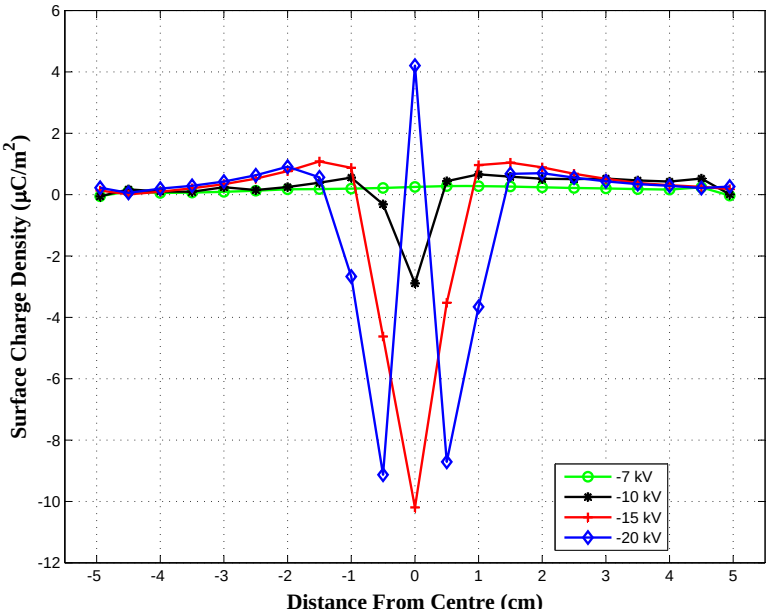

(b) Surface charge distribution, negative charging voltages

Fig. B.4: The small FRP sample a) surface potential and b) charge density distribution for -7 kV, -10 kV, -15 kV, and -20 kV.

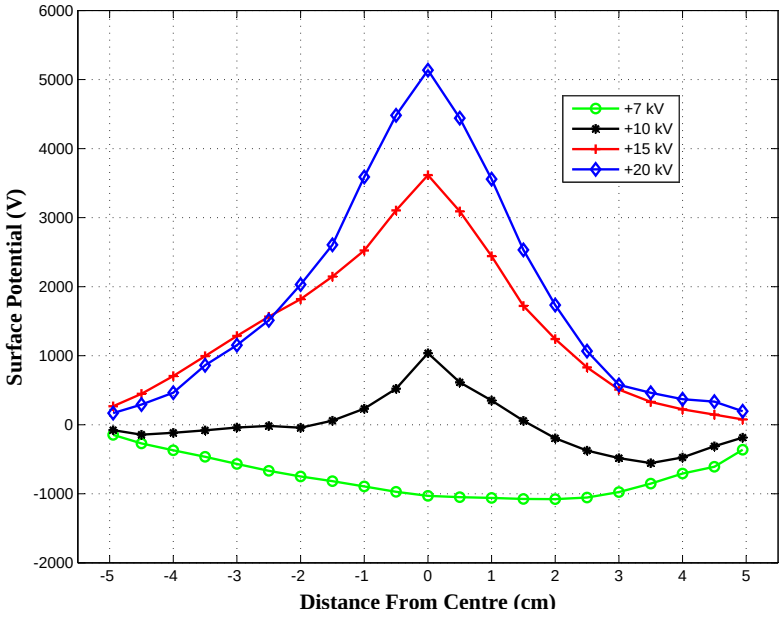

(a) Surface potential distribution, positive charging voltages

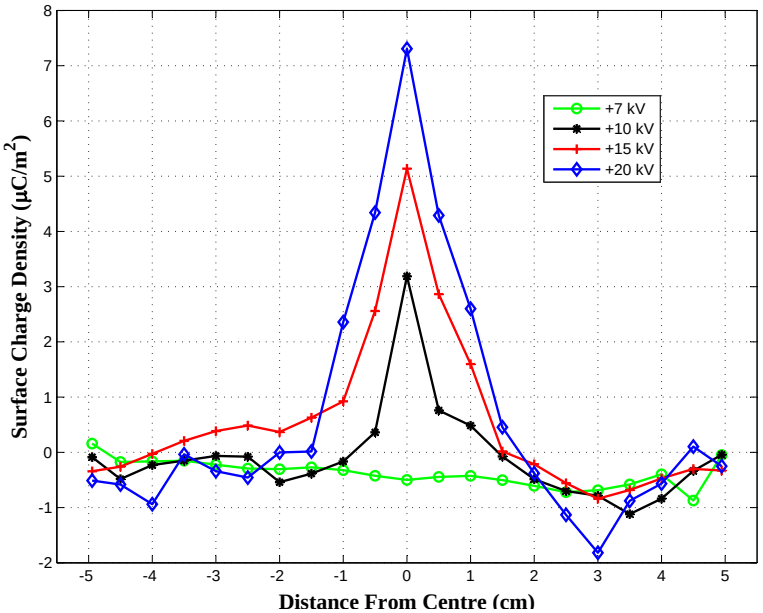

(b) Surface charge distribution, positive charging voltages

Fig. B.5: The large SIR sample a) surface potential and b) charge density distribution for + 7 kV, + 10 kV, +15 kV, and + 20 kV.

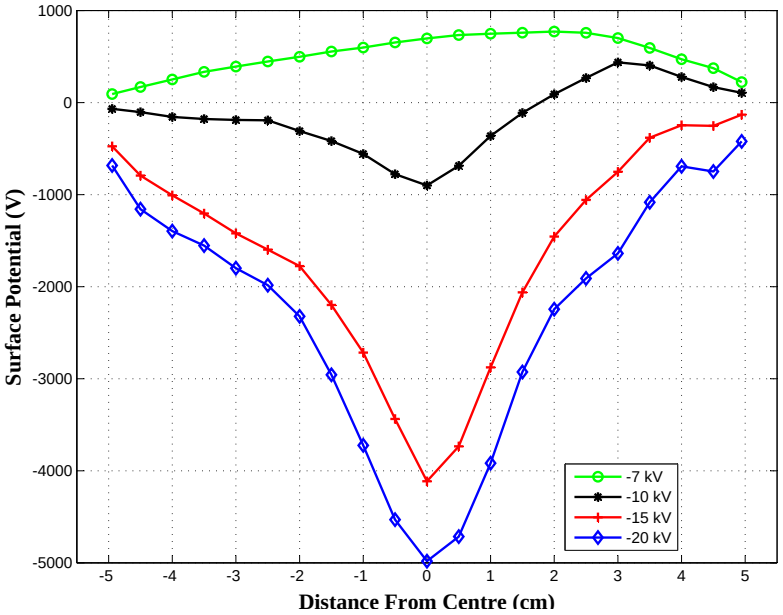

(a) Surface potential distribution, negative charging voltages

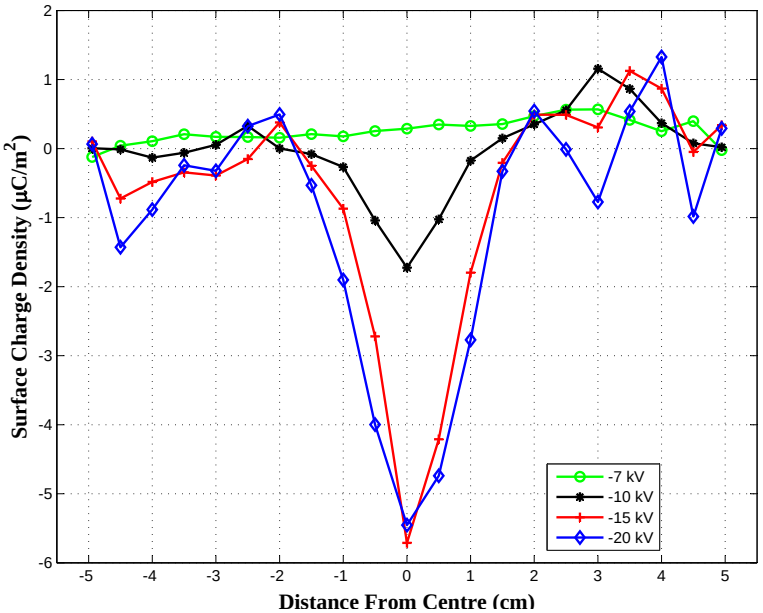

(b) Surface charge distribution, negative charging voltages

Fig. B.6: The large SIR sample a) surface potential and b) charge density distribution for -7 kV, -10 kV, -15 kV, and -20 kV.

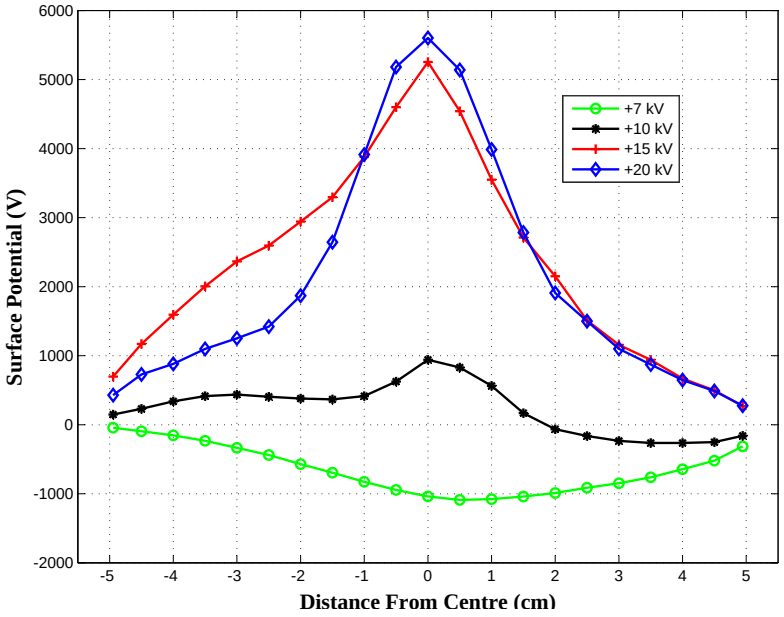

(a) Surface potential distribution, positive charging voltages

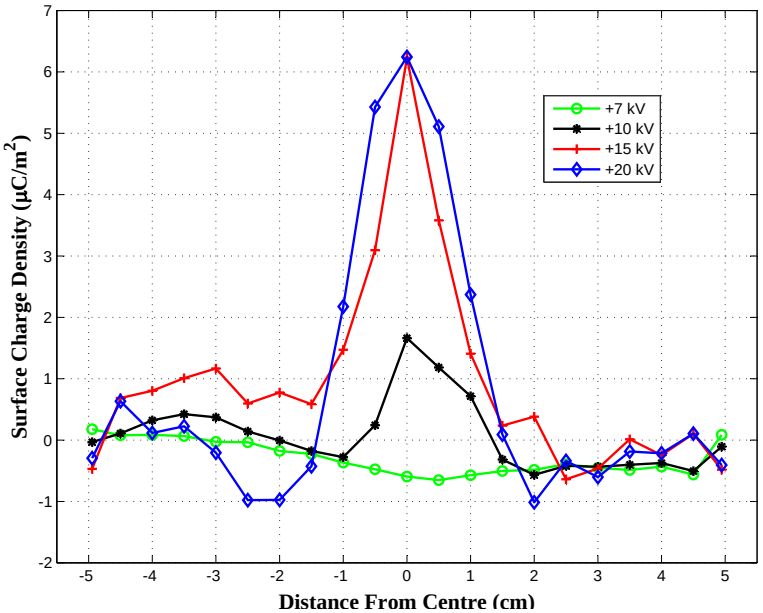

(b) Surface charge distribution, positive charging voltages

Fig. B.7: The small SIR sample a) surface potential and b) charge density distribution for + 7 kV, + 10 kV, +15 kV, and + 20 kV.

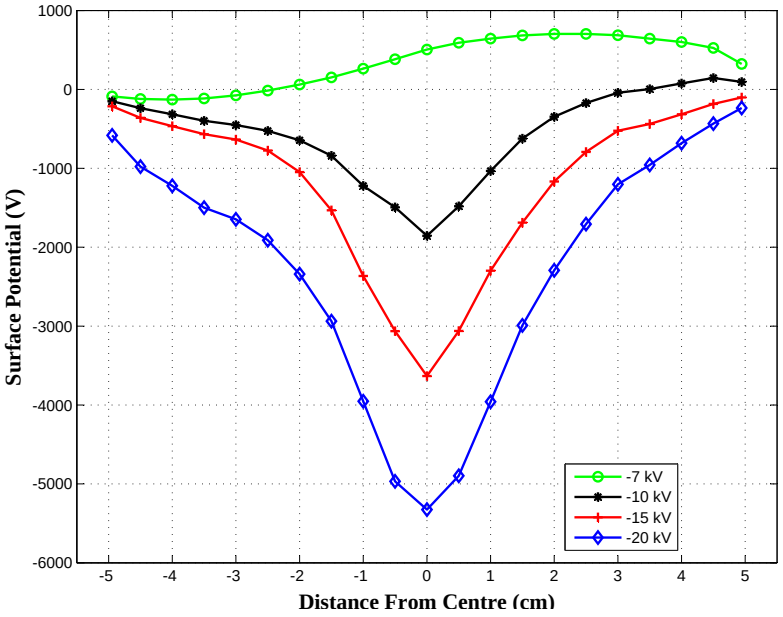

(a) Surface potential distribution, negative charging voltages

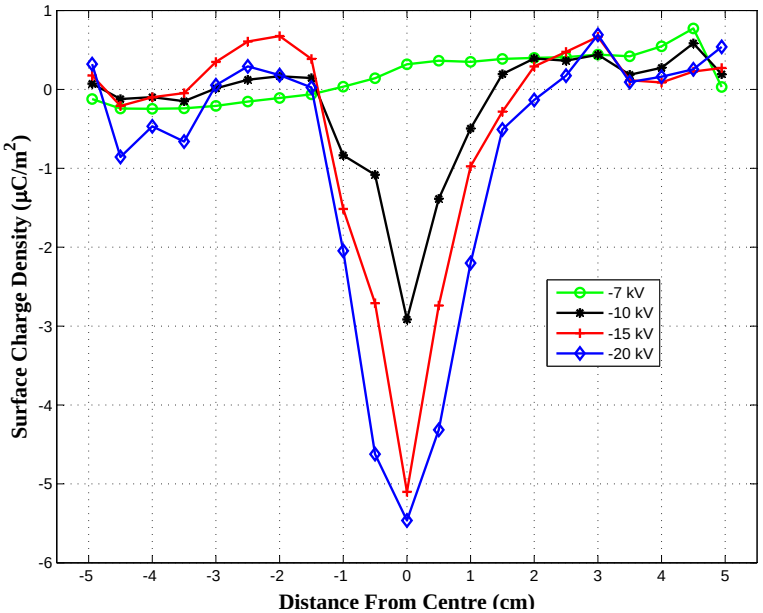

(b) Surface charge distribution, negative charging voltages

Fig. B.8: The small SIR sample a) surface potential and b) charge density distribution for -7 kV, -10 kV, -15 kV, and -20 kV.

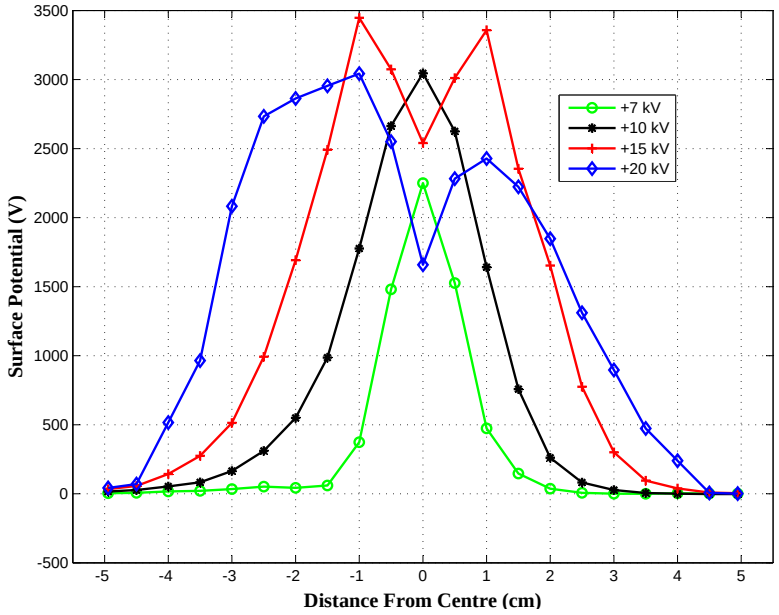

(a) Surface potential distribution, positive charging voltages

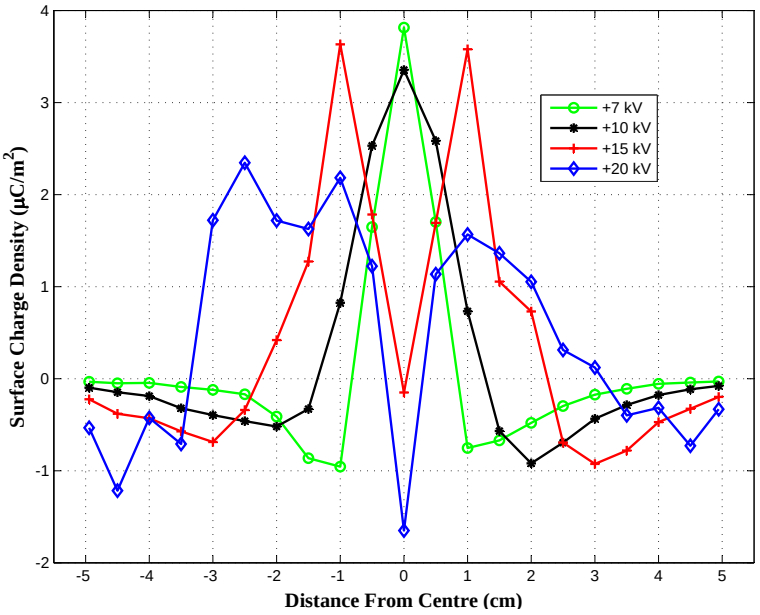

(b) Surface charge distribution, positive charging voltages

Fig. B.9: The wood sample a) surface potential and b) charge density distribution for + 7 kV, + 10 kV, +15 kV, and + 20 kV.

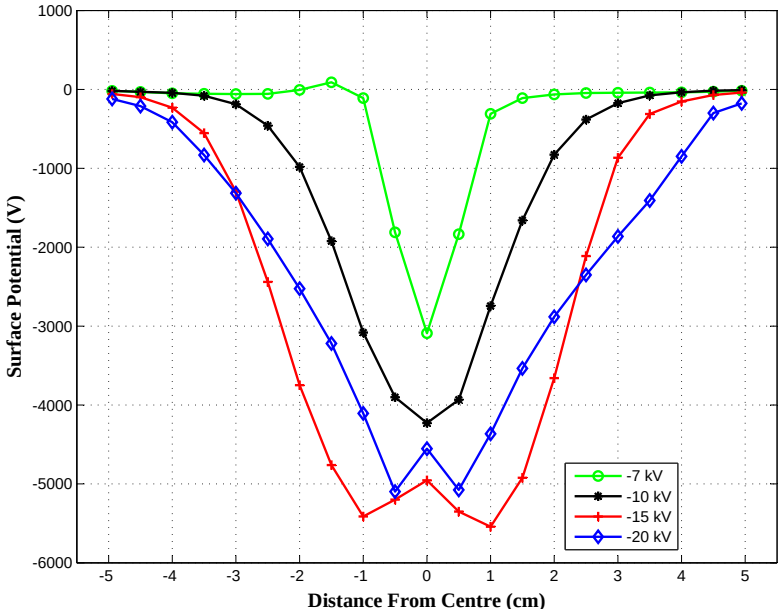

(a) Surface potential distribution, negative charging voltages

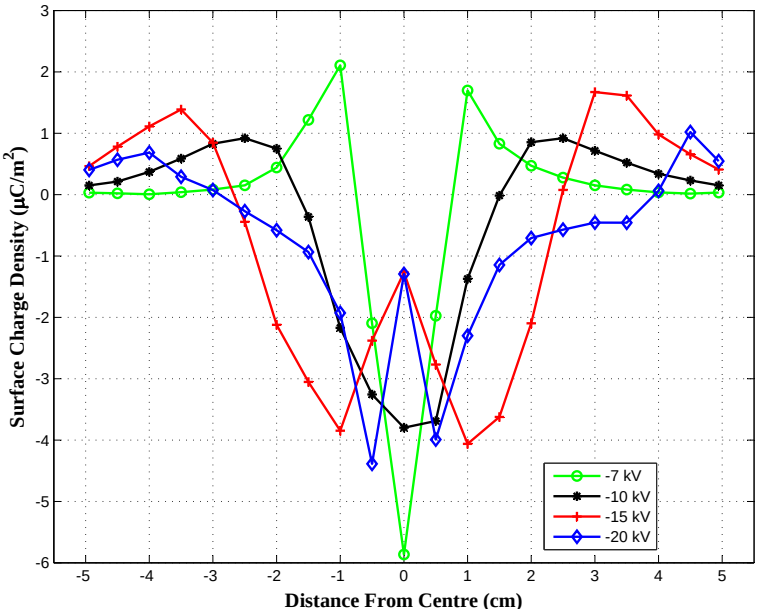

(b) Surface charge distribution, negative charging voltages

Fig. B.10: The wood sample a) surface potential and b) charge density distribution for -7 kV, -10 kV, -15 kV, and -20 kV.

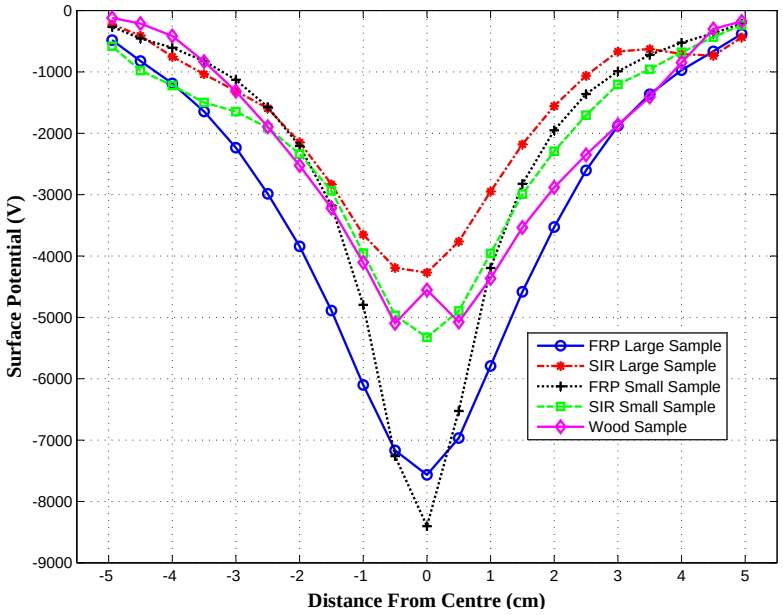

(a) Surface potential distribution all samples, -20 kV

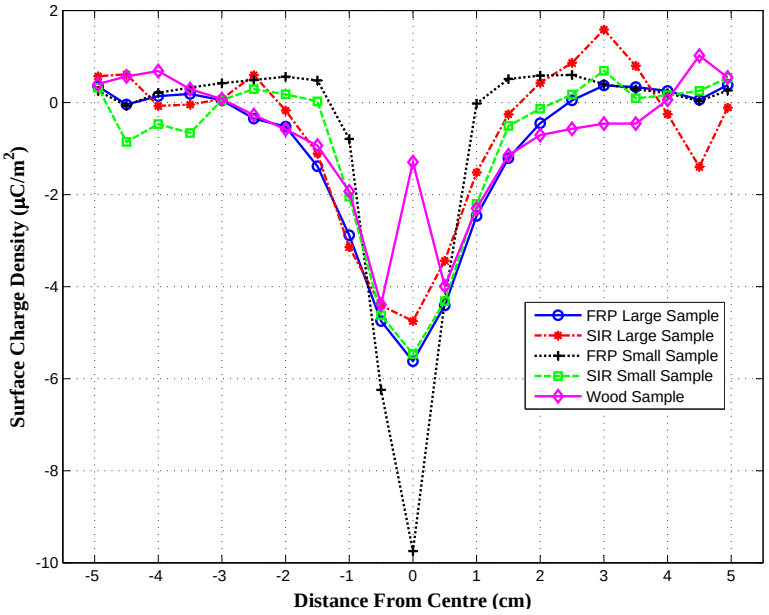

(b) Surface charge distribution, all samples, -20 kV

Fig. B.11: All samples a) surface potential and b) charge density distribution for -20 kV.

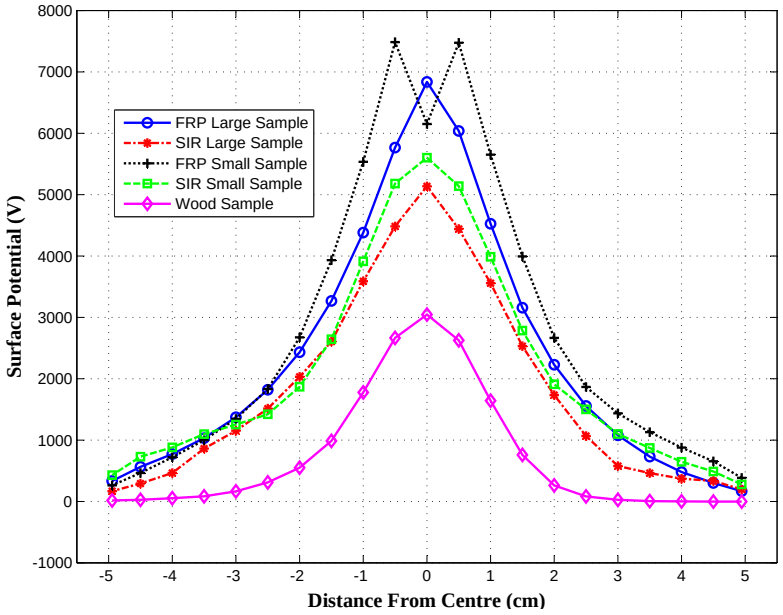

(a) Surface potential distribution all samples, +20 kV

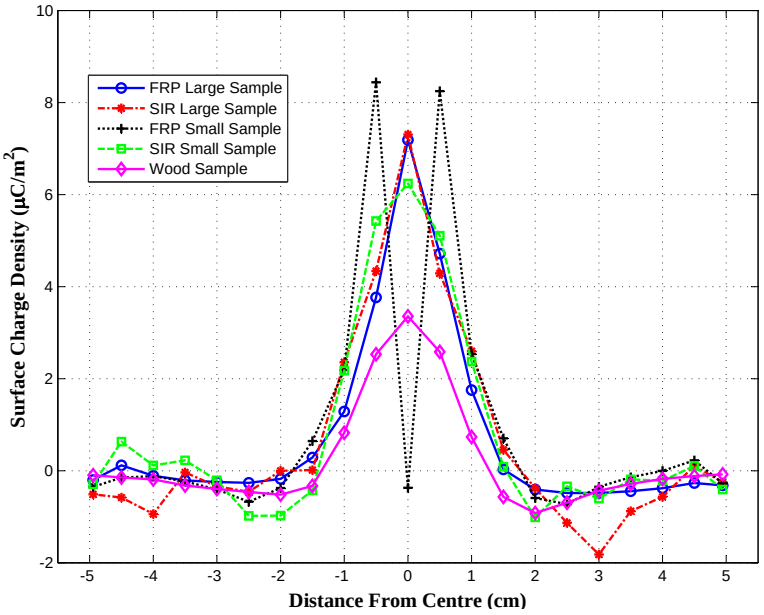

(b) Surface charge distribution, all samples, +20 kV

Fig. B.12: All samples a) surface potential and b) charge density distribution for +20 kV.

Appendix C

Figures of Surface Charge Decay for Insulator Samples

In the below figures the results of the surface charge decay tests are shown for -20 kV charging, with the ring of needles located at the center of the sample, 5 mm needle to surface distance, 2 minutes charging time and for up to a 240 minutes measurement period. The insulator samples are further described in 3.1.

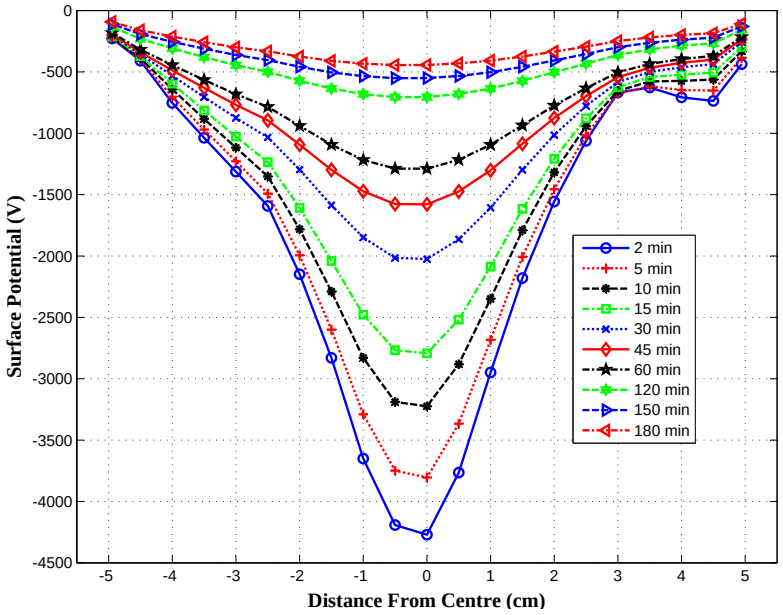

(a) Measured surface potential for charge decay test

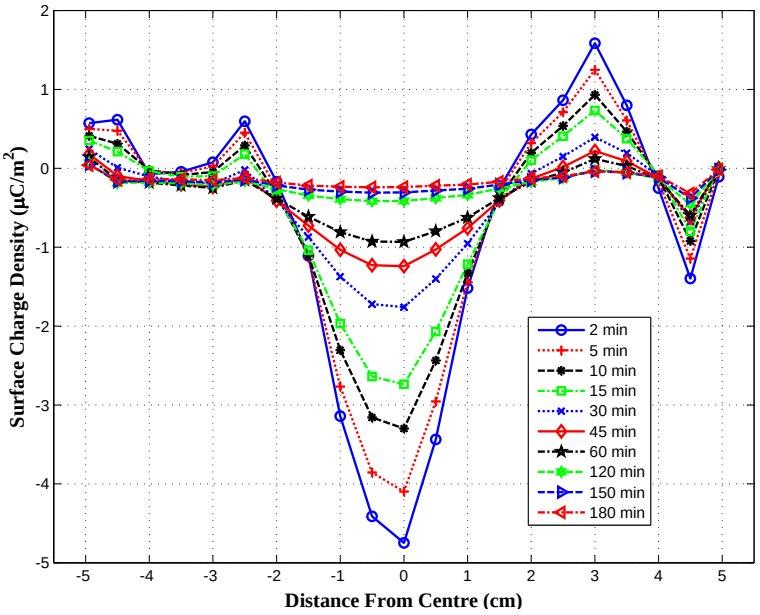

(b) Calculated charge density for charge decay test

Fig. C.1: Surface charge decay test for large SIR sample showing a) surface potential decay and b) surface charge density decay for -20 kV charging voltage.

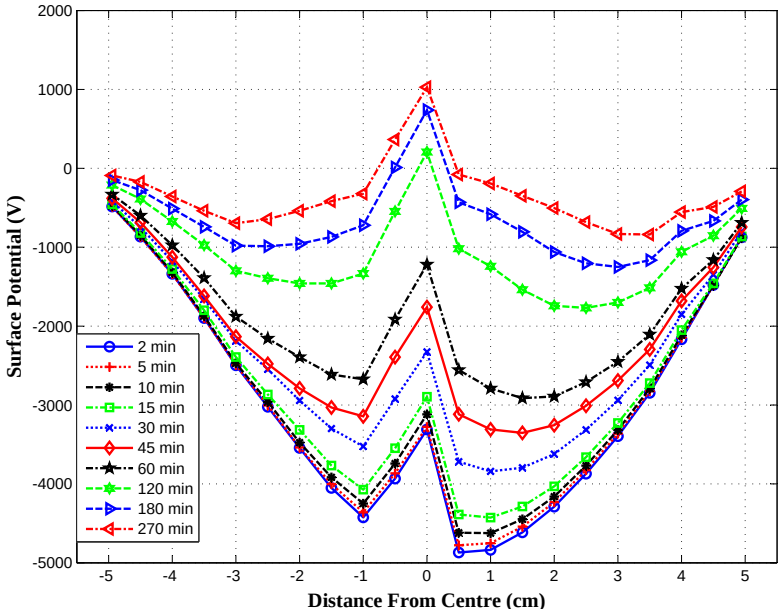

(a) Measured surface potential for charge decay test

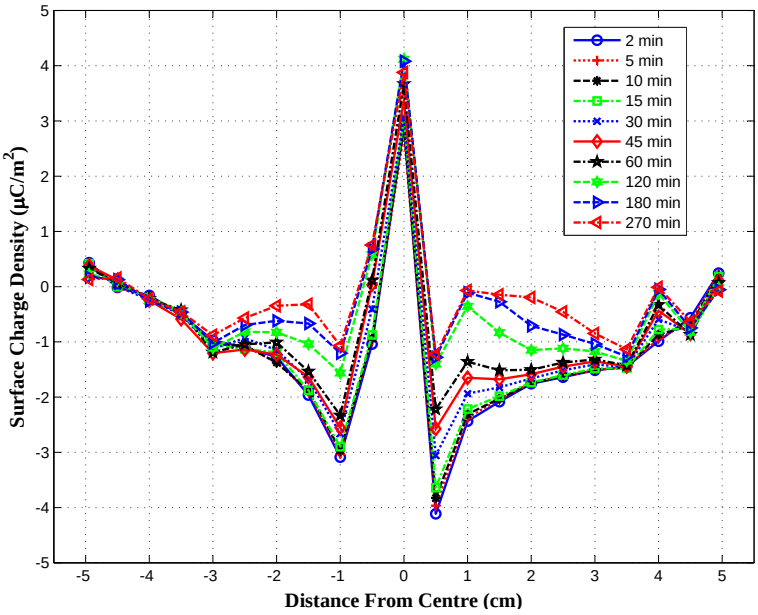

(b) Calculated charge density for charge decay test

Fig. C.2: Surface charge decay test for large FRP sample showing a) surface potential decay and b) surface charge density decay for -20 kV charging voltage.

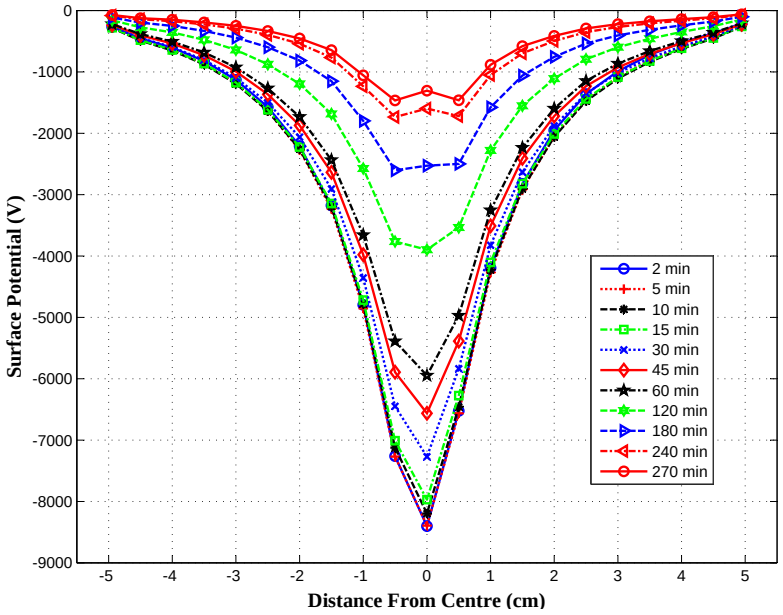

(a) Measured surface potential for charge decay test

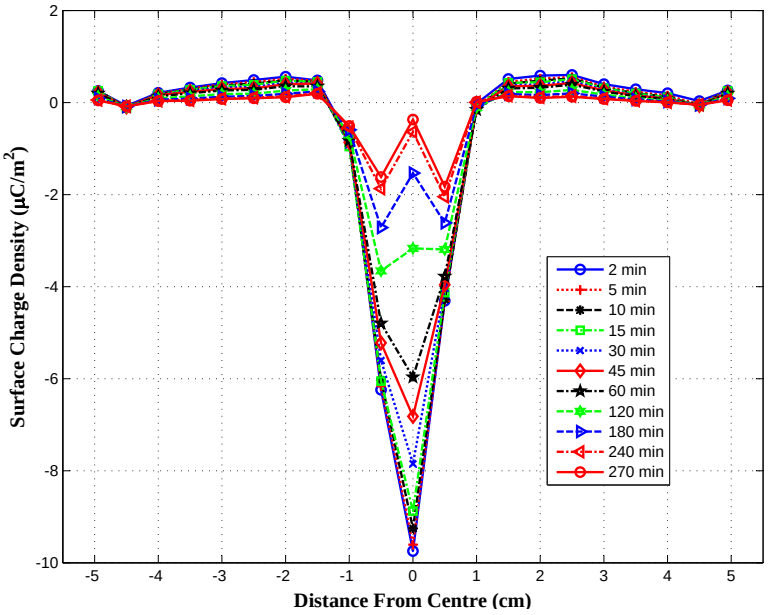

(b) Calculated charge density for charge decay test

Fig. C.3: Surface charge decay test for small FRP sample showing a) surface potential decay and b) surface charge density decay for -20 kV charging voltage.

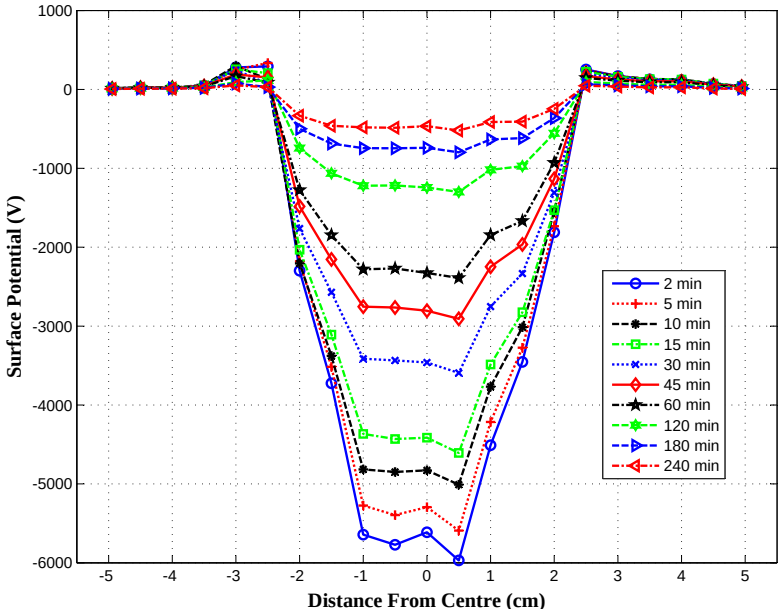

(a) Measured surface potential for charge decay test

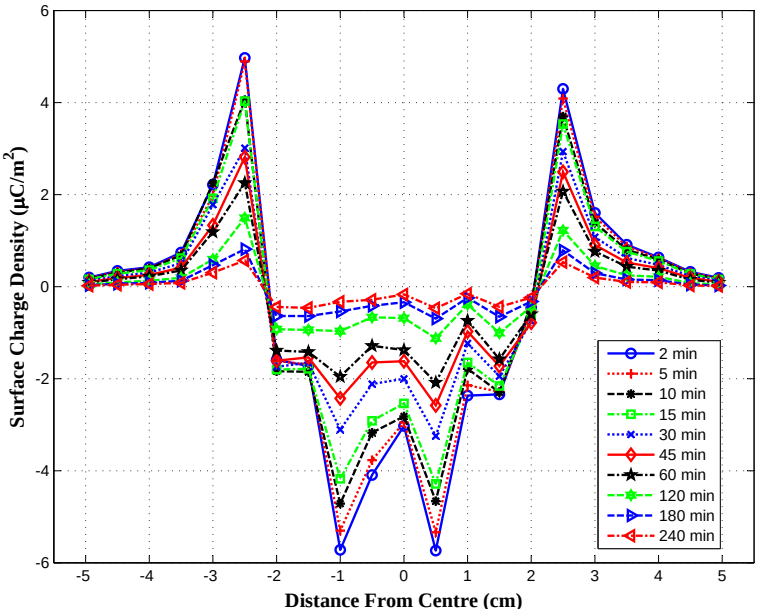

(b) Calculated charge density for charge decay test

Fig. C.4: Surface charge decay test for wood sample showing a) surface potential decay and b) surface charge density decay for -20 kV charging voltage.